Quantum Metrology for Biological Systems

by

Lea Gassab

A Dissertation Submitted to the
Graduate School of Sciences and Engineering
in Partial Fulfillment of the Requirements for
the Degree of

Doctor of Philosophy

in

Physics

KOÇ ÜNİVERSİTESİ

August 2024

Quantum Metrology for Biological Systems

Koç University

Graduate School of Sciences and Engineering

This is to certify that I have examined this copy of a doctoral dissertation by

Lea Gassab

and have found that it is complete and satisfactory in all respects,
and that any and all revisions required by the final
examining committee have been made.

Committee Members:

Prof. Dr. Özgür E. Müstecaplıoğlu

Asst. Prof. Onur Pusuluk

Assoc. Prof. Alkan Kabakçıoğlu

Date: August 5, 2024

Dedicated to all my teachers and friends

ABSTRACT

Quantum Metrology for Biological Systems
Lea Gassab
Doctor of Philosophy in Physics
August 2024

This thesis outlines three main projects which link biology, quantum information, and metrology. It culminates with future perspectives on quantum biology and various research related to the brain.

The first project begins with an examination of quantum information, moving from theoretical concepts to their practical implementation in biological environments. It tackles the issue of maintaining quantum coherence and entanglement despite the presence of environmental noise in open quantum systems. Geometrical optimization using buffer spins as a protective network of the quantum information in the central spin is introduced. Furthermore, the phenomenon of entanglement in a corresponding biological context is investigated by carrying out preliminary analysis of a more realistic system, the Posner cluster.

In the second project, the focus shifts to quantum sensing, with particular attention to the Nitrogen-Vacancy (NV) center, a point defect in diamond. The role of NV centers as sensitive probes is examined in biological contexts, particularly for detecting magnetic fields. The application of spin squeezing to NV centers, when considered as qutrit (three-level) systems, may potentially improve the precision of magnetic field measurements. This precision is quantified using Quantum Fisher Information. Moreover, the integration of a selective bioresponsive material, such as hydrogel, that act as a transducer in the measurement setup could open new avenues to a wider range of biological measurements.

The third project explores the use of quantum light to probe biological systems. It examines how quantum mechanics, particularly multipartite photon entanglement, can enhance our understanding of vision. This is achieved through simulations of psychophysical experiments, utilizing entanglement witnesses, a class of observables used to detect entanglement. Starting with bipartite entangled state,

and then, generalizing to tripartite case, the probability of seeing of the human eye is determined for a certain range of additive noise levels and visual thresholds. The results shed light on the human eye's capacity to witness entanglement.

The three topics covered demonstrate the intertwining relationship between biology and quantum physics. This is further detailed as future perspectives of research by posing some of the most intriguing and fundamental questions of all time in science. A special emphasis of the connection of this relationship to the brain is laid. Eventually, building on such endeavors will become the groundwork of significant potential contributions to future developments in biological and medical sciences.

ÖZETÇE

Biyolojik Sistemler için Kuantum Metroloji
Lea Gassab
Fizik, Doktora
Ağustos 2024

Bu tez, biyoloji, kuantum bilgisi ve metrolojiyi birleştiren üç ana projeyi özetlemektedir. Kuantum biyolojisi ve beyinle ilgili çeşitli araştırmalarla ilgili gelecekteki perspektiflerle bitmektedir.

İlk proje, kuantum bilgisi incelemesiyle başlar ve teorik kavramlardan biyolojik ortamlarda pratik uygulamalarına geçer. Açık kuantum sistemlerinde çevresel gürültünün varlığına rağmen kuantum koherens ve dolanıklığın nasıl sürdürülebileceği sorununu ele alır. Merkezi spinin kuantum bilgisini korumak için tampon spinlerin kullanıldığı geometrik optimizasyon yöntemi tanıtılmaktadır. Ayrıca, karşılık gelen biyolojik bağlamda dolanıklık fenomeni, daha gerçekçi bir sistem olan Posner kümesinin ön analizleri yapılarak incelenir.

İkinci projede, odak noktası kuantum algılamaya kayar ve özellikle elmas içindeki bir nokta kusuru olan Azot-Boşluk (NV) merkezine dikkat edilir. NV merkezlerinin biyolojik bağlamlarda, özellikle manyetik alanları tespit etmek için hassas prob olarak rolü incelenir. NV merkezleri, üç seviyeli (qutrit) sistemler olarak düşünüldüğünde, spin sıkıştırma tekniği kullanılarak manyetik alan ölçümlerinin hassasiyeti potansiyel olarak artırılabilir. Bu hassasiyet, Kuantum Fisher Bilgisi kullanılarak ölçülür. Ayrıca, ölçüm düzeninde transdüser olarak hareket eden hidrojel gibi seçici biyo-duyarlı bir malzemenin entegrasyonu, daha geniş bir biyolojik ölçüm yelpazesine yeni yollar açabilir.

Üçüncü proje, biyolojik sistemleri araştırmak için kuantum ışığının kullanımını araştırır. Kuantum mekaniğinin, özellikle çok parçacıklı foton dolanıklığının, görme anlayışımızı nasıl geliştirebileceğini inceler. Bu, psikofiziksel deneylerin simülasyonları, dolanıklığı tespit etmek için kullanılan bir gözlemler sınıfı olan dolanıklık tanıklarını kullanarak başarılır. İki parçacıklı dolanık durumla başlayıp ardından üç parçacıklı duruma genelleme yaparak, belirli bir aralıktaki gürültü seviyeleri ve

görsel eşikler için insan gözünün görme olasılığı belirlenir. Sonuçlar, insan gözünün dolanıklığı tanıklama kapasitesine ışık tutar.

Ele alınan üç konu, biyoloji ve kuantum fiziği arasındaki iç içe geçen ilişkiyi göstermektedir. Bu, bilimde tüm zamanların en ilginç ve temel sorularından bazılarını ortaya koyarak gelecekteki araştırma perspektifleri olarak daha ayrıntılı bir şekilde açıklanmıştır. Bu ilişkinin beyinle bağlantısına özel bir vurgu yapılmıştır. Sonuçta, bu tür çabalara dayanarak, biyolojik ve tıbbi bilimlerde gelecekteki gelişmelere önemli katkılar sağlayacak temeller oluşturulacaktır.

ACKNOWLEDGMENTS

I would like to first thank my supervisor, Professor Özgür E. Müstecaplıoğlu, who has been the best supervisor, always encouraging and present when needed, without putting pressure on me. I would also like to thank Professor Onur Pusuluk, with whom I have learned a lot and had the chance to work with. I would like to thank my colleagues for our discussions and laughter. I am especially thankful to Hamideh for her continuous assistance with Turkish translations and for being a great partner during our Hamam adventures. A special thanks to Ms. Merusha Naidoo, who is also completing her PhD in Human Genetics in South Africa, for verifying the contents regarding receptor proteins and hormones mentioned in Chapter 3. I would like to thank my partner, Yashine, for supporting me in the best way ever during these four years, especially for buying me sicak ekmek every morning ever since we have been living together. I would like to thank my parents, Catherine and Karim, my brother, Ugo, and my grandparents, Babaziz and Mamine, and my whole family and friends, especially Alizée and Elsa, for encouraging me and taking the time to come to visit me in the beautiful Türkiye. I would like to thank every person that I met and helped me to be where I am. Finally, I want to thank Türkiye for hosting me and showing its incredible beauty with hand on the heart people (avec la main sur le coeur), without forgetting all the cats and dogs who always accompany you in the streets of Istanbul and yunus (the dolphins) in the Bosphorus. Thank you. Teşekkür ederim. Muchas Gracias. Aychek. Merci beaucoup.

TABLE OF CONTENTS

List of Tables xiv

List of Figures xvi

Abbreviations xxvi

Chapter 1: General Introduction 1

1.1 The Quantum Vision Project 2
1.2 Quantum Effects in The Brain 2
1.3 Quantum Sensing 3
1.4 The Quantum Link to Biology 3
1.5 Outline 4

Chapter 2: Quantum Information Preservation In Biological Systems 5

2.1 Introduction 5
2.2 Quantum Information in Biology 10
2.2.1 Quantum Information 11
2.2.2 Coherence 11
2.2.3 Entanglement 13
2.3 Quantum Information as Metrological Tool 14
2.3.1 Quantum Fisher Information 14
2.3.2 Quantum Coherence Measures 15
2.3.3 Entanglement Measures 16
2.3.4 The Challenge of Quantifying Entanglement 18
2.4 Open Quantum Systems 19

2.5 Importance of Geometry . . . 21
2.5.1 Geometry in Engineering . . . 21
2.5.2 Geometry in Nanotechnology . . . 22
2.5.3 Geometry in Nature . . . 22
2.5.4 Is Geometry A Quantum Tool? . . . 23
2.6 Preservation of Quantum Coherence through Geometrical Optimization . . . 24
2.6.1 Spin-Star Network with Different Topologies . . . 24
2.6.2 Open Quantum System Dynamics . . . 28
2.6.3 Results . . . 29
2.6.4 Physical Mechanism of Coherence Protection . . . 33
2.6.5 Alternative Noise Model . . . 35
2.6.6 Parameter Dependence of The Model . . . 37
2.6.7 Preservation of Entanglement . . . 38
2.7 More Realistic System: Posner Cluster . . . 39
2.7.1 The Quantum Brain Proposal . . . 39
2.7.2 Generation of Entanglement in Posner Clusters: A Hypothesis 40
2.7.3 Analyzing Entanglement in One Posner Cluster . . . 42
2.8 Conclusion . . . 45

Chapter 3: Quantum Sensing With Nitrogen-Vacancy Centers 47
3.1 Introduction . . . 47
3.2 Quantum Sensing . . . 51
3.3 Nitrogen-Vacancy Centers . . . 52
3.3.1 Properties of NV Centers . . . 54
3.3.2 NV Centers as Probes in Biological Systems . . . 56
3.3.3 Enhancing Sensitivity with Quantum Correlations . . . 58
3.4 Quantum Fisher Information . . . 58
3.5 Spin Squeezing . . . 59

3.6 Spin Squeezing Enhanced Quantum Magnetometry with Nitrogen-Vacancy Center Qutrits . . . 61
3.6.1 Methodology . . . 61
3.6.2 Free Hamiltonian and Initial States . . . 63
3.6.3 Spin Squeezing Generation . . . 64
3.6.4 Open Quantum System Dynamics . . . 65
3.6.5 Spin Squeezing Parameter . . . 66
3.6.6 Results . . . 67
3.6.7 Analysis with Spin-1 Formalism . . . 68
3.6.8 Analysis with Spin-1/2 Formalism . . . 70
3.6.9 Entanglement . . . 72
3.7 Integrating NV Centers with Responsive Hydrogels for High-Precision Biological Measurements . . . 74
3.7.1 Hydrogels . . . 74
3.7.2 Choosing The Right Bioresponsive Material . . . 75
3.7.3 Our Proposal . . . 76
3.8 Conclusion . . . 77

Chapter 4: Quantum Light As A Biological Probe 79
4.1 Introduction to Vision . . . 79
4.2 Quantum Light and Metrology . . . 85
4.2.1 Light from Quantum Perspective . . . 85
4.2.2 Sub-Poissonian Light . . . 87
4.2.3 Applications in Biology . . . 89
4.3 Entanglement Witness . . . 90
4.3.1 Tripartite Entanglement Witness . . . 91
4.3.2 Distinguishing Between Two Classes of Tripartite Entanglement 92
4.3.3 Bipartite Entanglement Witness . . . 93
4.3.4 Is Entanglement Witness Experimentally Feasible? . . . 93

4.4 Ideal Photon Amplifiers 94
4.5 Human Eye Detection of Bipartite and Tripartite Entanglement in Psychophysical Experiments 97
4.5.1 Initial State and Amplification 97
4.5.2 Polarization Analyzers 100
4.5.3 Entanglement Witness Derivation 101
4.5.4 Detection by Human Eye or Photodetector 102
4.5.5 Probability of Seeing 104
4.5.6 Noise Addition 107
4.5.7 Results 107
4.5.8 Amplification via Amplitude Squeezing 110
4.6 Conclusion 115
4.6.1 The Different Scenarios 115
4.6.2 The Three Critical Factors 116
4.6.3 Alternative Approach 116
4.6.4 Orbital Angular Momentum States? 117
4.6.5 The Way Forward 118

Chapter 5: General Conclusion **119**
5.1 Summary 119
5.2 The Journey 120
5.3 Reflection on Physics 120
5.4 The Journey Continues... 120
5.5 Connection to The Brain 121

Chapter 6: Future Perspectives **122**
6.1 The Intertwining Relationship Between Biology and Quantum Physics 122
6.2 The Brain 123
6.2.1 Mind or Brain? 124

6.2.2 Brain Plasticity . . . 125
6.2.3 Effects of Electric Signals On The Brain and In The Brain . . 126
6.2.4 Stress . . . 126
6.2.5 Solutions to Stress and Brain Disorders . . . 128
6.2.6 Can Quantum Physics Address Pathological Issues? . . . 129
6.2.7 Does Quantum Physics Have All The Answers? . . . 130
6.2.8 Outlook . . . 131

Chapter 7: Dissemination Of Research **134**

7.1 Publications . . . 134
7.2 Conferences . . . 135
7.3 Events . . . 135

Bibliography **138**

LIST OF TABLES

2.1 The dimensionless time for which the relative entropy $S(\cdot\|\cdot)$, trace distance $T(\cdot\|\cdot)$, relative entropy of coherence $C_{RE}(\cdot)$ or L_1 norm of coherence $C_{L_1}(\cdot)$ become always inferior to 10^{-4} at the center of spin cluster for the parameters $\omega = 1$, $g = 0.002$, $\gamma = 0.0005$, and $T = 0.4$. The left and right columns compare the same quantity for the left and right geometries depicted in Figure 2.2, which correspond to vanishing and maximal connectivities in the buffer network, respectively. The initial state of the buffer spins is a maximally coherent superposition state. 29

2.2 The mean value of the relative entropy $S(\cdot\|\cdot)$, trace distance $T(\cdot\|\cdot)$, relative entropy of coherence $C_{RE}(\cdot)$ or L_1 norm of coherence $C_{L_1}(\cdot)$ of the central spin from time $t_1 = 29000$ to time $t_2 = 30000$ for the parameters $\omega = 1$, $g = 0.002$, $\gamma = 0.0005$, and $T = 0.4$. The left and right columns compare the same quantity for the left and right geometries depicted in Figure 2.2, which correspond to vanishing and maximal connectivities in the buffer network respectively. 30

2.3 The dimensionless time for which the relative entropy $S(\cdot\|\cdot)$, trace distance $T(\cdot\|\cdot)$, relative entropy of coherence $C_{RE}(\cdot)$ or L_1 norm of coherence $C_{L_1}(\cdot)$ become always inferior to 10^{-4} at the center of spin cluster for the parameters $\omega = 1$, $g = 0.002$, $\gamma_{\mathrm{d}} = 0.00059$, and $T = 0.4$. The left and right columns compare the same quantity for the left and right geometries depicted in Figure 2.2, which correspond to vanishing and maximal connectivity in the buffer network, respectively. The initial state of the buffer spins is a maximally coherent superposition state. The results are for the pure dephasing channel. . 36

2.4 The mean value of the relative entropy $S(\cdot\|\cdot)$, trace distance $T(\cdot\|\cdot)$, relative entropy of coherence $C_{RE}(\cdot)$ or L_1 norm of coherence $C_{L_1}(\cdot)$ of the central spin from time $t_1 = 29000$ to time $t_2 = 30000$ for the parameters $\omega = 1$, $g = 0.002$, $\gamma_{\mathrm{d}} = 0.00059$, and $T = 0.4$. The left and right columns compare the same quantity for the left and right geometries depicted in Figure 2.2, which correspond to vanishing and maximal connectivities in the buffer network, respectively. The results are for the pure dephasing channel. 36

2.5 Time, t_1, at which the logarithmic negativity between the two central spins becomes always inferior to 10^{-4} for various number of spins in the cluster. 40

LIST OF FIGURES

2.1 A central spin surrounded by four buffer spins, each one in its own thermal environment at temperature T. To illustrate how the central spin has negligible interaction with the environment, while the buffer spins can have frequent interactions, the thermal environment is depicted as a molecular bath. This system can be effectively viewed as a composite open quantum system, where the central spin is isolated from the environment, and the buffer spins each has their own local thermal dissipation channel. 25

2.2 Depiction of extreme geometries for central spin - buffer spins network for $N = 2, 3, 4, 5, 6$ buffer spins. The central spin, depicted in orange (light) color, is isolated from the environment, yet it is coupled to the blue (dark) colored buffer spins, which have local thermal dissipation pathways. For a particular number of buffer spins, N, we consider all the feasible buffer networks that can be embedded in a plane. Two extreme cases are depicted here: (left column) no connectivity and (right column) maximum connectivity within the buffer spin network. 26

2.3 The behavior of L_1 norm of coherence $C_{L_1}(\cdot)$ for four buffer spin networks with respect to dimensionless time t for the parameters $\omega = 1$, $g = 0.002$, $\gamma = 0.0005$, and $T = 0.4$. We use logarithmic scales for both vertical and horizontal axis. Two geometries are compared here. The first one is the tetrahedral buffer network which seems the best candidate to preserve coherence according to the results in Tables 2.1 and 2.2. The second one is a square buffer network, which is another planar graph with one less edge than the first. The solid (red) and the dash-dotted (green) curves illustrate the quantum coherence found in the central (A) and buffer (B) spins in the tetrahedral geometry. The dashed (dark blue) and pointed (black) curves represent the quantum coherence localized in the central (C) and buffer (D) spins in the square geometry. 31
2.4 The behavior of L_1 norm of coherence $C_{L_1}(\cdot)$ for a single spin connected to a thermal bath with respect to dimensionless time t. The initial state of the single spin is a maximally coherent superposition state. The time for which the L_1 norm of coherence becomes inferior to 10^{-4} is given by the vertically dotted gray line. The parameters are taken as $\omega = 1$ and $T = 0.4$. 32
2.5 Heat current as defined in Eq. (2.23) with respect to dimensionless time t. The solid red curve corresponds to the case in which there is no coupling between the buffer spins. The dotted blue curve illustrates the case with coupling between buffer spins. (a) Two buffer spin network. (b) Three buffer spin network. (c) Four buffer spin network. (d) Five buffer spin network. 33

2.6 The L1 norm difference between the three spin network and the four spin network with maximum connectivity (shown in Figure 2.2). (a) Mean value of the L1 norm from time $t_1 = 29000$ to time $t_2 = 30000$ with respect to coupling constant, g, and dissipative constant, γ. The graph corresponds to the tetrahedral geometry (4 spin network with maximal connectivity). (b) Difference of the L1 norm mean values from time $t_1 = 29000$ to time $t_2 = 30000$ with respect to coupling constant, g, and dissipative constant, γ. 37
2.7 Logarithmic negativity, E_N, of the reduced state composed on the two entangled spins with respect to dimensionless time, t. (a) Two buffer spin network. (b) Three buffer spin network. (c) Four buffer spin network. (d) Five buffer spin network. 39
2.8 Three-dimensional (left) and two-dimensional (right) arrangement of phosphorus atoms in a Posner molecule, $Ca_9(PO_4)_6$, with S_6 geometry: coupling constants, J_{jk}, in Eq. (2.27) are +0.178 Hz for the red pairs (1,2), (2,3), (3,1), (4,5), (5,6), (4,6); +0.145 Hz for the green pairs (1,4), (1,5), (2,4), (2,6), (3,5), 3,6); and −0.003 Hz for the yellow pairs (1,6), (2,5), (3,4). 41
2.9 The concurrence between different pairs of spins over time, starting from initial states with entanglement between spins 1 and 2. The graphs on the left illustrate the presence of entanglement between spins 1 and 2 and between spins 5 and 6, indicated by a non-zero concurrence. All other spin pairs do not show any entanglement generation, as their concurrence remains zero (graphs on the right). . . . 42

2.10 The concurrence between different pairs of spins over time, starting from initial states with entanglement between spins 1 and 4. The graphs on the right illustrate the presence of entanglement between spins 1 and 4 and between spins 3 and 6, indicated by a non-zero concurrence. All other spin pairs do not show any entanglement generation, as their concurrence remains zero (graphs on the left). 43

2.11 The concurrence between different pairs of spins over time, starting from initial states with entanglement between spins 1 and 6. The graphs on the right illustrate the presence of entanglement between spins 1 and 6, between spins 2 and 5, and between spins 3 and 4, indicated by a non-zero concurrence. All other spin pairs do not show any entanglement generation, as their concurrence remains zero (graphs on the left). 44

2.12 (a) Overlap between the 64 eigenstates and the initial states with entanglement between spins 1 and 2, and between spins 5 and 6. (b) Overlap between the 64 eigenstates and the initial states with entanglement between spins 1 and 3, and between spins 4 and 6. . . . 45

3.1 Configuration of the Nitrogen-Vacancy (NV) center in a diamond lattice. The black spheres represent the carbon atoms. The transparent sphere marked with a V represents the vacancy. The blue sphere represents the nitrogen impurity. The free electrons are depicted in yellow, with two electrons from the nitrogen atom and three from the carbon atoms adjacent to the vacancy. The red arrow represents an additional electron from the environment being added to form the negatively charged NV center. 53

3.2 An illustration of the spin dynamics in the Nitrogen-Vacancy (NV) center. When the NV center absorbs green light via a laser, it conserves the spin and transits from the ground-state triplet (^3A) to the excited-state triplet (^3E). The NV center emits red light when going back to the ground state. When the NV center first transits through the intermediate singlets (^1A and ^1E), spin polarization occurs between $m_s = \pm1$ and $m_s = 0$. The blue circle shows the Zeeman effect arising from the action of the static magnetic field, B_0, in the direction of the defect axis. γ_{NV} is the gyromagnetic ratio of the NV center. A qubit is generated by reducing the system to two-level, $m_s = 0$ and $m_s =$ -1, and forbidding the state $m_s = +1$. 55
3.3 The application of Ramsey-type sequence on two Nitrogen-Vacancy (NV) Centers with and without the introduction of spin squeezing. T_{fr} is the free evolution time. T_{sq} is the duration of the application of spin squeezing. 62
3.4 Illustration of the mean spin orientation and the variance of state preparation before the free evolution of the NV centers. At time t_1, the state is in its initial configuration (3.13) with homogeneous variance. At time t_2, the state reaches the end of the spin squeezing period, remaining aligned in the z-direction but with noise squeezed into an ellipse. Finally, at time t_3, a $\pi/2$ pulse is applied, shifting the state into the x-y plane. 68

3.5 The Quantum Fisher Information (QFI) as a function of time, t, with B = 50 G for the spin-1 formalism. The curves represents the free evolution as follows: the solid blue curve corresponds to a single NV center, the dashed-dotted red curve corresponds to two NV centers, the pointed cyan curve represents two NV centers subjected to spin squeezing ($c_1 = 2.5$ GHz, $T_{\text{sq}} = 3$ ns), and the dashed green curve represents two NV centers subjected to spin squeezing ($c_1 = 0.25$ GHz, $T_{\text{sq}} = 30$ ns). The different scenarios are illustrated as: (a) without including any noise terms, (b) including thermalization and dephasing with $\gamma_t = 0.2$ MHz and $\gamma_d = 0.1\gamma_t$, and (c) including thermalization and dephasing with $\gamma_t = 0.2$ MHz and $\gamma_d = \gamma_t$. 69
3.6 The squeezing parameter, ξ^2, for the spin-1 formalism, as a function of time, t, during the free evolution of two NV centers subjected to spin squeezing with $c_1 = 2.5$ GHz for a time of $T_{\text{sq}} = 3$ ns, including thermalization and dephasing with $\gamma_t = 0.2$ MHz, $\gamma_d = 0.1\gamma_t$, and $B = 50$ G. 71
3.7 The Quantum Fisher Information (QFI) as a function of time, t, with B = 50 G for the spin-1/2 formalism. The curves represents the free evolution as follows: the solid blue curve corresponds to a single NV center, the dashed-dotted red curve corresponds to two NV centers, the pointed cyan curve represents two NV centers subjected to spin squeezing ($c_1 = 2.5$ GHz, $T_{\text{sq}} = 3$ ns), and the dashed green curve represents two NV centers subjected to spin squeezing ($c_1 = 0.25$ GHz, $T_{\text{sq}} = 30$ ns). The different scenarios are illustrated as: (a) without including any noise terms, (b) including thermalization and dephasing with $\gamma_t = 0.2$ MHz and $\gamma_d = 0.1\gamma_t$, and (c) including thermalization and dephasing with $\gamma_t = 0.2$ MHz and $\gamma_d = \gamma_t$. 72

3.8 The logarithmic negativity, E_N, for the spin-1 formalism, as a function of time, t, during the free evolution of two NV centers subjected to spin squeezing with $c_1 = 2.5$ GHz for a time of $T_{\text{sq}} = 3$ ns, including thermalization and dephasing with $\gamma_t = 0.2$ MHz, $\gamma_d = 0.1\gamma_t$, and $B = 50$ G. Entanglement appears when $E_N > 0$ at the start of free evolution which is right after the application of spin squeezing. Afterward, entanglement decreases due to noise. 73
3.9 Schematic representation of the experimental setup: the blue cloud represents the biological system at temperature T, the gray box signifies the hydrogel with a thickness of d_t, the orange box denotes the static magnetic source B, and the green disc represents the NV center. (a) Configuration for a single NV center. (b) Configuration for two entangled NV centers, with entanglement symbolized by the yellow star. 75

4.1 A schematic representation of the setup for human eye detection of bipartite and tripartite entanglement in psychophysical experiments. The red boxes (labeled by A) are schematic representation of the interferometric entanglement generation setups. Upper (a) and lower (b) panels are respectively for the bipartite and tripartite cases. The blue boxes (labeled by B) represent the polarization analyzers complexes, which includes a Quarter Wave Plate (QWP), a Half Wave Plate (HWP) and a Polarized Beam Splitter (PBS). The pink boxes (labeled by C) represent the coherent amplification processes. The green boxes (labeled by D) represent the detection part of the horizontal polarization by the human eye. A horizontal black line appears at one of the outputs of the PBS to illustrate the beam being blocked. The numbers 1,2 and 3 correspond to the branches in the interferometric setup. 99

4.2 Simplified representation of the detection method. The light source is represented by a yellow star. The light coming into the human eye is represented by the solid yellow line. Then, the human subject answers by yes or no according to whether he/she sees or does not see the light. After N simulations of the experiment, we calculate the probabilities needed in the different witnesses (4.32) and (4.33). From these probabilities, we can calculate the expectation value of the entanglement witness and conclude if the human subject can differentiate between entangled and non-entangled light or multipartite and biseparable light. 103
4.3 Probability of seeing, P_{see} (4.44), as a function of the coherence parameter α of the coherent amplification. The solid black line represents P_{see} for the state $|1'\rangle$ and the dashed red line represents P_{see} for the state $|0'\rangle$. The dotted blue line represents P_{see} for the state $|1'\rangle$ with additive noise $D = 2$ and the dashed dotted green line represents P_{see} for the state $|0'\rangle$ with additive noise $D = 2$. The threshold K is taken as 7 and $\eta = 0.08$. The dashed vertical gray line is given for $\alpha = 2.5$. 105
4.4 Results for the expectation values $\langle W \rangle$ of the Bell state witness (4.32) with respect to the number of runs N and for different values of the human vision threshold K. The black circles, the blue star, the red triangle, and the green square represent $K = 1$, $K = 3$, $K = 5$, $K = 7$ respectively. The markers on the graph are represented every hundred steps. For each threshold, the horizontal solid lines represent the last value of the witness expectation values. The probability of seeing is evaluated for $\eta = 0.08$. In these graphs, a human eye and an ideal photodetector have been used. $\langle W \rangle$ is plotted for the additive noise (a) $D = 0$, (b) $D = 2$, and (c) $D = 5$. 108

4.5 Results for the expectation values $\langle W \rangle$ of the W state witness (4.33) with respect to the number of runs N and for different values of the human vision threshold K. The black circles, the blue star, the red triangle, and the green square represent $K = 1$, $K = 3$, $K = 5$, $K = 7$ respectively. The markers on the graph are represented every hundred steps. For each threshold, the horizontal solid lines represent the last value of the witness expectation values. The probability of seeing is evaluated for $\eta = 0.08$. In these graphs, a human eye and two ideal photodetectors have been used. $\langle W \rangle$ is plotted for the additive noise (a) $D = 0$, (b) $D = 2$, and (c) $D = 5$. 109

4.6 Statistics of different amplification methods. The solid green curve represents the mean photon number, while the dashed red curve and the dashed-dotted blue curve depict the variance and standard deviation of the photon number respectively. (a) and (b) correspond to the application of the displacement operator plotted against the displacement parameter, r, for $n = 0$ and $n = 1$, respectively. (c) and (d) correspond to the application of the squeezing operator plotted against the squeezing parameter, z, for $n = 0$ and $n = 1$ respectively. (e) and (f) illustrate amplitude squeezing for different values of r, which represents the modulus of the displacement (coherence) parameter, for $n = 0$ and $n = 1$ respectively. The phase of the squeezing parameter is set to $s = 0.2$ with $\theta = \phi - \frac{\pi}{2}$, and the phase of the displacement parameter is $\phi = \pi$. 112

4.7 Probability distribution, P_n, according to the photon number n. The red dotted curve corresponds to the case of applying a displacement operator to $|0'\rangle$. The solid red curve corresponds to the case of applying a displacement operator to $|1'\rangle$. The black dotted curve corresponds to the case of applying amplitude squeezing to $|0'\rangle$ and the solid red curve corresponds to the case of applying amplitude squeezing to $|1'\rangle$. The modulus of the displacement (coherence) parameter is taken as $r = \sqrt{50}$. The modulus and the phase of the squeezing parameter are $s = 0.5$ and $\theta = 0$ respectively. The phase of the displacement parameter is taken as $\phi = 0$. 114

ABBREVIATIONS

GHZ	Greenberger-Horne-Zeilinger
HWP	Half Wave Plate
NV	Nitrogen-Vacancy
OAM	Orbital Angular Momentum
PBS	Polarized Beam Splitter
QFI	Quantum Fisher Information
QWP	Quarter Wave Plate
SLD	Symmetric Logarithmic Derivative

Chapter 1

GENERAL INTRODUCTION

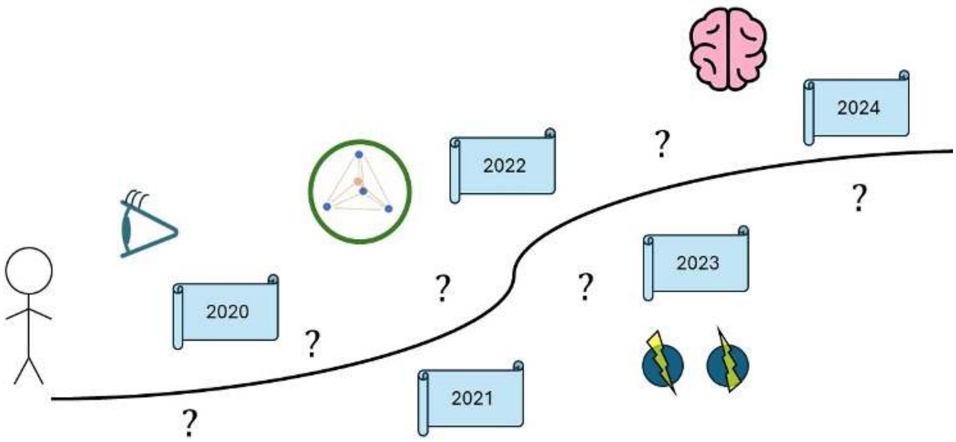

This thesis summarizes the various research that I embarked upon during my four-year journey as a PhD student. Due to the vastness of the three main topics (two of them having been published, and another submitted already - see Chapter 7), I have chosen to introduce each of them separately at the beginning of each chapter. For a more stimulating experience, some photographs that I have taken in Türkiye during my stay here and that I deemed relevant for each topic have also been included in order to illustrate the chapters. Similarly, in other places, I have inserted a simplified figure which illustrates that particular section or chapter.

1.1 The Quantum Vision Project

When I started my PhD, I was first enrolled in a project linked to Quantum Vision. Quantum and vision can be related in several ways; the project focused on the quantum effects in the biological phenomenon of vision. My interest has been in the interaction of quantum light, especially entangled light, and vision. I wanted to understand whether human beings could be good detectors of the quantum properties of light. To do this, I simulated a psychophysical experiment, involving some entanglement witnesses, which are mathematical tools to tell us if there is a presence of entanglement or not. The simulation was also based on the probability of seeing. This work helped us to understand the limitations of human vision, and for the sake of curiosity, to answer whether human beings could detect multipartite entanglement.

1.2 Quantum Effects in The Brain

In parallel to this work, I have been interested in "quantum brain" models. Starting with a presentation about the Posner model of cognition in the Journal Club of our group, the Quantum Enabling System Technologies (QuEST) Group, I subsequently worked on how quantum properties are preserved in different geometries. It consisted of manipulating several spins or qubits and arranging them in different geometric clusters around a central spin that has quantum information to preserve, such as quantum coherence or entanglement. This entertaining project allowed me to play easily with the model, and we discovered that the tetrahedral geometry was the best candidate. Despite simplification beyond its biological inspiration, this toy model's results surprisingly led us back to biology. Indeed this tetrahedral geometry is found a lot in nature, and also in the phosphate molecule used by Matthew Fisher in his model of cognition. That is why after publishing this work, we focused back on this model of cognition, this time playing with the geometry of a more realistic model, closer to biology, and this is the Posner cluster.

1.3 Quantum Sensing

A third topic caught my attention a bit later and also because it was linked to a project I was involved in. It is about the Nitrogen-Vacancy Center. This promising defect in diamond allows scientists to try conceiving a quantum computer based on it, but more applications are possible and one of them was what I got interested in. It is a very good candidate for biological sensing. I explored, using quantum correlations generated by spin squeezing, how we could improve this sensor, and also how we could make it a universal sensor using hydrogel and subsequently being able to detect any biological property such as pH, temperature, etc. This is an important and relevant topic notably for the health sector where sensors need to be more and more precise.

1.4 The Quantum Link to Biology

These three works that I encountered in my PhD allowed me to learn several topics all linked to biology, quantum information, measurement, and optimization. Whether it was the optimization of geometry to keep quantum information as long as possible to be able to use it in metrology, whether it was the improvement of quantum sensing using quantum information to be able to capture the biological property needed, or whether it was the design of a psychophysical experiment to see if a human can measure the quantum information by their biological system, which is their eyes, there was always a link between quantum physics and biology.

In some parts of the thesis, simple examples, and sometimes a little more complex ones have been cited especially related to the human body. This is done on purpose to relate to one of the main aims of the field of biology, that is, the understanding of the functionalities within the human being. At the same time, I hope this thesis will help to bridge the gap between various branches of science, starting with physics and biology. In my opinion, science has been progressing mainly through the cross-collaboration between all the fields of science that generate interdisciplinary research. To illustrate this point, we can look no further than the cell as an example.

What is considered as the basic unit of life, that is, the cell, is at the same time a biological entity, a complex composition of chemical substances and it is made of quarks, electrons and other particles at the very fundamental level. If we wish to take measurements with regards to the cell, at some point we definitely need to take into consideration the biology, chemistry and physics happening within and around the cell to retrieve the most accurate information.

1.5 Outline

Despite the variety of contents pertaining to the title of this thesis, I have come to realize that in four years, I have only scratched the surface of the door of this vast field. My work is only a very minute footstep toward achieving significant quantum metrology for biological systems. Hence, I encourage future research students and scholars to undertake the task of further expanding this field.

I have structured my thesis as follows: In Chapter 2, I introduce the preservation of quantum information in biological systems. Chapter 3 covers quantum sensing with Nitrogen-Vacancy Centers. Following this, Chapter 4 inspects the use of quantum light as a biological probe. In Chapter 5, I conclude with a general and personal reflection on this journey. In Chapter 6 I share some future perspectives of the relationship between quantum physics and biology. Lastly, in Chapter 7, I detail the dissemination of my research through various publications, conferences, and events.

Chapter 2

QUANTUM INFORMATION PRESERVATION IN BIOLOGICAL SYSTEMS

2.1 Introduction

Information is a concept that may have started with the creation of the universe or, existed even before that given that energy cannot be created or destroyed and therefore was always present. How come, one may ask. This is a discussion beyond the scope of this thesis. Here, we will focus on some mathematical aspects only.

Information can be understood as a quantity representing choice and therefore can be related to statistical probability. This definition is based on Shannon's work [Shannon, 1948] who can somehow be considered as the founder of artificial intelligence for having built one of the first machine learning devices. In his regard, information is more or less the synonym of entropy. More precisely, Shannon defined entropy as a measure of the content of information. In so doing, he set the basis for the field that is of major interest to us here, that is, information theory.

Information theory [Gray, 2011, Ash, 2012] deals with the exchange of information and therefore lays the ground for communication. Two other pioneers that are often acknowledged for this field are Harry Nyquist and Ralph Hartley. Is information really useful if it is not communicated or transmitted? For centuries, studies have been carried out to improve the transmission of information [Hartley, 1928, Fano, 1949, Anderson and Johnnesson, 2006]. Mostly, in the digital world, 0 and 1 have been the main representation of information. However, can data, that is, the binary digits 0 and 1 express sadness, happiness, anger, beauty or other aspects of feelings and art? This remains debatable to day. A voice message that is originally an analog signal can easily be converted into digital form, but what about the expression of that voice? And then there is the ever presence of noise. In almost all forms of communication, there can be disturbance. This will be further discussed later on.

Despite the advent of quantum mechanics [Born M, 1925] being around the same time as that of information theory, only around thirty years later were proposals independently formulated by Gordon [Gordon, 1962, Gordon, 1964], Stratonovich [Stratonovich, 1966] and Helstrom [Helstrom, 1967] to relate the two fields [Hayashi, 2006]. The resulting merged field eventually became known as quantum information theory [Hayashi, 2016].

Today, quantum information theory can be viewed as an intersection of quantum mechanics and information science, unfolding the intricate behavior and capabilities of quantum systems. At its core, quantum information may refer to the state of a quantum system, describing phenomena that defy classical understanding. One of them is quantum coherence. While classical information would be constrained to being 0 or 1, quantum information can take both values at the same time due to the effect of superposition which arises when a particle occupies more than one state at a time. There is also the property of entanglement whereby two particles or more are connected to each other beyond space and time and a change to one of them affects the others.

In nature, there are some phenomena that cannot be explained accurately enough with classical physics. For instance, photosynthesis is a biological process in which the transfer of energy through pigment molecules is probably so efficient due to the effect of quantum coherence [Ishizaki and Fleming, 2012]. Similarly, it is plausible that quantum entanglement could be influencing protein folding and enzymatic reactions [Baiesi et al., 2017]. Investigating quantum coherence and entanglement hold tremendous potential for enhancing our fundamental understanding of the underlying physics of living systems [Chin et al., 2012].

Now, in order to find evidence of these phenomena, we need to take a step back to one of the most important usage of information, that is measurement. Without refined measuring devices, we cannot get to the nitty-gritty of these processes. That is where metrology, the science of measurement comes in. As quantum information is the quantum analogy of classical information, likewise, the field of quantum metrology has also become an active domain [Hotter et al., 2024, Chen and Jing, 2024], and it is of particular interest here.

Since quantum coherence and entanglement can enhance the precision of measurements, this has enabled advancements in atomic clocks [Vanier, 2005], interferometers [Rarity et al., 1990], and, quantum-enhanced sensors [Szigeti et al., 2021]. These technologies promise unprecedented accuracy in measuring time, gravitational fields, magnetic flux, and other physical quantities, pushing the boundaries of what is measurable [Ye and Zoller, 2024].

Indeed, quantum coherence plays a vital role in a wide range of quantum technologies, including quantum computing [Unruh, 1995, Duan and Guo, 1997], quantum sensing [Degen et al., 2017a], quantum metrology [Shlyakhov et al., 2018b], and quantum cryptography [Gisin et al., 2002]. However, the presence of environmental noise and the detrimental effects of decoherence pose substantial challenges [Schlosshauer, 2019, Brandt, 1999].

Noise can arise from various sources, such as thermal fluctuations, electromagnetic radiation, and interactions with neighboring particles. To address this challenge, several strategies have been proposed. These encompass intentionally introducing supplementary noise during the coupling process [Yang et al., 2022], using periodical kicks [Viola et al., 1999], implementing a non-Hermitian driving potential [Huang et al., 2021a], employing correlated channels for interaction [Sk and Panigrahi, 2022], leveraging topological edge states [Bahri et al., 2015, Nie et al., 2020, Yao et al., 2021], integrating auxiliary atoms [Faizi and Ahansaz, 2019], or even surfaces [Bluvstein et al., 2019] to safeguard coherence [Faizi and Ahansaz, 2019].

Furthermore, understanding and quantifying quantum coherence and entanglement require sophisticated mathematical tools. Measures like relative entropy, trace distance, L_1 norm, and various entanglement metrics such as negativity, concurrence, and entropy of formation, provide frameworks for assessing the extent and impact of these quantum properties. As quantum systems grow more complex, particularly in multipartite systems, these measures help navigate the increasing computational and interpretative challenges.

In the context of open quantum systems, which are quantum systems that interact with their environment, understanding the dynamics becomes essential. These systems are described using density matrices and quantum master equations, which account for dissipation and decoherence. The interplay between a system and its environment affects the system's evolution, with implications for quantum computing and information processing.

Finally, geometry plays a pivotal role in both molecular structures and engineering design. In molecular biology, the spatial arrangement of atoms influences chemical reactivity and stability. In engineering, precise geometric design ensures the structural integrity and performance of various systems, from buildings to nanotechnology. The interdisciplinary connections between molecular geometry and engineering highlight the importance of geometric considerations in both scientific and technological advancements.

The existing strategies for protecting coherence in artificial systems predominantly rely on external drives [Viola et al., 1999], the presence of spontaneously occurring coherence [Faizi and Ahansaz, 2019], localization on edge states or positioning near surfaces [Bluvstein et al., 2019], sophisticated interaction control methods [Sk and Panigrahi, 2022], or tailored noise control techniques [Yang et al., 2022].

In contrast, nature appears to have discovered a simpler solution by leveraging the arrangement and connectivity of molecular networks, as argued in light-harvesting complexes containing chromophores. Although the presence and beneficial effects of quantum coherence in such biological systems are still a subject of debate, we propose a theoretical exploration to identify ideal molecular geometries for coherence protection.

By doing so, we aim to guide the engineering of artificial molecules or materials that could store quantum coherence. Our approach holds the potential to shed light on the lifetime and possible existence of quantum coherence in physiological conditions in nature. Our studies may be further complemented by quantum chemistry calculations to assess the energetic stability of these artificial quantum networks and search for their natural analogs.

We have a specific focus on investigating the influence of geometrical degrees of freedom on the preservation of quantum coherence within the core of an atomic cluster, where the atoms are assumed to be two-level systems, modelled as spin-1/2 particles. In order to achieve this objective, we thoroughly examine spin-star networks to evaluate the efficacy of peripheral spins as protective barriers, shielding the central spin from its surrounding environment. The sub-network, comprised of these peripheral spins known as the buffer network, serves as an intermediary layer that adeptly absorbs and dissipates environmental noise, while simultaneously upholding the coherence of the central spin. The utilization of buffer networks holds significant potential for applications in quantum computation, quantum sensing, and the study of biological molecules [Thatcher and Campbell, 1993, Fisher, 2015].

Our findings carry practical implications for various applications that demand long-lived coherent spin states, including quantum memories [Gentile et al., 2017], quantum magnetometry [Barry et al., 2020], quantum control and computation [Vandersypen et al., 2001, Vandersypen and Chuang, 2005], as well as biomedical imaging [Gossuin et al., 2010].

This chapter sifts through the potential role of quantum information preservation in biological systems. Section 2.2 introduces the theoretical basis of quantum information by citing the plausible implications of coherence and entanglement in biological mechanisms such as photosynthesis, avian compass, microtubules and protein folding. Section 2.3 examines quantum information as a metrological tool, addressing methods such as Quantum Fisher Information, coherence measures, and entanglement measures to quantify and analyze quantum phenomena in biological settings. Section 2.4 presents the open quantum systems and Section 2.5 the geometry in nature and engineering. Building on these concepts, Section 2.6 focuses on a specific approach to maintain quantum coherence in open systems using geometric optimization. It elucidates the details of this model, including its behavior under different conditions and its ability to preserve entanglement. Finally, Section 2.7 applies these ideas to a more realistic biological model system, the Posner cluster, with the possibility of generating entanglement within it. The chapter concludes in Section 2.8 by summarizing the findings and outlining future research directions.

2.2 Quantum Information in Biology

Quantum mechanics, the fundamental theory governing the behavior of particles at the atomic and subatomic scale, has long fascinated scientists. While quantum phenomena are often associated with the exotic world of quantum computers and teleportation, recent research suggests that these effects may play a crucial role in biological processes [Lloyd, 2011]. In particular, coherence and entanglement, have captured the attention of biophysicists and biochemists. Let us discover how these quantum phenomena intersect with biology.

2.2.1 Quantum Information

Quantum information refers to the state of a quantum system [Nielsen and Chuang, 2010]. While this concept may seem abstract, it is fundamental to understanding the quantum nature of a state. Quantum coherence, a form of quantum information, describes a scenario where particles exist in a delicate balance of multiple states at once [Streltsov et al., 2017]. Another form of quantum information, entanglement, connects the quantum states of particles across vast distances. The measurement of one particle instantly influences the other, a nonlocality phenomenon famously known as "spooky action at a distance," which challenges classical intuition [Hardy, 1998].

2.2.2 Coherence

Coherence appears to help in different biological mechanisms.

Photosynthesis

Photosynthesis is the process by which plants and certain bacteria convert sunlight into chemical energy. It has been observed that plants achieve this with remarkable efficiency, approaching nearly 100%. Scientists have explored a quantum approach to explain this phenomenon, making photosynthesis a prominent subject in the emerging field of quantum biology [Ishizaki and Fleming, 2012, Zhu et al., 2024, Panitchayangkoon et al., 2010].

During photosynthesis, light energy is efficiently captured through a process called coherent energy transfer. Unlike short-lived electronic coherence, this method relies on long-lasting quantum coherence. Researchers speculate that exciton-vibrational coherence within photosynthetic systems contributes to this sustained effect. However, understanding how this coherence operates in a living organism remains challenging due to the noisy environment at room temperature. Recent explanations propose that long-lasting coherences are safeguarded by quantum phase synchronization, facilitated by exciton-vibrational coupling.

Resonant anti-symmetric collective modes play a crucial role in dissipating unwanted effects [Zhu et al., 2024].

Avian Compass

The quantum model of the avian compass explains how birds achieve remarkable precision in their migration journeys. According to this proposed mechanism, when blue or green light is absorbed, a radical pair of electrons forms within an oriented molecule (possibly a cryptochrome) in the bird's eye. These electrons undergo coherent quantum oscillations between entangled singlet and triplet states, influenced by the orientation of the host molecule relative to the Earth's magnetic field. A spin-dependent electron transition allows current flow only when the spins in the pair align in a specific symmetric state. The rate of current flow depends on the molecule's orientation with respect to the magnetic field.

This purely quantum mechanical process accounts for various observed behaviors in birds, including their inability to distinguish the North from the South. Ongoing experimental and theoretical research aim to identify the specific molecules or molecular complexes where this mechanism operates and develop detailed, testable models [Ritz, 2011, Kominis, 2020].

Microtubules

Some current research focuses on the coherent transfer in microtubules. These microtubules consist of "tubulin" subunit proteins, which exhibit a unique architecture of chromophores, including aromatic amino acids like tryptophan. Interestingly, the geometry and dipolar properties of these aromatics resemble those found in photosynthetic units. This suggests that tubulin may facilitate coherent energy transfer. When tubulin aggregates into geometric lattices within microtubules, it could play a crucial role in living organisms for essential processes such as biological signaling and communication and brain processes [Babcock et al., 2024, Craddock et al., 2014, Jibu et al., 1994].

2.2.3 Entanglement

Entanglement occurs when two or more particles become correlated in such a way that their quantum states are interdependent. While entanglement is typically associated with isolated quantum systems, recent studies hint at its relevance in biological contexts:

- Protein Folding: Proteins, the workforce of cellular function, fold into specific three-dimensional structures. Entanglement between distant amino acids could influence the folding process. Understanding how quantum entanglement affects protein stability and function remains an active area of research [Baiesi et al., 2017, Salicari et al., 2023].

- As previously discussed, entanglement may play a role in the bird navigation mechanism. Specifically, the entangled singlet and triplet states are relevant in the context of the radical pair mechanism.

- The brain is an intricate biological system with many mysteries yet to be unraveled. In the quest for understanding, quantum mechanics has been proposed as a tool. Notably, entanglement could play a role, as seen in Matthew Fisher's proposal. Here, two phosphorus atoms take on the role of entangled spins, akin to the behavior of qubits in quantum computing [Fisher, 2015].

The interplay between coherence and entanglement is intriguing. Coherence facilitates efficient energy transfer, while entanglement may underlie subtle biological processes. Organisms may exploit both phenomena to optimize their survival strategies. Other quantum effects, such as quantum tunneling, also play a role in biological systems, such as the sense of smell [Tirandaz et al., 2017] or enzymatic reactions [Truhlar, 2010]. Identifying quantum effects in living systems is challenging due to environmental noise and temperature fluctuations. However, ongoing research using techniques like ultrafast spectroscopy and quantum biology aims to unveil the mysteries of life.

2.3 Quantum Information as Metrological Tool

In metrology, quantum information is a powerful tool for precision measurement. Quantum metrology uses the intrinsic properties of quantum systems to enhance our ability to measure physical quantities with unprecedented accuracy.

Coherence, the persistence of phase relationships, lies at the heart of quantum metrology. When particles remain in phase, their collective behavior enhances measurement precision. Consider an atomic clock: the coherence of atomic transitions allows us to measure time with remarkable accuracy [Vanier, 2005, Shiddiq et al., 2016]. Quantum interference, a consequence of coherence, enables interferometers to measure length, rotation, and other parameters. In a Mach-Zehnder interferometer, for instance, coherent light splits into two paths, recombining to create interference patterns. Minute phase shifts reveal changes in the measured quantity. Applications range from navigation devices, magnetometry and thermometry to remote sensing and super-resolution imaging [Streltsov et al., 2017, Rarity et al., 1990].

Entanglement offers a unique advantage. When particles are entangled, their states become correlated, even across vast distances. This correlation allows for ultra-sensitive measurements. Entangled particles serve as very promising sensors. For instance, entangled photons can detect minuscule changes in gravitational fields or magnetic flux. Quantum-enhanced sensors promise breakthroughs in geophysics, navigation, and medical imaging [Watts et al., 2021, Pezzè, 2021, Cappellaro and Lukin, 2009].

2.3.1 Quantum Fisher Information

The Quantum Fisher Information (QFI) quantifies the optimal precision achievable in estimating a parameter through a suitable optimal measurement. It directly measures the optimal precision of the estimation process and is therefore considered the primary figure of merit in quantum metrology. A mathematical description is provided in Section 3.4.

When a probe state is prepared and measured multiple times ($n > 1$), the mean square error in estimating a parameter q is bounded by the quantum Cramér-Rao bound. Quantum coherence, particularly asymmetry, plays a crucial role in achieving precision beyond classical limits. Furthermore, entanglement enhances quantum metrology. When the probe state is entangled across multiple subsystems, correlations emerge, enabling measurements with precision surpassing classical strategies. The increase in QFI reflects this enhancement.

To achieve Heisenberg scaling, we start with a coherent probe state and apply unitary transformations before measurement. Given ρ is the probe state, and $\hat{H}$ the Hamiltonian, the QFI, $I(\rho, \hat{H})$, scales as $I(\rho, \hat{H}) \sim n^2$ with n being the number of measurements, indicating a quadratic improvement in precision compared to classical methods [Streltsov et al., 2017]. Indeed if we use probe states without any coherence or entanglement, the QFI can scale at most linearly with n, $I(\rho, \hat{H}) \sim n$.

In summary, quantum coherence and entanglement are the primary resources driving the superior performance of quantum metrology, allowing significant improvements in precision estimation.

2.3.2 Quantum Coherence Measures

We first introduce two general measures to compare quantum states based on their density matrices, which characterize the system:

- The first measure is the relative entropy [Cover et al., 1991], defined as

$$S(\rho\|\sigma) = \mathrm{Tr}[\rho \log_2 \rho] - \mathrm{Tr}[\rho \log_2 \sigma], \tag{2.1}$$

  for the Hermitian matrices ρ and σ.

- The second measure is the trace distance [Shao et al., 2015], which can be reduced to

$$T(\rho, \sigma) = \frac{1}{2}\mathrm{Tr}\left[\sqrt{(\rho - \sigma)^2}\right]. \tag{2.2}$$

L_1 norm of coherence

The L_1 norm of coherence quantifies the quantum coherence possessed in a state [Baumgratz et al., 2014]. It is equal to the sum of the magnitude of all the off-diagonal elements of a given density matrix,

$$C_{L_1}(\rho) = \sum_{i \neq j} |\rho_{ij}| \, . \tag{2.3}$$

C_{L_1} neglects the signs of distinct coherences in a basis and takes them into account independently of each other.

Relative entropy of coherence

Another measure that we utilize to determine the amount of coherence is the relative entropy of coherence [Baumgratz et al., 2014],

$$C_{RE}[\rho] = \min_{\varsigma \in \mathrm{IC}} \left(S\left(\rho \| \varsigma\right) \right) = S\left(\rho \| \rho_d\right), \tag{2.4}$$

where the minimum is taken over the set of incoherent states (IC) that are diagonal in the basis and ρ_d is the diagonal part of the density matrix ρ. C_{RE} measures the distinguishability of a density matrix with a modified copy which is subjected to a full dephasing process.

2.3.3 Entanglement Measures

Quantum entanglement, a phenomenon where the states of two or more particles become intertwined in such a way that their properties are inherently correlated, lies at the heart of quantum mechanics. While entanglement is a fundamental feature of quantum systems, quantifying it remains a challenging task, especially as we move beyond simple qubit (two-level) systems.

Researchers have proposed several measures to quantify entanglement. These measures aim to capture different aspects of entanglement, such as its strength, structure, and suitability for specific applications. Some well-known measures are listed below.

Logarithmic Negativity

The negativity, denoted as $N(\rho)$, quantifies entanglement in bipartite quantum systems ρ_{AB} [Benabdallah et al., 2021]. It is given by summing over the absolute of the negative eigenvalues, λ_i, of the partially transposed density matrix, ρ_A^T,

$$N(\rho_{AB}) = \sum_i |\lambda_i|. \tag{2.5}$$

The logarithmic negativity, denoted as E_N, is related to the negativity and serves as a good indicator of the degree of entanglement. It is defined as

$$E_N(\rho_{AB}) = \log_2(2N(\rho_{AB}) + 1). \tag{2.6}$$

Concurrence

Concurrence is another measure used in quantum information theory to quantify the entanglement present in a bipartite quantum state. It is particularly useful for two-qubit systems [Hill and Wootters, 1997]. The formula for concurrence is given by

$$C(\rho) = \max\{0, \lambda_1 - \lambda_2 - \lambda_3 - \lambda_4\}, \tag{2.7}$$

where $\lambda_1, \lambda_2, \lambda_3$, and λ_4 are the square roots of the eigenvalues of the non-Hermitian matrix $\rho\tilde{\rho}$ in descending order. Here, $\tilde{\rho} = (\sigma_y \otimes \sigma_y)\rho^*(\sigma_y \otimes \sigma_y)$, where σ_y is the Pauli matrix and ρ^* denotes the complex conjugate of ρ.

Generalized Concurrence

A generalized version of concurrence for multi-particle pure states in arbitrary dimensions exists and is defined as

$$C_M(\rho_{AB}) = \sqrt{2(1 - \mathrm{Tr}(\rho_A^2))}\ , \tag{2.8}$$

where ρ_A is the reduced density matrix obtained by tracing out subsystem B [Rungta et al., 2001].

Entanglement of Formation

The entanglement of formation (E_f) is a measure used in quantum information theory to quantify the entanglement present in a bipartite quantum state. It is particularly useful for understanding how entangled a given state is relative to a maximally entangled state. The entanglement of formation E_f for a bipartite quantum state ρ is defined as

$$E_f(\rho) = \min \left\{ \sum_i \mathrm{p_i} S(\rho_i) \right\}, \tag{2.9}$$

where the minimum is taken over all decompositions of $\rho = \sum_i \mathrm{p_i} \rho_i$, with ρ_i being pure states, $\mathrm{p_i}$ being probabilities, and $S(\rho_i)$ is the von Neumann entropy of the reduced density matrix, ρ_i [Wootters, 2001].

2.3.4 The Challenge of Quantifying Entanglement

Going beyond qubit systems and considering multipartite systems (involving more than two particles), quantifying entanglement becomes increasingly complex:

- Computational Complexity: Calculating entanglement measures for multipartite systems is computationally demanding. The number of possible entangled states grows exponentially with the system size.

- Entanglement Structure: Multipartite entanglement exhibits intricate structures, including genuine multipartite entanglement [Palazuelos and De Vicente, 2022]. Capturing these structures requires sophisticated tools.

- Physical Interpretation: Interpreting entanglement measures physically becomes less intuitive as the system size increases.

2.4 Open Quantum Systems

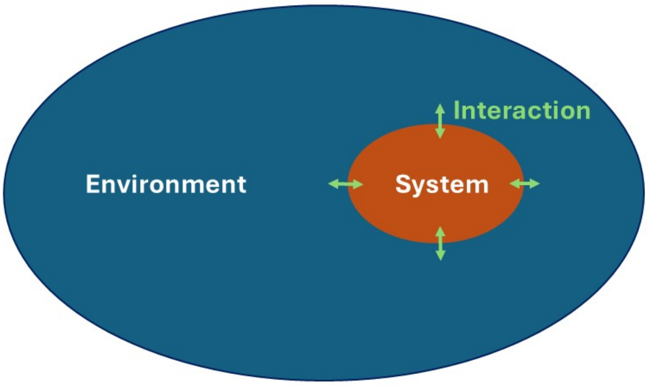

An open quantum system interacts with an external quantum environment, leading to dissipation and decoherence. The interaction with the environment occurs over a specific correlation time. Although the environment is in thermal equilibrium, it does not preserve minor changes induced by its interaction with the system for extended periods. There exists a competition between the correlation time and the time scale for significant changes in the system.

Open quantum mechanics plays a crucial role in physics because no system can be entirely isolated from its environment. The general approach involves deriving the dynamics of an open system from an underlying microscopic theory by eliminating the environmental degrees of freedom [Breuer et al., 2002]. Instead of using a wave function, we describe open quantum systems using the density matrix. The general Hamiltonian can be expressed as

$$\hat{H}(t) = \hat{H}_S \otimes I_E + I_S \otimes \hat{H}_E + \hat{H}_I(t) = \hat{H}_0 + \hat{H}_I(t), \tag{2.10}$$

where $\hat{H}_S$ is the system's Hamiltonian, $\hat{H}_E$ is the environment's Hamiltonian, $\hat{H}_I(t)$ represents the interaction Hamiltonian between the system and the environment, and $\hat{H}_0$ is the free part of the Hamiltonian. I_E and I_S are identity matrices for the environment's and system's Hilbert spaces respectively. Throughout the chapter, we take $\hbar = 1$.

Starting from the interaction picture given by the von Neumann equation,

$$\frac{d\rho}{dt} = -i\left[\hat{H}_I(t), \rho\right], \tag{2.11}$$

where ρ is the density matrix of the whole system, we then trace out the environment's degrees of freedom. The reduced density matrix of the system, $\rho_S(t)$, evolves according to

$$\frac{d\rho_S}{dt} = -i\mathrm{Tr}_{\mathrm{E}}\left(\left[\hat{H}_I(t), \rho\right]\right), \tag{2.12}$$

where Tr_{E} denotes the trace over the environment. Assuming weak interaction and applying the Born approximation, we consider the separability of the states throughout the evolution as

$$\rho(t) = \rho_S(t) \otimes \rho_E, \tag{2.13}$$

where ρ_E represents a reference state of the environment. Subsequently, we apply the Markov approximation, assuming the environment has a short memory, meaning its correlation functions decay rapidly compared to the system's evolution timescale. We also use the secular approximation, which neglects fast-rotating terms that average out to zero over time due to their high frequency relative to the system's evolution timescale.

After these approximations, and further calculations which are not listed here but available in the literature [Breuer et al., 2002, Manzano, 2020], the Lindblad master equation can then be written as

$$\frac{d}{dt}\rho_S(t) = -i\left[\hat{H}_S, \rho_S(t)\right] + D(\rho_S(t)), \tag{2.14}$$

where the dissipator $D(\rho_S)$ is given by

$$D(\rho_S) = \sum_{k,\omega} \gamma_k(\omega)\left(A_k(\omega)\rho_S A_k^\dagger(\omega) - \frac{1}{2}A_k^\dagger(\omega)A_k(\omega)\rho_S - \frac{1}{2}\rho_S A_k^\dagger(\omega)A_k(\omega)\right). \tag{2.15}$$

Here, A_k are the operators through which the environment couples to the system in $\hat{H}_I$ and are called the jump operators, γ_k are the corresponding rates, and ω are the relevant frequency in our system [Manzano, 2020].

This formulation is based on the global master equation approach, where the entire system is considered as a whole interacting with a common environment. Such an approach is necessary when the subsystems are strongly interacting, requiring the full system Hamiltonian to be considered to accurately describe the dissipative dynamics. In contrast, the local master equation simplifies this approach by assuming each subsystem interacts independently with its own local environment. This is valid when the subsystems are weakly interacting compared to their coupling with their respective environments.

Open quantum systems play a fundamental role in understanding dissipation, decoherence, and the behavior of quantum systems in realistic environments. It is important to note that only the main steps have been shown in this section to illustrate how the master equation used in Section 2.6 and Section 3.6 is derived.

2.5 Importance of Geometry

Geometry plays a crucial role in both molecular structures and engineering design, influencing the properties and functionality of materials at different scales [Testa, 1982].

2.5.1 Geometry in Engineering

In engineering, geometry is a fundamental aspect of design and construction. Whether in civil, mechanical, or aerospace engineering, the shape and arrangement of components profoundly impact the performance and durability of structures. Precision in geometric design is crucial for ensuring the structural integrity of buildings, bridges, and mechanical systems. Furthermore, geometric considerations are pivotal in the design of advanced technologies, such as microelectronics and nanotechnology, where minute details at the molecular level can significantly affect device performance [Xu et al., 2019a].

2.5.2 Geometry in Nanotechnology

The interdisciplinary connection between molecular and engineering geometry is particularly evident in the emerging field of nanotechnology. Engineers manipulate the geometric arrangement of atoms and molecules to create materials with tailored properties and functionalities, leading to innovations in multiple fields such as material science and medicine. Some examples are: crystal design [Hart et al., 2012], the effect of the shapes of particles in nanomedicine [Liu et al., 2012], DNA nanotechnologies [Seeman, 2007] and magnetic antidot [Wang et al., 2006].

2.5.3 Geometry in Nature

An intriguing question to ponder about nature is why things we did not shape ourselves, starting from the molecular level, are the way they are. Initially, considering energy packets and fundamental particles, they do not have definite shapes. However, as we observe larger structures, they become organized and take on geometric forms, such as molecules.

At the level of molecules, the spatial arrangement of atoms, known as molecular geometry, determines key characteristics such as chemical reactivity, bond angles, and overall stability. Understanding molecular geometry is essential in fields like chemistry and biochemistry, where it influences the behavior of compounds, reactions, and biological processes [Gillespie and Robinson, 2005].

Some geometries, like those in chiral molecules, are very similar; yet, two chiral molecules can have vastly different functions [Patočka et al., 2004]. One chiral molecule may be abundant in nature while the other is absent [Quack, 1989]. Chirality is a significant subject in physics and has recently become relevant in quantum mechanics through the Chiral-Induced Spin Selectivity effect, which describes how the chirality of molecules influences the spin of electrons passing through them [Aiello et al., 2022].

2.5.4 Is Geometry A Quantum Tool?

The intricate interplay between geometry, whether at the molecular or macroscopic level, underpins advancements in both scientific understanding and technological applications. In nature, why are some geometries preferred? Perhaps the answer lies in preserving quantum properties from the beginning to facilitate biological functions. There must be a reason why certain geometries are favored. In the following section, we will demonstrate how geometry influences the preservation of quantum information.

2.6 Preservation of Quantum Coherence through Geometrical Optimization

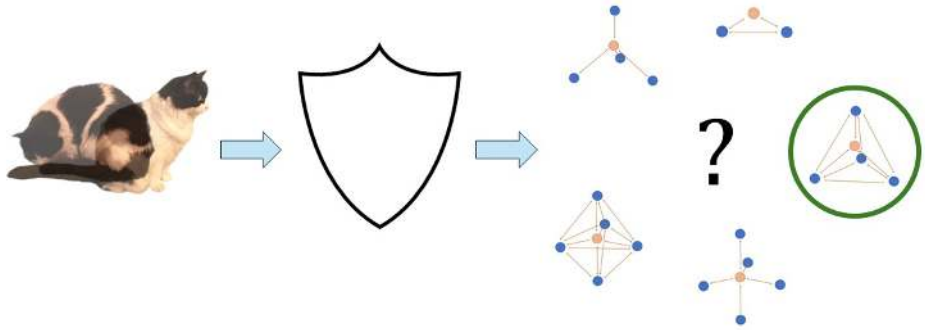

The work in this section is based on one of my published works [Gassab et al., 2024b].

2.6.1 Spin-Star Network with Different Topologies

Consider a cluster of $N+1$ spins that consists of a central spin surrounded by a buffer network, as illustrated in Figure 2.1. Each buffer spin is individually connected to a thermal bath, while the central spin does not engage in direct interactions with the environment. Our objective is to analyze the impact of buffer network size and topology on the coherence of the central spin. To achieve this, we focus on buffer networks that can be represented as planar graphs.

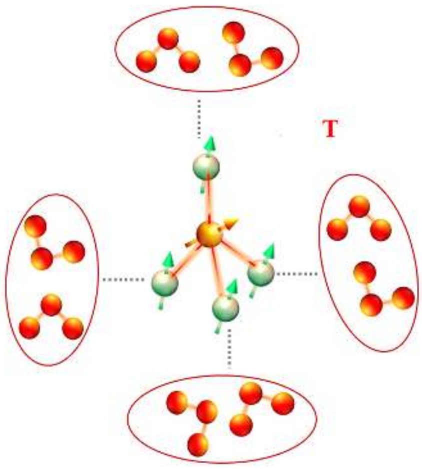

Figure 2.1: A central spin surrounded by four buffer spins, each one in its own thermal environment at temperature T. To illustrate how the central spin has negligible interaction with the environment, while the buffer spins can have frequent interactions, the thermal environment is depicted as a molecular bath. This system can be effectively viewed as a composite open quantum system, where the central spin is isolated from the environment, and the buffer spins each has their own local thermal dissipation channel.

We explore various scenarios by considering different numbers of buffer spins, ranging from the two extremes (see Figure 2.2):

- no coupling between buffer spins,
- pairwise interactions between all nearest neighbor buffer spins.

For the sake of simplicity, we assume that all spins are identical with a magnitude of 1/2. When subjected to a magnetic field aligned along the quantization axis z, an energy difference denoted by $\hbar\omega$ emerges between the lower state $|0\rangle$ (spin-up) and the upper state $|1\rangle$ (spin-down), enabling a two-level description.

The buffer spins are brought into thermal equilibrium with the surrounding environment at an inverse temperature β, while the central spin is initially prepared in a maximally coherent superposition state.

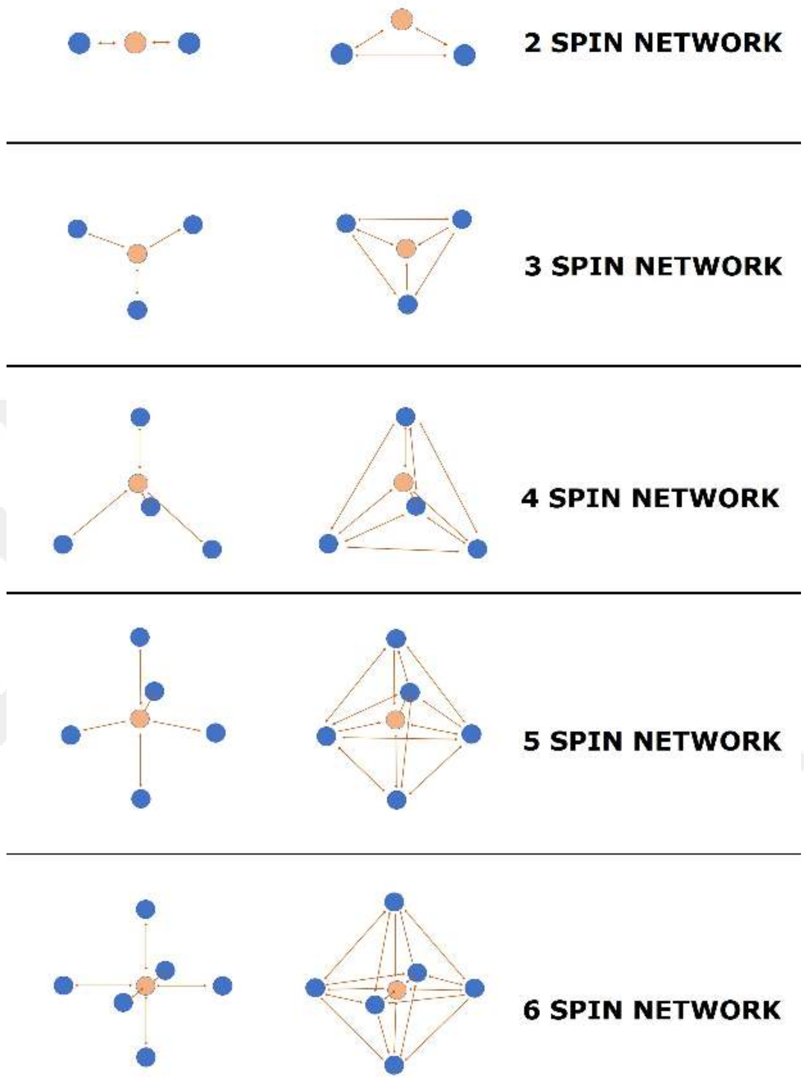

Figure 2.2: Depiction of extreme geometries for central spin - buffer spins network for $N = 2, 3, 4, 5, 6$ buffer spins. The central spin, depicted in orange (light) color, is isolated from the environment, yet it is coupled to the blue (dark) colored buffer spins, which have local thermal dissipation pathways. For a particular number of buffer spins, N, we consider all the feasible buffer networks that can be embedded in a plane. Two extreme cases are depicted here: (left column) no connectivity and (right column) maximum connectivity within the buffer spin network.

Then, the initial cluster state can be represented as a product state,

$$\rho(0) = \frac{|0\rangle + |1\rangle}{\sqrt{2}} \otimes \rho_{th}^{\otimes n}. \tag{2.16}$$

The thermal state of the buffer spins is defined as

$$\rho_{th} = \frac{\mathrm{e}^{-\beta \frac{\omega}{2} \hat{\sigma}_z}}{\mathcal{Z}}, \tag{2.17}$$

where $\hat{\sigma}_z = |0\rangle\langle 0| - |1\rangle\langle 1|$ represents the Pauli-z operator and $\mathcal{Z} = 2\cosh[\beta\,\omega/2]$ denotes the partition function. Here, we assume the Boltzmann constant, k_B, to be equal to 1. The total Hamiltonian of the spin cluster reads as an XX central spin model, which is a simplified case of general Richardson-Gaudin spin cluster models [Gaudin, 1976],

$$\hat{H} = \sum_{i=1}^{N+1} \frac{\omega}{2} \hat{\sigma}_z^{(i)} + \sum_{i \neq j} g_{ij} \left(\hat{\sigma}_x^{(i)} \hat{\sigma}_x^{(j)} + \hat{\sigma}_y^{(i)} \hat{\sigma}_y^{(j)} \right) . \tag{2.18}$$

The Pauli spin-1/2 operators for the i^{th} spin are denoted by $\hat{\sigma}_x^{(i)}$, $\hat{\sigma}_y^{(i)}$, and $\hat{\sigma}_z^{(i)}$, and the interaction strength between the spin pair (i, j) is represented by g_{ij}. The central spin, labeled by "1", is coupled to the buffer spins at strength $g_{1j} = g \neq 0$ in all geometries under consideration.

On the other hand, each buffer network is defined by a different array of coupling constants consisting of zero or g values, which can be represented by a planar graph. That is to say, the coupling constants between buffer spins can be drawn in the plane so that buffer spins and their non-zero coupling constants are represented by vertices and edges, respectively, and no two edges of the resulting graph intersect at a point other than a vertex. The maximum number of edges between the vertices corresponding to the buffer spins in such a graph is $3N - 6$, in the case of $N \geq 3$ buffer spins. This means that the array of coupling constants between buffer spins cannot include more than $3\,N - 6$ non-zero values. Hence, the number of possible geometries for a cluster of $N + 1$ spins becomes

$$M = \sum_{k=0}^{3\,N-6} \binom{E}{k} . \tag{2.19}$$

$E = N(N-1)/2$ is the number of edges for a complete graph. Figure 2.2 shows two extreme geometries, contributing to this sum, for $N = 2, 3, 4, 5, 6$ buffer spins representing the buffer network. k classifies the buffer network geometries with respect to the number of edges in them. The left geometry corresponds to the $k = 0$ term, whereas the right geometry corresponds to one of the $k = 3N - 6$ terms, which allows putting the central spin right in the middle of the bulk network.

2.6.2 Open Quantum System Dynamics

We describe the open quantum system dynamics of the spin-star network by the following Lindblad master equation [Breuer et al., 2002],

$$\dot{\rho}(t) = -i\left[\hat{H}, \rho(t)\right] + \mathcal{D}(\rho(t))\,, \tag{2.20}$$

where the unitary contribution to the dynamics is provided by the self-Hamiltonian of the system given in Eq. (2.18). By assuming weakly coupled buffer spins, local thermal dissipation channels are described by the dissipator in Eq. (2.20), which reads as

$$\begin{aligned} \mathcal{D}(\rho) = &\sum_{i=2}^{N+1} \gamma_i \left(1 + n(\omega)\right) \left[\hat{\sigma}_i^- \rho(t) \hat{\sigma}_i^+ - \frac{1}{2}\left\{\hat{\sigma}_i^+ \hat{\sigma}_i^-, \rho(t)\right\}\right] \\ &+ \sum_{i=2}^{N+1} \gamma_i\, n(\omega) \left[\hat{\sigma}_i^+ \rho(t) \hat{\sigma}_i^- - \frac{1}{2}\left\{\hat{\sigma}_i^- \hat{\sigma}_i^+, \rho(t)\right\}\right]\,, \end{aligned} \tag{2.21}$$

where $n(\omega)$ is the Planck distribution at the spin resonance frequency ω. $\hat{\sigma}^{\pm}$ are the Pauli spin ladder operators. $\gamma_i = \gamma$ is the coupling constant between the environment and the i^{th} buffer spin, taken to be homogeneous for each buffer spin independent of the network structure for simplicity.

To determine whether the dissipator (2.21) achieves local thermalization in our simulations, we compare the reduced spin states $\rho_i = \mathrm{Tr}_{j_1 \cdots j_n}[\rho]$, $j_k \neq i$ with the local thermal state ρ_{th} using two different measures. The first measure is the relative entropy (2.1), and the second measure is the trace distance (2.2).

Table 2.1: The dimensionless time for which the relative entropy $S(\cdot\|\cdot)$, trace distance $T(\cdot\|\cdot)$, relative entropy of coherence $C_{RE}(\cdot)$ or L_1 norm of coherence $C_{L_1}(\cdot)$ become always inferior to 10^{-4} at the center of spin cluster for the parameters $\omega = 1$, $g = 0.002$, $\gamma = 0.0005$, and $T = 0.4$. The left and right columns compare the same quantity for the left and right geometries depicted in Figure 2.2, which correspond to vanishing and maximal connectivities in the buffer network, respectively. The initial state of the buffer spins is a maximally coherent superposition state.

$N+1$	$S(\rho_1\|\rho_{th})$		$T(\rho_1,\rho_{th})$		$C_{RE}(\rho_1)$		$C_{L_1}(\rho_1)$	
3	20640	24210	20630	23710	38970	46680	41770	50150
4	17270	29870	16870	29730	32310	58320	34590	62020
5	14990	**32930**	14250	**32360**	27250	**64660**	29600	**66870**
6	13460	25440	12410	24800	24410	48070	25820	52010
7	12930	19410	11030	17780	23260	35320	23260	37450

For a given number of buffer spins N, we investigate the open system dynamics of M different spin clusters and search for the geometry that optimizes the protection of the central spin coherence. For this aim, we quantify the quantum coherence possessed in the reduced state of the central spin $\rho_1 = \mathrm{Tr}_{2\cdots n+1}[\rho]$ by the L_1 norm of coherence (2.3). Another measure that we utilize to determine the amount of coherence in the central spin is the relative entropy of coherence (2.4).

2.6.3 Results

The simulations are performed by using scientific Python packages along with key libraries from QuTiP [Johansson et al., 2012]. The spin transition frequency ω is taken as the time and energy scale (such that $\omega = 1$) and dimensionless scaled parameters are used. Particularly, inter-spin coupling strength g and bath dissipation rate γ are taken to be 0.002 and 0.0005 respectively. The temperature of the environment ($T = \beta^{-1}$) is taken as 0.4. The simulations are continued until the quantum coherence of the central spin vanishes. Specifically, we record the time after which the quantum coherence is always inferior to 10^{-4}. The buffer spins are in a thermal initial state at the same temperature as their local bath ($T = 0.4$).

Table 2.2: The mean value of the relative entropy $S(\cdot\|\cdot)$, trace distance $T(\cdot\|\cdot)$, relative entropy of coherence $C_{RE}(\cdot)$ or L_1 norm of coherence $C_{L_1}(\cdot)$ of the central spin from time $t_1 = 29000$ to time $t_2 = 30000$ for the parameters $\omega = 1$, $g = 0.002$, $\gamma = 0.0005$, and $T = 0.4$. The left and right columns compare the same quantity for the left and right geometries depicted in Figure 2.2, which correspond to vanishing and maximal connectivities in the buffer network respectively.

$N+1$	$S(\rho_1\|\rho_{th})$		$T(\rho_1,\rho_{th})$		$C_{RE}(\rho_1)$		$C_{L_1}(\rho_1)$	
3	1.13×10^{-6}	1.46×10^{-5}	1.12×10^{-6}	1.33×10^{-5}	4.60×10^{-4}	1.80×10^{-3}	9.17×10^{-4}	3.54×10^{-3}
4	9.60×10^{-8}	1.12×10^{-4}	9.35×10^{-8}	1.07×10^{-4}	1.36×10^{-4}	5.07×10^{-3}	2.68×10^{-4}	1.01×10^{-2}
5	8.26×10^{-9}	$\mathbf{2.54\times10^{-4}}$	6.73×10^{-9}	$\mathbf{2.14\times10^{-4}}$	3.89×10^{-5}	$\mathbf{7.38\times10^{-3}}$	7.25×10^{-5}	$\mathbf{1.42\times10^{-2}}$
6	1.83×10^{-9}	2.47×10^{-5}	5.04×10^{-10}	2.07×10^{-5}	1.54×10^{-5}	2.29×10^{-3}	1.94×10^{-5}	4.41×10^{-3}
7	1.35×10^{-9}	9.41×10^{-7}	5.32×10^{-11}	4.35×10^{-7}	1.17×10^{-5}	3.89×10^{-4}	6.32×10^{-6}	6.39×10^{-4}

Our simulations show that the dissipator (2.21) provides local thermalization for both central and buffer spins. For this aim, we compare the steady-state spin states $\rho_i(\infty)$ with the local thermal state ρ_{th} using the relative entropy and trace distance. Moreover, we identify the thermalization time at which the relative entropy between the reduced spin states and ρ_{th} diminishes.

The findings regarding the central spin are summarized in the first two columns of Table 2.1 for the geometries depicted in Figure 2.2. Table 2.1 also presents the times at which the relative entropy of coherence vanishes. Notably, the disappearance of $C_{RE}(\rho_1)$ consistently occurs later than $S(\rho_1\|\rho_{th})$, indicating that complete decoherence occurs after the populations have reached equilibrium values.

Our results demonstrate a correlation between the protection time of quantum coherence in the central spin and the connectivity of the buffer network, considering a specific number of buffer spins. We observe that the network with maximal planar graph embedding yields the longest protection time. To illustrate this, Table 2.1 presents a comparison of the protection time for different cluster sizes, depicted in Figure 2.2, with left and right geometries representing minimal and maximal connectivity in the buffer network, respectively.

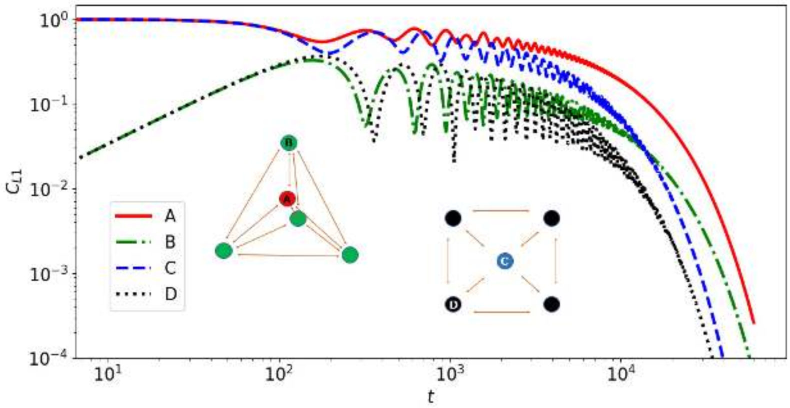

Figure 2.3: The behavior of L_1 norm of coherence $C_{L_1}(\cdot)$ for four buffer spin networks with respect to dimensionless time t for the parameters $\omega = 1$, $g = 0.002$, $\gamma = 0.0005$, and $T = 0.4$. We use logarithmic scales for both vertical and horizontal axis. Two geometries are compared here. The first one is the tetrahedral buffer network which seems the best candidate to preserve coherence according to the results in Tables 2.1 and 2.2. The second one is a square buffer network, which is another planar graph with one less edge than the first. The solid (red) and the dash-dotted (green) curves illustrate the quantum coherence found in the central (A) and buffer (B) spins in the tetrahedral geometry. The dashed (dark blue) and pointed (black) curves represent the quantum coherence localized in the central (C) and buffer (D) spins in the square geometry.

Additionally, Figure 2.3 depicts the time-dependent behavior of central spin quantum coherence in four buffer spin networks with tetrahedral and square geometries. Notably, the former exhibits a longer survival time for quantum coherence. Thus, our conclusion is that a higher number of buffer spin interactions results in a more effective protective shell around the central spin.

In the scenario of vanishing connectivity, we observe a continuous decrease in quantum coherence as the number of buffer spins increases. This is expected since each buffer spin introduces an additional local thermalization channel, thereby accelerating the thermalization process.

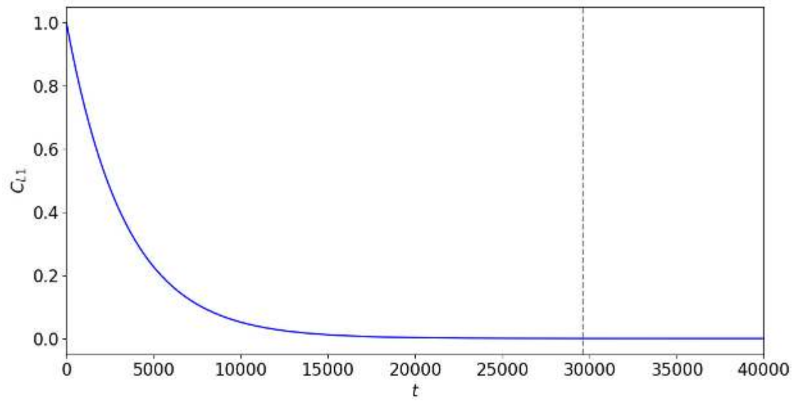

Figure 2.4: The behavior of L_1 norm of coherence $C_{L_1}(\cdot)$ for a single spin connected to a thermal bath with respect to dimensionless time t. The initial state of the single spin is a maximally coherent superposition state. The time for which the L_1 norm of coherence becomes inferior to 10^{-4} is given by the vertically dotted gray line. The parameters are taken as $\omega = 1$ and $T = 0.4$.

However, the behavior of protection time differs in the maximal connectivity scenario. It does not increase monotonically with the number of buffer spins in the cluster. The optimal protection against environmental decoherence, as indicated in the last column of Table 2.1, is achieved by a four buffer spin network with a tetrahedral geometry.

Furthermore, Table 2.2 provides the mean value of quantum coherence in the central spin. The mean value is calculated between t_1=29000 and t_2=30000, which corresponds to the thermalization time of a single spin initially in a maximally coherent superposition state within a thermal bath, as depicted in Figure 2.4. According to Table 2.2, the tetrahedral geometry with four buffer spins yields the highest mean coherence value.

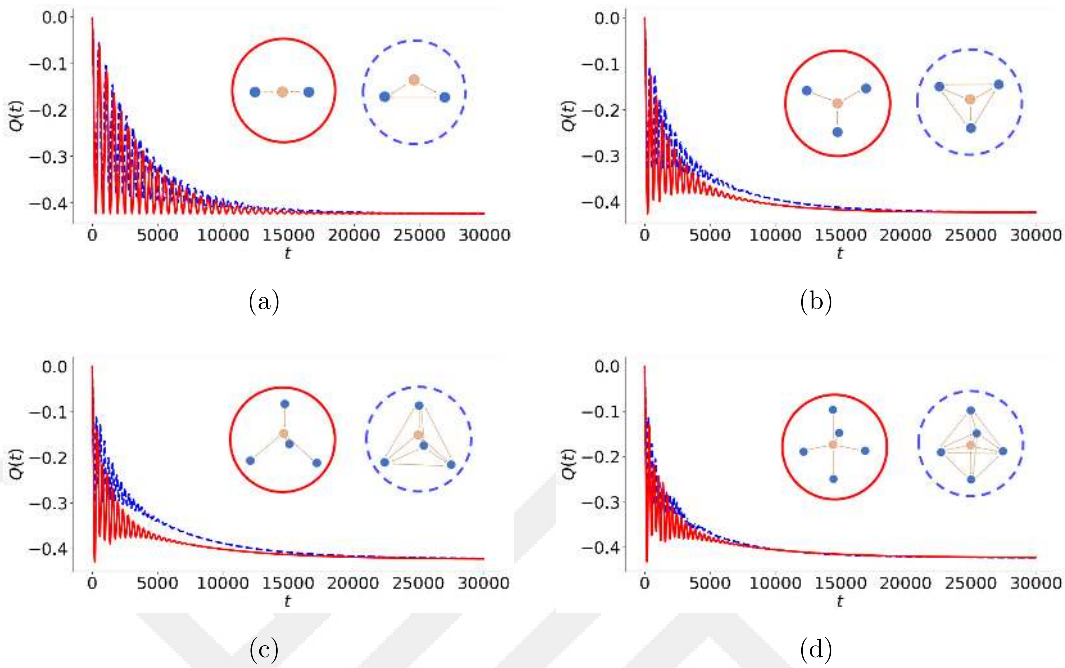

Figure 2.5: Heat current as defined in Eq. (2.23) with respect to dimensionless time t. The solid red curve corresponds to the case in which there is no coupling between the buffer spins. The dotted blue curve illustrates the case with coupling between buffer spins. (a) Two buffer spin network. (b) Three buffer spin network. (c) Four buffer spin network. (d) Five buffer spin network.

2.6.4 Physical Mechanism of Coherence Protection

The erasure of quantum coherence has been a subject of extensive discussion in the context of quantum computation, primarily as a means to efficiently reset quantum bits before executing quantum algorithms [Landauer, 1961, Bennett, 1982, Piechocinska, 2000, Shizume, 1995, Miller et al., 2020]. Landauer's pioneering ideas and erasure protocol have undergone both experimental and theoretical scrutiny [Croucher et al., 2018, Buffoni and Campisi, 2023, Scandi et al., 2022]. We focus on the simplest scenario in which the coherence of a qubit diminishes due to the process of thermalization, similar to the scenario outlined by [Wang et al., 2023].

Information erasure, often called “bit reset”, represents a critical operation occurring between successive thermodynamic cycles, enabling feedback control of subsystems. Nevertheless, it is imperative to acknowledge that this operation entails a significant energy exchange between the subsystem and its surrounding thermal bath, a concept consistent with Landauer’s principle. This principle sets a lower bound on the amount of heat dissipation required for information erasure, thus establishing a close connection between the energy cost and the reduction in entropy within the subsystem.

The work of [Wang et al., 2023] introduces an inequality for the dissipated energy, which imposes a more stringent lower limit than Landauer’s classical formulation. This further underscores the energy-intensive nature of information erasure, frequently surpassing the information gain divided by the inverse of the temperature. It is noteworthy that a more rapid decline in coherence results in a heightened heat transfer during the erasure process.

In our specific system, we can make a comparative analysis of energy transfer between a configuration lacking coupling between buffer spins and one that incorporates such coupling. Our investigation centers on the assessment of the local energy current within our system, which is defined as follows,

$$J(t) = \mathrm{Tr}\left(\hat{H}_s \frac{d}{dt}\rho_s(t)\right). \tag{2.22}$$

In this equation, $\hat{H}_s = \omega\sigma_z/2$ represents the Hamiltonian and ρ_s the density matrix for the central spin. The total heat exchange in and out of the central spin can be calculated by

$$Q(t) = \int_0^t J(\tau)\mathrm{d}\tau. \tag{2.23}$$

To illustrate how the buffer-central spins network structure influences the coherence protection time in the central spin, we consider the different geometries of Figure 2.2.

Figure 2.5 exhibits a time delay in the exchange of the same amount of heat with the central spin when the buffer spins are coupled. The time delay in exchanging the same amount of heat energy in the transient regime results in a delay in achieving the minimum energy transfer essential for erasing the coherence within the central qubit. In our specific case, the energy cost (E_c) of coherence erasure is given by

$$E_c = \mathrm{Tr}\left(\hat{H}_s(\rho_{\mathrm{fin}} - \rho_{\mathrm{int}})\right) = -0.42, \tag{2.24}$$

where ρ_{int} and ρ_{fin} are respectively the initial and final density matrix of the central spin. As it can be observed in Figure 2.5, all the heat exchange curves corresponding to the different geometries are converging to E_c.

The current analysis serves to elucidate the underlying physical principles supporting our approach to preserving coherence. From an analytical standpoint, it remains an open question to determine which network geometry, involving buffer and central spins, is most effective in delaying the heat exchange required to erase the coherence within the central spin. However, by conducting a numerical investigation systematically, the tetrahedral geometry emerges as the most favorable choice.

2.6.5 Alternative Noise Model

The case of the pure dephasing channel is also checked. The dissipator (2.21) is changed to

$$\mathcal{D}(\rho) = \sum_{i=2}^{N+1} \gamma_d \left[\hat{\sigma}_i^z \rho(t) \hat{\sigma}_i^z - \rho(t)\right], \tag{2.25}$$

where γ_d is the dephasing rate. We consider different dephasing rates. Table 2.3 and Table 2.4 are reported for $\gamma_d = 0.00059$. The conclusion of tetrahedral geometry of buffer qubits offering the best protection against decoherence remains robust in case of a dephasing environment as well.

Table 2.3: The dimensionless time for which the relative entropy $S(\cdot\|\cdot)$, trace distance $T(\cdot\|\cdot)$, relative entropy of coherence $C_{RE}(\cdot)$ or L_1 norm of coherence $C_{L_1}(\cdot)$ become always inferior to 10^{-4} at the center of spin cluster for the parameters $\omega = 1$, $g = 0.002$, $\gamma_{\rm d} = 0.00059$, and $T = 0.4$. The left and right columns compare the same quantity for the left and right geometries depicted in Figure 2.2, which correspond to vanishing and maximal connectivity in the buffer network, respectively. The initial state of the buffer spins is a maximally coherent superposition state. The results are for the pure dephasing channel.

$N+1$	$S(\rho_1\|\rho_{th})$		$T(\rho_1,\rho_{th})$		$C_{RE}(\rho_1)$		$C_{L_1}(\rho_1)$	
3	6890	9990	6890	9990	13600	20440	15120	22210
4	6930	13600	6930	13600	13780	27160	15090	29520
5	7130	**16960**	7130	**16960**	13830	**33770**	15010	**36700**
6	7060	13540	7060	13540	13760	27380	14840	29810
7	6800	13020	6800	13020	13540	26530	14800	28900

Table 2.4: The mean value of the relative entropy $S(\cdot\|\cdot)$, trace distance $T(\cdot\|\cdot)$, relative entropy of coherence $C_{RE}(\cdot)$ or L_1 norm of coherence $C_{L_1}(\cdot)$ of the central spin from time $t_1 = 29000$ to time $t_2 = 30000$ for the parameters $\omega = 1$, $g = 0.002$, $\gamma_{\rm d} = 0.00059$, and $T = 0.4$. The left and right columns compare the same quantity for the left and right geometries depicted in Figure 2.2, which correspond to vanishing and maximal connectivities in the buffer network, respectively. The results are for the pure dephasing channel.

$N+1$	$S(\rho_1\|\rho_{th})$		$T(\rho_1,\rho_{th})$		$C_{RE}(\rho_1)$		$C_{L_1}(\rho_1)$	
3	4.00×10^{-14}	2.34×10^{-11}	7.87×10^{-15}	2.34×10^{-11}	5.25×10^{-8}	2.66×10^{-6}	8.92×10^{-8}	5.33×10^{-6}
4	3.03×10^{-11}	1.15×10^{-8}	2.95×10^{-11}	1.15×10^{-8}	5.81×10^{-5}	2.05×10^{-6}	2.98×10^{-6}	1.16×10^{-4}
5	1.48×10^{-11}	$\mathbf{2.68\times10^{-7}}$	1.46×10^{-11}	$\mathbf{2.68\times10^{-7}}$	2.05×10^{-6}	$\mathbf{2.75\times10^{-4}}$	4.09×10^{-6}	$\mathbf{5.51\times10^{-4}}$
6	5.59×10^{-15}	1.09×10^{-8}	1.64×10^{-15}	1.09×10^{-8}	3.03×10^{-8}	5.48×10^{-5}	4.02×10^{-8}	1.10×10^{-4}
7	7.09×10^{-16}	6.53×10^{-9}	1.85×10^{-16}	6.53×10^{-9}	5.53×10^{-9}	4.21×10^{-5}	1.11×10^{-8}	8.42×10^{-5}

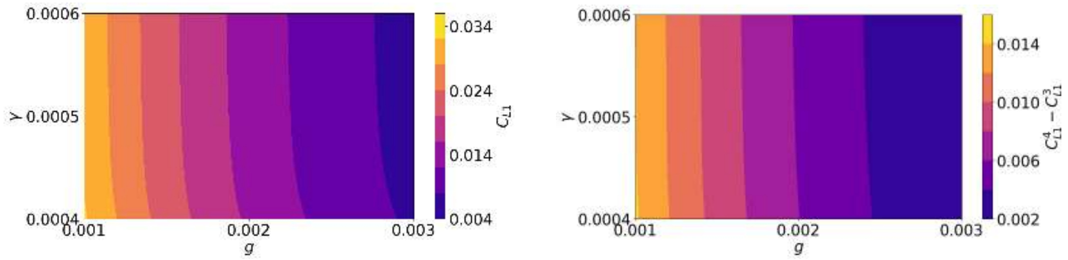

(a) (b)

Figure 2.6: The L1 norm difference between the three spin network and the four spin network with maximum connectivity (shown in Figure 2.2). (a) Mean value of the L1 norm from time $t_1 = 29000$ to time $t_2 = 30000$ with respect to coupling constant, g, and dissipative constant, γ. The graph corresponds to the tetrahedral geometry (4 spin network with maximal connectivity). (b) Difference of the L1 norm mean values from time $t_1 = 29000$ to time $t_2 = 30000$ with respect to coupling constant, g, and dissipative constant, γ.

2.6.6 Parameter Dependence of The Model

Specific coupling constants, denoted as g for the inter-spin coupling and γ for coupling with the environment, are set at 0.002 and 0.0005 respectively. We further explore variations in coupling constants in the context of a four buffer spin network arranged in a tetrahedral geometry, as illustrated in Figure 2.6a.

Interestingly, we observe that changes in these coupling constants have minimal impact on the behavior of the L1 norm. Moreover, our analysis in Figure 2.6b confirms that our key findings remain consistent across different coupling scenarios. Specifically, we compare the L1 norm of the tetrahedral geometry with that of a three buffer spin network. The L1 norm of the tetrahedral geometry consistently exceeds that of the three buffer spin network. This underscores the robustness of our main conclusion across various coupling constant settings.

2.6.7 Preservation of Entanglement

In the previous part, we found that the tetrahedral geometry is the best candidate for coherent protection, which closely resembles the structure of the phosphate molecule. Building upon this result, we now extend our investigation to the preservation of entanglement.

In our approach, we treat each atom within a phosphate molecule as an identical spin having a magnitude of 1/2. In the context of a phosphate molecule, a cluster of five spins consists of a central spin (associated with the phosphorus atom) surrounded by buffer spins (corresponding to oxygen atoms). The buffer spins interact with individual thermal baths, while the central spin remains isolated from direct environmental interactions. When exposed to a magnetic field along the z-axis, an energy difference arises between the lower state (spin-up) and the upper state (spin-down), allowing for a two-level description. The buffer spins eventually reach thermal equilibrium with the environment at an inverse temperature β.

Here, we focus on the preservation of the initial entanglement over time between two spins, each in a separate network. To achieve this, we simulate the system as an open system. The central spins within both networks are entangled with each other, while the buffer spins exist in a thermal state. There is no direct coupling between the spins of the two networks, considering they are well separated. We consider two clusters of $N+1$ spins, each cluster consisting of a central spin surrounded by a buffer network. The initial cluster state can be represented as a product state,

$$\rho(0) = \frac{|01\rangle + |10\rangle}{\sqrt{2}} \otimes \rho_{th}^{\otimes 2N}. \tag{2.26}$$

To verify the entanglement protection of different geometries, we look at the logarithmic negativity (2.6). Notably, Figure 2.7 illustrates the entanglement negativity over time between the two central spins of two separate clusters, considering the different geometries. We observe that entanglement is conserved for an extended duration in the tetrahedral geometry as outlined in Table 2.5. This result further supports the previous section's conclusion that tetrahedral geometry is optimal for quantum information protection.

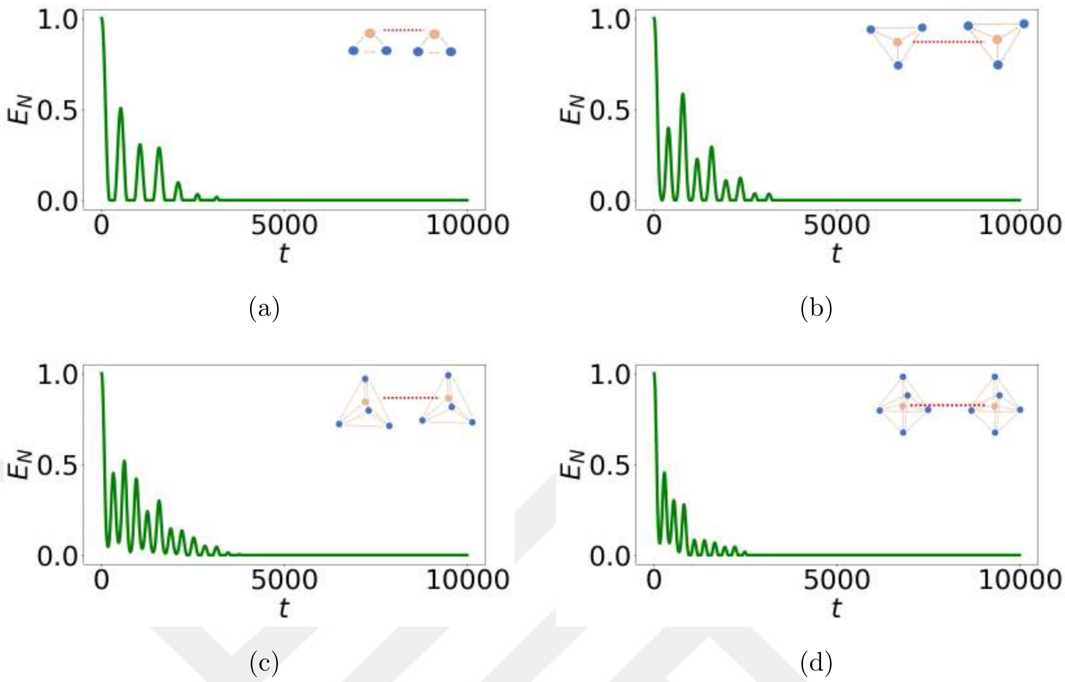

Figure 2.7: Logarithmic negativity, E_N, of the reduced state composed on the two entangled spins with respect to dimensionless time, t. (a) Two buffer spin network. (b) Three buffer spin network. (c) Four buffer spin network. (d) Five buffer spin network.

A parallel can be drawn with biological systems, but to make it closer to real scenarios, we need to create a more realistic model. The aim of the next section is to develop such a model of the Posner cluster.

2.7 More Realistic System: Posner Cluster

2.7.1 The Quantum Brain Proposal

[Fisher, 2015] proposes a comparison between quantum computing and our brain, suggesting that our brain might function like a quantum computer [Weingarten et al., 2016]. This model aligns closely with neuroscience conventions, where consciousness is associated with the network of neurocells.

Table 2.5: Time, t_1, at which the logarithmic negativity between the two central spins becomes always inferior to 10^{-4} for various number of spins in the cluster.

N+1	3	4	5	6
t_1	3210	3230	**3800**	2540

To facilitate quantum computing in the brain, we first need to identify a suitable candidate to act as a qubit. Moreover, the brain's mechanism should meet the following criteria:

- Long nuclear-spin coherence time;
- Mechanism for transporting the qubit into neurons;
- Qubit storage at the molecular level;
- Biological process for entangling qubits;
- Initiation of a chemical reaction that triggers quantum measurements, affecting neuronal function.

2.7.2 Generation of Entanglement in Posner Clusters: A Hypothesis

The optimal candidate for a neural qubit in our brain should have a nuclear spin of 1/2 to ensure long-lived coherence. Therefore, phosphorus emerges as the best candidate for a neural qubit. The phosphate ion and the pyrophosphate ion (PPi) serve as transporters for this qubit. In our body, adenosine triphosphate (ATP) undergoes a hydrolysis reaction,

$$\text{ATP} \longrightarrow \text{AMP} + \text{PPi},$$

producing adenosine monophosphate (AMP) and the pyrophosphate ion. Occasionally, further hydrolysis results in the production of two separate phosphate ions. Once the transporter is identified, a mechanism is needed to protect the coherence of the phosphorus qubit. This is where the Posner molecule comes into play.

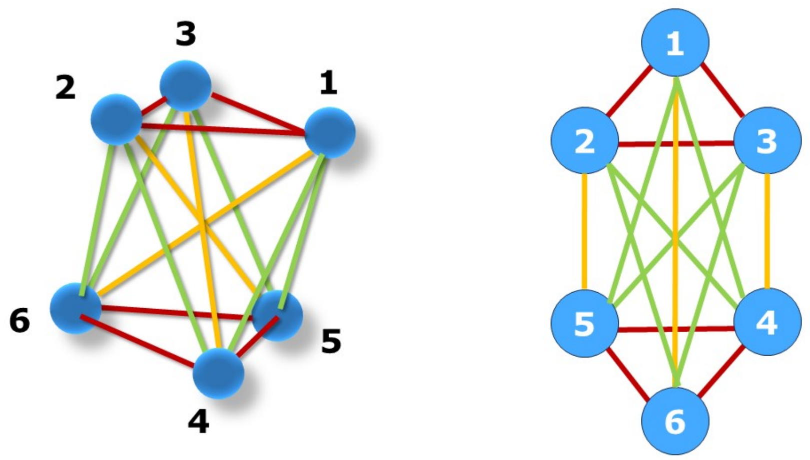

Figure 2.8: Three-dimensional (left) and two-dimensional (right) arrangement of phosphorus atoms in a Posner molecule, $Ca_9(PO_4)_6$, with S_6 geometry: coupling constants, J_{jk}, in Eq. (2.27) are +0.178 Hz for the red pairs (1,2), (2,3), (3,1), (4,5), (5,6), (4,6); +0.145 Hz for the green pairs (1,4), (1,5), (2,4), (2,6), (3,5), 3,6); and −0.003 Hz for the yellow pairs (1,6), (2,5), (3,4).

The existence of stable calcium-phosphate molecules in our body indicates that phosphate ions will bind to calcium cations, protecting them from proton binding. This mechanism extends the coherence time for phosphorus nuclear spin. The calcium-phosphate molecule, $Ca_9(PO_4)_6$, is called the Posner cluster.

Next, we need a mechanism to entangle two qubits present in one or two different Posner clusters. The enzyme pyrophosphatase could ensure this entanglement. The two phosphorus nuclear spins could be entangled and would be located in two different Posner clusters. When these Posner molecules are present in two different presynaptic neurons, they undergo a binding reaction with other Posner clusters, influencing the firing of the corresponding neurons. Thus, the two reactions occurring in two different neurons could be entangled.

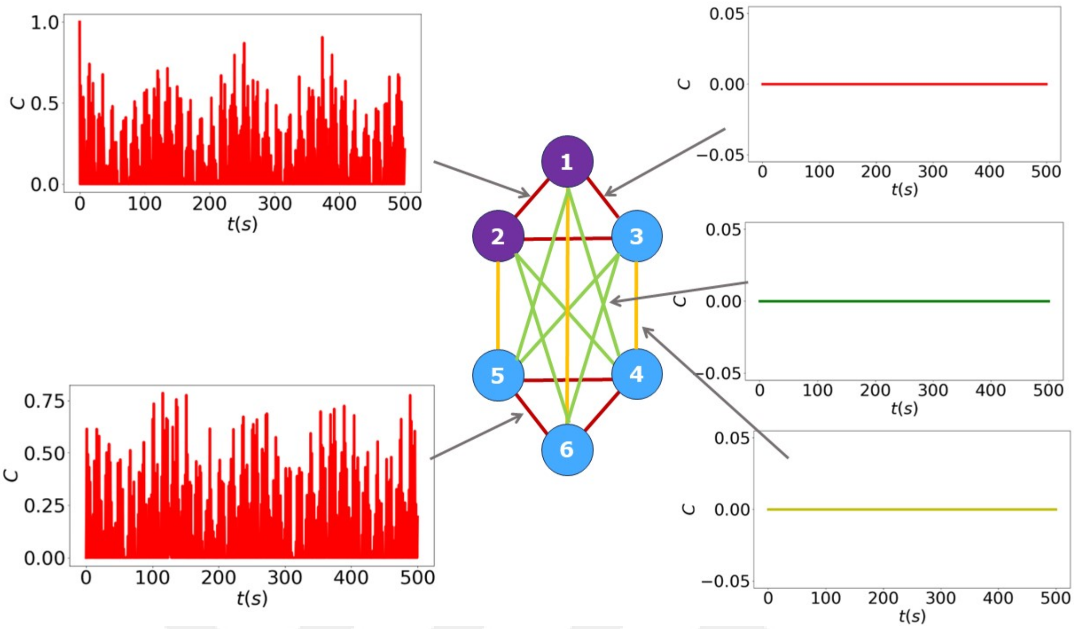

Figure 2.9: The concurrence between different pairs of spins over time, starting from initial states with entanglement between spins 1 and 2. The graphs on the left illustrate the presence of entanglement between spins 1 and 2 and between spins 5 and 6, indicated by a non-zero concurrence. All other spin pairs do not show any entanglement generation, as their concurrence remains zero (graphs on the right).

2.7.3 Analyzing Entanglement in One Posner Cluster

Following the literature [Player and Hore, 2018, Adams et al., 2023], we consider that we can model the Posner cluster as an ensemble of six spins-1/2 with the following Hamiltonian,

$$\hat{H}_0 = \omega_0 \sum_k \hat{S}_{kz} + \sum_{j<k} \sum_k 2\pi J_{jk} \hat{\mathbf{S}}_j \cdot \hat{\mathbf{S}}_k, \tag{2.27}$$

where J_{jk} represents the spin interaction values as described in Figure 2.8 and $\hat{S}_k$ the spin-1/2 matrix for the k^{th} spin. This corresponds to S_6 symmetry.

For the beginning of our analysis, we do not consider any open quantum system approach; instead, we focus on the dynamics of entanglement in a closed system.

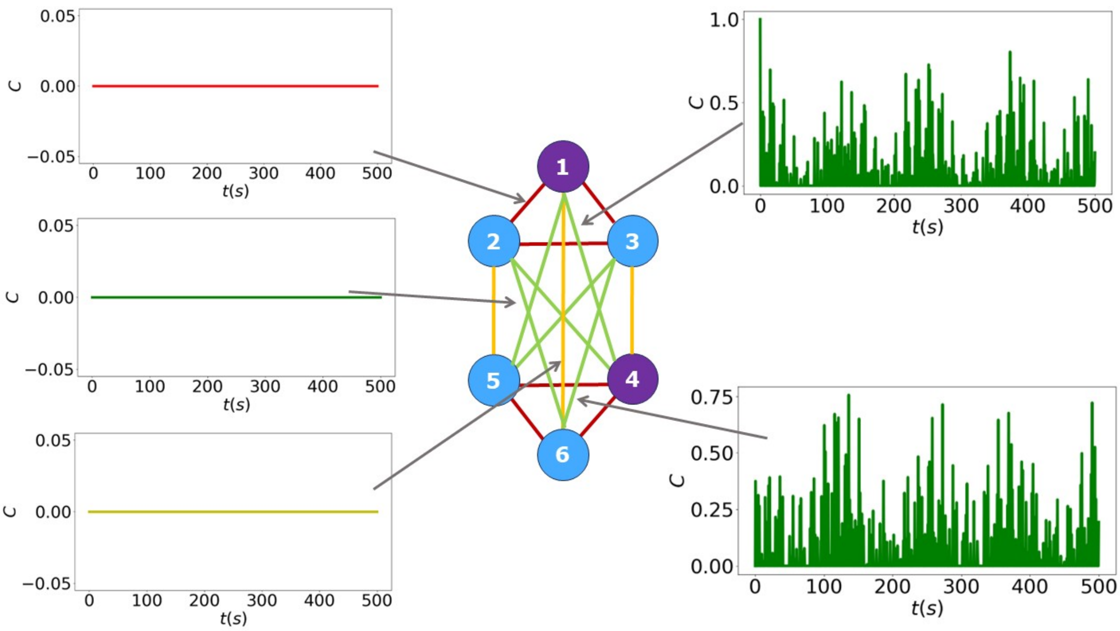

Figure 2.10: The concurrence between different pairs of spins over time, starting from initial states with entanglement between spins 1 and 4. The graphs on the right illustrate the presence of entanglement between spins 1 and 4 and between spins 3 and 6, indicated by a non-zero concurrence. All other spin pairs do not show any entanglement generation, as their concurrence remains zero (graphs on the left).

The initial state consists of two selected spins in a singlet state,

$$|\psi_0\rangle = \frac{1}{\sqrt{2}}(|01\rangle - |10\rangle). \tag{2.28}$$

The other spins are in a maximal mixed state.

In Figure 2.9, we investigate the evolution of concurrence (2.7). The results show that when we begin with an entangled state in spins 1 and 2, entanglement only appears in the symmetric pair (spins 5 and 6) and not in any other spin pair. This observation is further supported by the analysis of different initial states presented in Figure 2.10 and Figure 2.11.

A possible explanation for this behavior can be found in Figure 2.12. Here, we see that starting with an entangled pair of spins leads to the same overlap between the initial state and the eigenvector as when we start with the entangled symmetric pair.

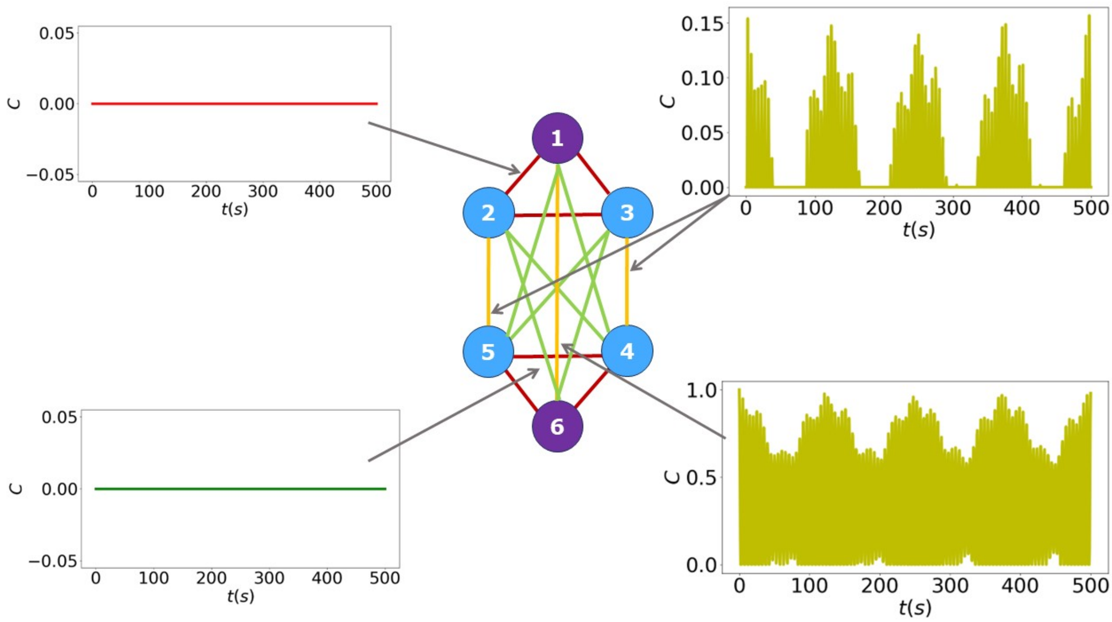

Figure 2.11: The concurrence between different pairs of spins over time, starting from initial states with entanglement between spins 1 and 6. The graphs on the right illustrate the presence of entanglement between spins 1 and 6, between spins 2 and 5, and between spins 3 and 4, indicated by a non-zero concurrence. All other spin pairs do not show any entanglement generation, as their concurrence remains zero (graphs on the left).

The overlap is defined as $\mathrm{Tr}(\rho_0\rho_\mathrm{e})$ with ρ_0 being the density matrix of the initial state and ρ_e being the density matrix of the eigenvector. With these exciting results, we characterize the significance of symmetry in the system for entanglement generation, which is a preliminary step for analyzing larger numbers of Posner molecules.

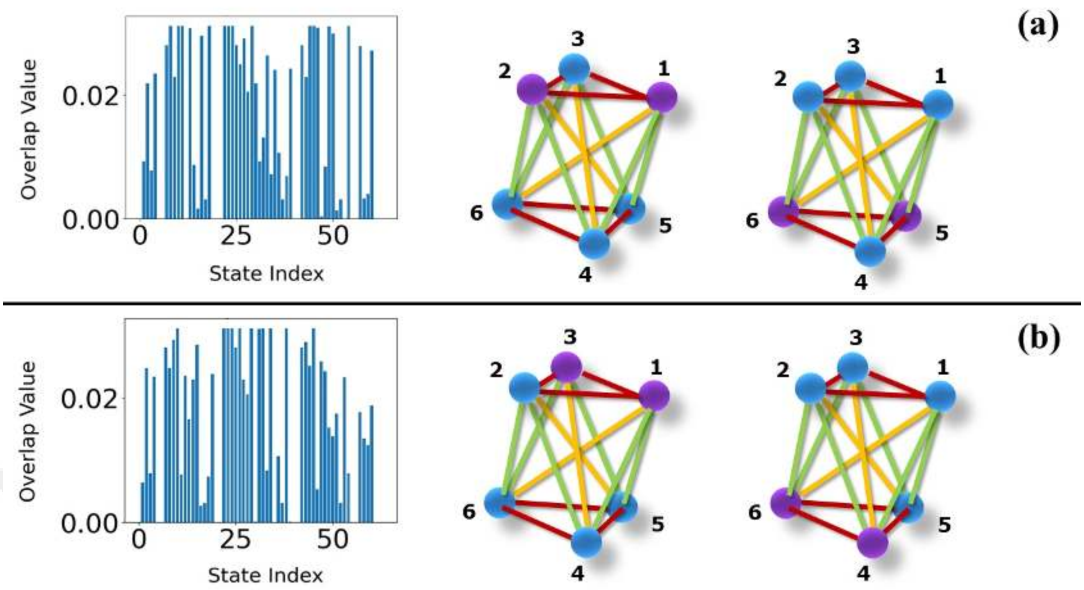

Figure 2.12: (a) Overlap between the 64 eigenstates and the initial states with entanglement between spins 1 and 2, and between spins 5 and 6. (b) Overlap between the 64 eigenstates and the initial states with entanglement between spins 1 and 3, and between spins 4 and 6.

2.8 Conclusion

In this chapter, we have examined the influence of buffer network size and topology on the preservation of quantum coherence in a central spin. Our analysis has specifically concentrated on weak inter-spin coupling, considering buffer networks that could be embedded in a plane without intersecting edges. The results have yielded a noteworthy observation: the preservation time of quantum coherence did not exhibit a consistent increase with the addition of more buffer spins in the cluster.

Remarkably, we have identified that a four buffer spin network, characterized by maximum connectivity and adopting a tetrahedral geometry, provided the most effective means of preserving quantum coherence against the perturbations arising from the thermal environment. This finding highlighted the significance of carefully optimizing the buffer network's structural features to enhance the protection of quantum coherence in practical applications.

Furthermore, within the same model, we investigated the preservation of entanglement between two separate clusters protecting a centrally located entangled spin. Our analysis confirmed that the tetrahedral geometry remained the optimal choice for this scenario.

Notably, this tetrahedral geometry is frequently observed in natural molecules, such as water-ice systems in hexagonal phases [Raza et al., 2011], magnetic spin-ice substances [Bramwell and Gingras, 2001], and phosphate molecules in Posner clusters [Fisher, 2015]. It is worth mentioning that our simplified model did not fully account for such complex molecules. Nevertheless, the correspondence between the tetrahedral network and the optimal geometry holds potential significance for both understanding biochemical processes and advancing artificial quantum technologies.

Inspired by the existing Posner cluster model, we analyzed entanglement dynamics in a more realistic model. This analysis yielded intriguing results: entangled initial states shared their entanglement symmetrically during time evolution inside one Posner cluster. This further emphasized the significant role of configuration in entanglement evolution within a molecule.

In the future, we should start by examining the effects of environmental noise and characterizing the time scales involved in typical neuronal processes. This approach will enable us to study entanglement under environmental noise conditions which could more accurately reflect that which may be present in the brain. Consequently, we should explore various entanglement scenarios, including cases where entanglement is shared among multiple Posner clusters. Investigating how two Posner clusters could be entangled through their subunits in the phosphate network may also be crucial. In conclusion, this work has significant potential for extension beyond Posner clusters to different biological scenarios, such as reactive oxygen species [Paul, 2015].

Chapter 3

QUANTUM SENSING WITH NITROGEN-VACANCY CENTERS

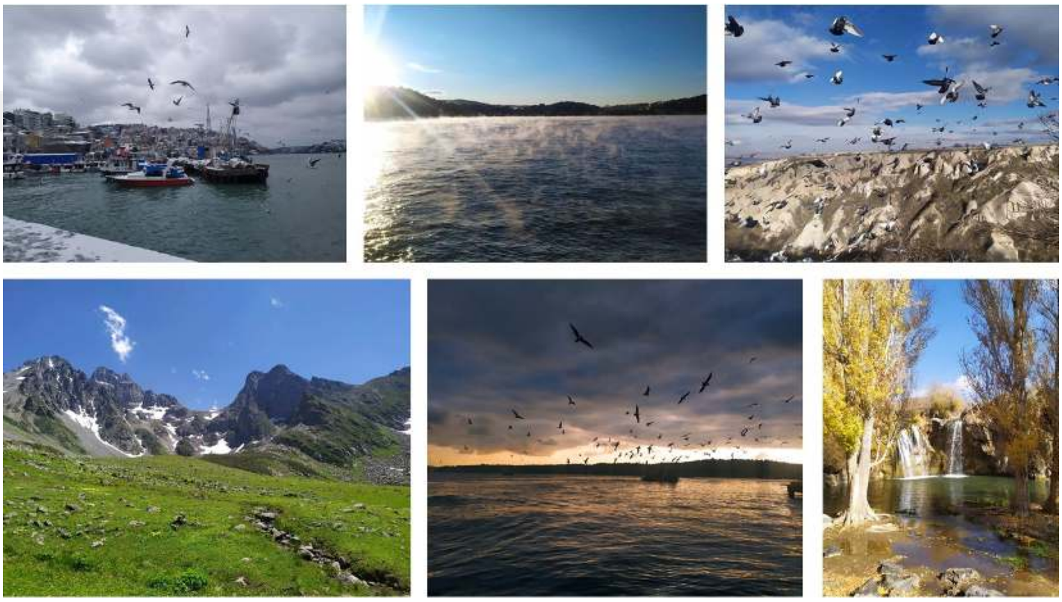

3.1 Introduction

The fact that you can read this text means that you can see. Still, you could be "reading" this text by listening, or even by touching if it is put in braille form.

In the previous chapter, we discovered the importance of information and how we could preserve that information in a specific scenario. Now, in this chapter we will see how we can receive and/or collect information. The three ways of "reading" mentioned above are three ways of receiving information [Fisher et al., 2004]. Our body is equipped with specific organ systems to enable us to receive information all the time. Sometimes we are even overwhelmed by the amount of information coming through. These organ systems rely mostly on sensory organs to retrieve data [Hazenberg and van Lier, 2016].

Beside the eyes, the ears and our hands, there is also our nose and our tongue that bring in information to our brain [Silverstein et al., 2002, Szwed et al., 2017]. These faculties have been defined as our basic senses: to see, to hear, to touch, to smell and to taste. Does the human body have more senses? The answer lies in a matter of perspective [Parma et al., 2024]. Some cells can perceive other cells [Taniguchi, 2010, Plum et al., 2023]. Certain interior organs can sense what is going on outside the human body, for example the stomach reacting in a certain way in a state of fear or worry [Klarer et al., 2014].

Recently, a receptor protein has been discovered in human that can identify amino acids [Gumerov et al., 2022]. Some other receptor proteins in the human body sense hormones in the blood, and bind to their intended hormonal targets [Schreiber, 2023]. Alternatively, hormones may "communicate" with each other by means of a feedback mechanism, which involves the regulatory hormone acting on the target endocrine gland to then promote or suppress synthesis of the other hormone [Hiller-Sturmhöfel and Bartke, 1998]. Furthermore, some hormones are merely produced by the effect of sensing, for example reflex tears running out of the eyes [Murube, 2009], or saliva secreted as one bites into a chilli [Riantiningtyas et al., 2024].

The same way, scientists have taken sensing to the atomic level [Malik et al., 2020, Kitching et al., 2011]. First, they started by creating sensing devices that mimic the eyes [Kingslake, 1989] and ears, such as cameras and microphones, followed by more sophisticated apparatus, especially those used in the medical field [Togawa et al., 2011, Mukhopadhyay et al., 2018]. Then, as our understanding of what is smaller grew bigger, the world needed more refined, tinier and tinier detectors [Vaseashta and Dimova-Malinovska, 2005, Cristiano et al., 2015, El-khatib et al., 2021, Singh et al., 2024, Yao et al., 2024]. This brings us to the objective of this chapter: quantum sensing [Ye and Zoller, 2024, Degen et al., 2017b, DeMille et al., 2024, Bass and Doser, 2024].

The exploration of precisely controlled quantum systems as highly sensitive nanoscale detectors holds significant promise in advancing our comprehension of intricate processes within biological and condensed-matter systems, operating at molecular and atomic scales [Hasselbach et al., 2000, Kirtley et al., 1995]. The demanding criteria for both high sensitivity and spatial resolution have prompted suggestions to employ spin-based quantum systems as nanoscale magnetometers [Chernobrod and Berman, 2005] or to utilize imaging through the detection of sample-induced decoherence [Cole and Hollenberg, 2009].

A particularly appealing physical platform for realizing these concepts is the Nitrogen-Vacancy (NV) center in diamond [Doherty et al., 2013]. This choice is motivated by the center's prolonged coherence times at room temperature and its convenient optical readout of the spin state [Degen et al., 2017b, Jelezko and Wrachtrup, 2006, Balasubramanian et al., 2009, Hanks et al., 2017, Hong et al., 2013, Schirhagl et al., 2014]. Given the considerable potential of the NV center, researchers have conducted studies to enhance the sensing capabilities of this probe. Specific pulse sequences, such as Carr-Purcell-Meiboom-Gill (CPMG) and Dynamic Decoupling (DD) [Shim et al., 2012, Wang et al., 2012], have been used to prolong coherent time. Likewise, researchers have investigated the use of entangled NV centers [Qiu et al., 2021, Xie et al., 2021] and, finally, spin squeezing [Dooley et al., 2016].

Spin squeezing, as introduced by [Kitagawa and Ueda, 1993], involves the quantum redistribution of uncertainties along two orthogonal spin directions. This operation holds significance in quantum sensing and metrology, providing a means to enhance measurement precision beyond the standard quantum limit in experiments [Brask et al., 2015, Buchmann et al., 2016, Gross, 2012]. Consequently, spin squeezing emerges as a valuable resource in applications of quantum technology.

In the context of spin squeezing generation for NV centers, ensembles of qubits are typically considered. However, this approach has limitations as the qubit model is an approximation that necessitates a bias field.

Hence, we dig into the possibility of using qutrits for NV centers. Pulsed dynamical generation of spin squeezing has been surveyed in the literature for spin-1 systems [Begzjav and Agarwal, 2021, Huang et al., 2021b] and other methods, including generation via nonadiabatic control [Xin et al., 2022]. In the context of NV centers, Ramsey interferometry is recognized as a straightforward and efficient protocol for measuring magnetic fields. It has been extensively studied in qubit systems [Güldeste and Bulutay, 2023, Oshnik et al., 2022, Coto et al., 2021, Rondin et al., 2014] and has also been discussed for qutrit systems [Oon et al., 2022, Hart et al., 2021].

In this project, we analyze the potential enhancements in quantum metrological performance achievable by transitioning from two-level (qubits) to three-level (qutrits) spin systems and incorporating spin squeezing within typical quantum magnetometry settings, specifically NV center Ramsey interferometry. We adopt a foundational approach, comparing qubit versus qutrit Ramsey quantum magnetometry scenarios, both with and without spin squeezing, in terms of Quantum Fisher Information (QFI). Considering the influence of quantum dephasing and relaxation during the spin system's evolution, our findings suggest that qutrits, coupled with the additional step of spin squeezing, can outperform qubits in terms of QFI, provided that the spin squeezing magnitude, the timing of squeezing and free evolution are optimally determined.

In order to apply this result to biological systems, we draw upon the suggestion of [Zhang et al., 2018] to use hydrogel as a spacer between a nanodiamond with NV centers and magnetic nanoparticles (MNPs). Upon stimulation, the hydrogel experiences a volume phase transition, which alters the distance between the MNPs and the NV centers. This shift in distance markedly influences the magnetic field that the highly sensitive NV centers can then detect.

Our proposition is to enhance bio-sensing sensitivity by employing correlated NV centers. The biologically reactive hydrogel would serve as an intermediary. A transducer translates these alterations into discernible magnetic signals. By integrating correlated NV centers, we aim to improve sensitivity.

Here is a summary of the sections in Chapter 3. Section 3.2 presents the concept of quantum sensing. Section 3.3 explains the unique properties of NV centers and explores their potential as probes within biological systems as well as how quantum correlations can further enhance measurement sensitivity. To quantify this improvement, Section 3.4 introduces a tool called Quantum Fisher Information. Next, Section 3.5 focuses on a technique called spin squeezing, explaining its role in boosting sensitivity for specific quantum measurements. Building on this foundation, Section 3.6 is a detailed breakdown of how spin squeezing can be applied to improve quantum magnetometry using NV center qutrits. Finally, the chapter ventures into a new application with Section 3.7 proposing a method that combines NV centers with bioresponsive materials such as hydrogels for precise biological measurements. In Section 3.8, the chapter ends by summarizing the key takeaways from this exposition of quantum sensing with NV centers.

3.2 Quantum Sensing

Quantum sensing utilizes quantum objects to measure any physical quantity. These objects are characterized by quantized energy levels, which can include electronic, magnetic, or vibrational states of superconducting or spin qubits, neutral atoms, and even more [Degen et al., 2017b]. To function as a quantum sensor, the object must meet certain criteria:

- Discrete energy levels: The object must have distinct energy levels for the measurement to be effective. Often, these are two-level systems (qubits) or a collection of them. Recently, three-level systems (qutrits) have shown promise as well [Shlyakhov et al., 2018a].

- State initialization: The sensor needs to be easily initialized into a known state for reliable measurements.

- Controllability: It should be readily manipulated by applying time-dependent fields.

- Selective interaction: The sensor must interact strongly with the physical quantity of interest, causing a change in its energy level. This interaction should be weak for other signals to avoid noise.

The term "quantum sensing" is also used to refer to the application of quantum coherence in measuring any physical parameter. Quantum coherence plays a crucial role in quantum sensing. The sensor needs to have a long enough coherence time to effectively utilize superposition and achieve high sensitivity. Quantum sensing can also be described as the utilization of quantum entanglement, where multiple entangled sensors are employed to enhance measurement sensitivity or precision. This approach, recognized for achieving Heisenberg-limited measurements, necessitates the use of more than one sensor. Quantum sensors encompass a variety of examples such as atomic vapor cells [Shah et al., 2007], Rydberg atoms [Haroche, 2013], quantum dots [Elzerman et al., 2004], and NV centers [Doherty et al., 2013], among others. Quantum sensing is an emerging field with immense potential. Despite being in its early stage, progress in this domain is expected to have a profound influence on a range of scientific pursuits and technological innovations in the future, some of which will be mentioned throughout the chapter.

3.3 Nitrogen-Vacancy Centers

A Nitrogen-Vacancy center appears when a nitrogen atom takes the place of a carbon atom in the diamond lattice, creating a defect which consists of the nitrogen impurity adjacent to a vacant lattice site. The electronic structure of the NV center is formed with five non-bonded electrons, where two electrons are from the nitrogen atom and three from the carbon atoms adjacent to the lattice vacancy. The NV center can exist in neutral, positive, and negative charge states. For quantum technology applications, mostly the negatively charged NV center is used. This state is formed when the NV center captures an electron, from the environment, at the vacancy site creating a spin-1 pair with one of the non-bonded electrons. Figure 3.1 illustrates the overall geometry of the NV center.

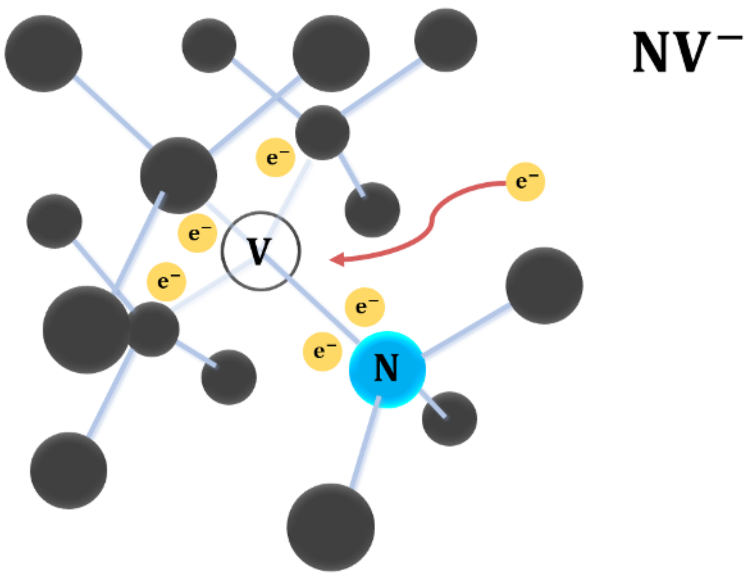

Figure 3.1: Configuration of the Nitrogen-Vacancy (NV) center in a diamond lattice. The black spheres represent the carbon atoms. The transparent sphere marked with a V represents the vacancy. The blue sphere represents the nitrogen impurity. The free electrons are depicted in yellow, with two electrons from the nitrogen atom and three from the carbon atoms adjacent to the vacancy. The red arrow represents an additional electron from the environment being added to form the negatively charged NV center.

3.3.1 Properties of NV Centers

NV centers exhibit long spin coherence times even at room temperature, and also, optical addressability, biocompatibility, and photostability. This presents unique opportunities for biological applications in quantum metrology [Taylor and Bowen, 2016]. The three significant properties of NV centers are:

1. Spin initialization: Efficient spin state preparation;

2. Coherent control: Coherent manipulation of the spin state to be able to control the interaction with the environment;

3. Optical readout: To be able to read the optical spin state in order to translate the spin state, after the interaction with its environment, to a measurable parameter.

These properties match with the characteristics of a quantum sensor as highlighted in Section 3.2. The spin dynamics are summarized in Figure 3.2. The negatively charged NV center consists of:

- ^3A: a ground-state triplet composed of the spin states, m_s= -1, 0, +1;

- ^3E: an excited-state triplet composed of the spin states, m_s= -1, 0, +1;

- ^1A: an intermediate-state singlet composed of the spin state, m_s= 0;

- ^1E: an intermediate-state singlet composed of the spin state, m_s= 0.

For ^3A and ^3E, the electrons have total spin 1, and $m_s = 0$ state has a lower energy than m_s = +1 and m_s = -1. Furthermore, due to the Zeeman shift, m_s = +1 and m_s = -1 will be split with the action of an external magnetic field in the direction of the defect axis, but the state $m_s = 0$ will not be affected. Other properties of the environment as temperature can also have an effect on these energy levels.

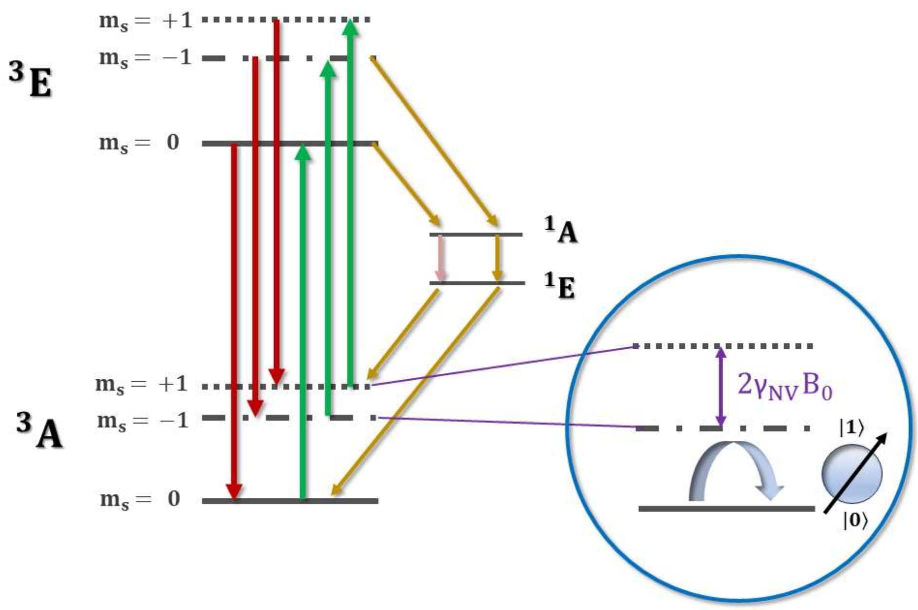

Figure 3.2: An illustration of the spin dynamics in the Nitrogen-Vacancy (NV) center. When the NV center absorbs green light via a laser, it conserves the spin and transits from the ground-state triplet (^3A) to the excited-state triplet (^3E). The NV center emits red light when going back to the ground state. When the NV center first transits through the intermediate singlets (^1A and ^1E), spin polarization occurs between $m_s = \pm 1$ and $m_s = 0$. The blue circle shows the Zeeman effect arising from the action of the static magnetic field, B_0, in the direction of the defect axis. $\gamma_{\rm NV}$ is the gyromagnetic ratio of the NV center. A qubit is generated by reducing the system to two-level, $m_s = 0$ and $m_s =$ -1, and forbidding the state $m_s = +1$.

If a green laser is shone upon the NV center, it will absorb the green light and then, the ground-state triplet will jump to the excited-state triplet. Then, the emitted wavelength will be in the red range as it goes back to the ground state. Sometimes this takes place via the intermediate state. In the middle of the transition ($^1A \rightarrow {}^1E$), no visible light but instead infrared is emitted. The emitted light over the whole transition ($^3E \rightarrow {}^1A \rightarrow {}^1E \rightarrow {}^3A$) has a broader wavelength which however remains in the red part of the spectrum [Jelezko and Wrachtrup, 2006, Acosta and Hemmer, 2013].

The NV center emits more light when $m_s = 0$ than when $m_s = \pm 1$. Therefore, NV centers can be used to check in which state is the spin [Doherty et al., 2013].

The energy of the NV center is different when its spin is aligned with the magnetic field rather than against it. This means that the NV center needs one microwave frequency to flip its spin from 0 to +1, and another to flip from 0 to -1. Measuring the difference between the microwaves reveals the strength of the magnetic field. Thus, NV centers can also be used as sensitive compass to accurately measure the natural magnetic field around us. [Graham et al., 2024] demonstrate applications in Global Positioning System (GPS).

The qubit in Figure 3.2 shows that NV center is a promising candidate for quantum computing. It offers the long-lived coherence and scalability to two-level systems that are essential for this application [Childress and Hanson, 2013, Weber et al., 2010].

3.3.2 NV Centers as Probes in Biological Systems

The NV center is a prominent point defect found in diamond. Unlike other color centers, NV centers possess several unique properties that make them particularly attractive for biological applications [Balasubramanian et al., 2014]. Firstly, they are magnetic, meaning they have a non-zero spin. Secondly, their luminescence is directly linked to their spin state, allowing control of light emission through magnetic fields [Schirhagl et al., 2014]. Finally, the biocompatibility of NV centers makes them ideal candidates for probing biological systems [Wu et al., 2016].

Following its discovery, numerous applications have emerged for NV centers [Petrini et al., 2020]. They can be employed to measure various physical quantities within biological systems, including temperature [Wu et al., 2022], magnetic fields [Hong et al., 2013, Grinolds et al., 2013], and pressure [Doherty et al., 2014]. NV centers have significantly impacted the field of nanoscale Magnetic Resonance Imaging (MRI) [Boretti et al., 2019]. Their unique properties allow for high-resolution imaging at the cellular and even molecular level [Mamin et al., 2013, Suter and Jelezko, 2017]. Recent advancements have seen NV centers combined with Electron-Spin Labels (ESLs) for the detection of molecular transitions within biological environments [Munuera-Javaloy et al., 2022]. This opens exciting possibilities for studying biomolecular interactions. As comprehensively reviewed by [Schirhagl et al., 2014], various sensing protocols exist for utilizing NV centers in biological systems. These protocols include:

- Pulsed experiments,
- Continuous-wave experiments,
- Relaxometry.

These diverse sensing techniques allow researchers to tailor their approach to specific biological questions, offering a powerful toolbox for probing biological processes at the nanoscale. Finally NV centers excel at magnetic field sensing but struggle with other biological parameters like temperature and pH. To bridge this gap, researchers are looking at transducers, like hydrogels, that convert these biological changes into magnetic signals detectable by NV centers [Zhang et al., 2018]. This “translation” of physical quantities opens doors to using NV centers for a wider range of biological measurements.

3.3.3 Enhancing Sensitivity with Quantum Correlations

The NV center presents a lot of advantages but it is not perfect. Indeed it is affected by the surrounding noises. Quantum correlations and entanglement can be used to suppress measurement noise, and consequently improve the measurement sensitivity. Such techniques are relevant to nanodiamond NV sensors, because of its physical dimensions and the NV-NV interactions causing decoherence. Some techniques to generate quantum correlations have been discussed in the literature and could in theory improve the sensitivity.

For example, by using dynamical decoupling pulse sequences to suppress NV spin decoherence, [Bar-Gill et al., 2013] improve the spin coherence time by more than two orders of magnitude. Another way to improve the current result would be to use bath engineering methods. [Ullah et al., 2022] show the advantage of using a common bath for protection against local dephasing and dissipation channels and to make robust entanglement with NV centers. [Hou et al., 2019] have also shown a way to obtain maximal steady-state quantum correlation between NV centers thanks to squeezed-reservoir engineering.

One of the aims of this thesis is to improve the sensitivity of the NV centers even with the presence of environmental noise in close proximity to the sample.

3.4 Quantum Fisher Information

In the context of quantum parameter estimation, particularly in magnetic field sensing, fundamental results in quantum metrology become imperative. Let us consider a scenario where a quantum state encodes a parameter θ, and the goal is to estimate this parameter with optimal precision. The lower bound for the variance of any unbiased estimator $\tilde{\theta}$ is encapsulated by the Quantum Cramér-Rao Bound (QCRB), expressed as:

$$(\Delta\tilde{\theta})^2 \geq \frac{1}{\nu F_Q(\theta)}. \tag{3.1}$$

F_Q denotes the QFI, a quantum analog of the classical Fisher information, and ν represents the number of measurement repetitions [Luo, 2000, Liu et al., 2020].

The QFI (F_Q) is a pivotal quantity, and its definition depends on whether the quantum state is pure or mixed. For a pure state $|\psi\rangle$,

$$F_Q(\theta) = 4\left[\langle\partial_\theta\psi|\partial_\theta\psi\rangle - |\langle\partial_\theta\psi|\psi\rangle|^2\right]. \tag{3.2}$$

For a mixed state described by the density operator, ρ, the QFI can be defined, using the Symmetric Logarithmic Derivative (SLD) operator ($\hat{L}_\theta$), as

$$F_Q(\theta) = \mathrm{Tr}\left[\rho\hat{L}_\theta^2\right]. \tag{3.3}$$

The SLD operator is implicitly determined by the equation,

$$\partial_\theta\rho = \frac{\hat{L}_\theta\rho + \rho\hat{L}_\theta}{2}. \tag{3.4}$$

Expressing $\hat{L}_\theta$ in the eigenbasis of ρ, the QFI takes the form,

$$F_Q(\theta) = 2\sum_{k,l}\frac{|\langle k|\partial_\theta\rho|l\rangle|^2}{\lambda_k + \lambda_l}. \tag{3.5}$$

Here, $|k\rangle$ and $|l\rangle$ are the eigenvectors, and λ_k and λ_l are the eigenvalues of the density operator, ρ.

3.5 Spin Squeezing

Spin squeezing is a crucial concept in quantum information processing and metrology, offering a means to enhance the precision of quantum measurements beyond classical limits [Tóth and Apellaniz, 2014]. In systems involving NV centers, which are vital for various quantum applications, understanding electron spin behavior is essential. Spin squeezing occurs when the variance of a spin component perpendicular to the mean spin is reduced below the standard quantum limit. The definition of spin squeezing varies depending on the context [Ma et al., 2011]. This concept has significant applications in detecting quantum entanglement, which is fundamental to quantum physics and quantum information processing. Additionally, spin squeezing plays a key role in improving measurement precision in techniques such as Ramsey spectroscopy [Wineland et al., 1992, Wineland et al., 1994], atomic clocks [Bigelow, 2001, Polzik, 2008], and gravitational-wave interferometers [Walls and Zoller, 1981].

In order to quantify spin squeezing, the most widely studied squeezing parameters were proposed by [Kitagawa and Ueda, 1993] in analogy to photon squeezing, given by

$$\xi_S^2 = \frac{4\left(\Delta \hat{J}_{n_\perp}^2\right)_{\min}}{N}. \tag{3.6}$$

In this context, $n_\perp$ represents an axis perpendicular to the mean-spin direction $\hat{n}$, and N denotes the total number of spins. The collective spin is defined as $\hat{J} = \frac{1}{2}\sum_i \hat{\sigma}_i$, where $\hat{\sigma}_i$ represents the Pauli matrix of the spin-1/2 particle i. Another spin squeezing parameter is introduced by [Wineland et al., 1994] in Ramsey experiments, defined as

$$\xi_R^2 = \frac{N\left(\Delta \hat{J}_{n_\perp}\right)^2}{|\langle \vec{J} \rangle|}, \tag{3.7}$$

with

$$\hat{n} = \frac{\left(\langle \hat{J}_x \rangle, \langle \hat{J}_y \rangle, \langle \hat{J}_z \rangle\right)}{|\langle \hat{J} \rangle|}. \tag{3.8}$$

It is worth noting that other derived spin squeezing parameters have been discussed, along with their links to entanglement [Ma et al., 2011].

3.6 Spin Squeezing Enhanced Quantum Magnetometry with Nitrogen-Vacancy Center Qutrits

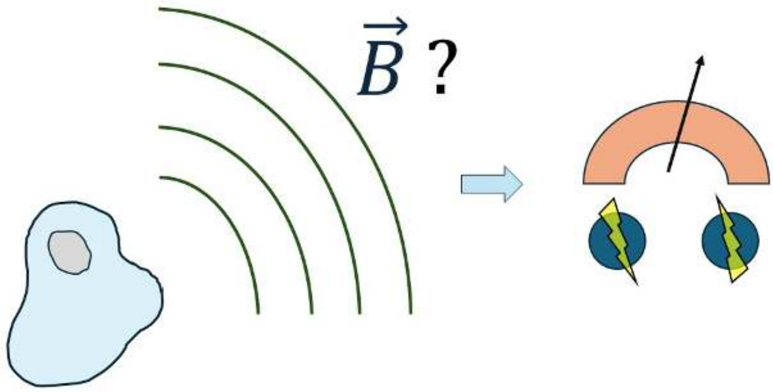

My latest results that have been submitted [Gassab and Müstecaplıoğlu, 2024] are presented in this section.

3.6.1 Methodology

In a scenario where there exists an unknown, potentially weak magnetic field within a defined region, our objective is to measure this magnetic field with the utmost precision possible. To accomplish this, we utilize one or two NV centers as our probes.

The NV center, characterized as an optically active color defect, results from a substitutional nitrogen impurity and a neighboring carbon vacancy in the diamond lattice. Comprising six electrons from nitrogen and the surrounding carbon atoms, the negatively charged NV center is described as a spin-1 (qutrit) system. We opt to elicit the full capabilities of the NV center by modeling it as a qutrit system [Yan et al., 2010, Shlyakhov et al., 2018a].

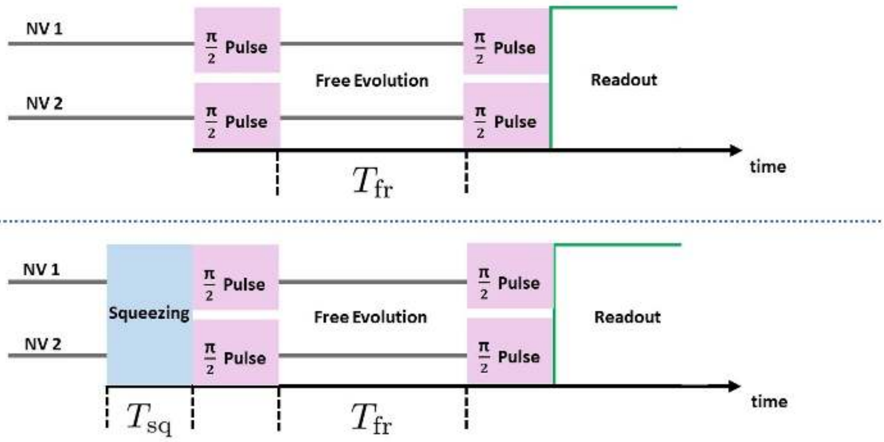

Figure 3.3: The application of Ramsey-type sequence on two Nitrogen-Vacancy (NV) Centers with and without the introduction of spin squeezing. T_{fr} is the free evolution time. T_{sq} is the duration of the application of spin squeezing.

This choice is motivated by the potential advantages that qutrits offer in metrology when compared to qubits (spin-1/2 system). Its ground state is a spin triplet (^3A) denoted as $|Sm_S\rangle$ with $S = 1$ and $m_S = 0, \pm1$. The NV center Hamiltonian captures these properties, while the excited-state triplet (^3E) is acknowledged at a higher energy level and is not explored in this context [Barry et al., 2020, Doherty et al., 2013].

Initially, our focus is on a single NV center. We then extend our consideration to two NV centers, exploring Ramsey interferometry with and without the application of spin squeezing as illustrated in Figure 3.3. When incorporating spin squeezing, the initial state, $|\psi_0\rangle$, is first driven through spin squeezing, and then subjected to the $\pi/2$ pulse.

3.6.2 Free Hamiltonian and Initial States

Neglecting interactions with nuclear spins or spin-strain effects [Sewani et al., 2020, Ullah et al., 2022], the Hamiltonian governing N NV centers is expressed as follows,

$$\hat{H}_0 = \sum_{i=1}^{\mathrm{N}} \left[D\hat{S}_{zi}^2 + g_S \vec{B} \cdot \vec{\hat{S}}_i \right]. \tag{3.9}$$

Hereon, we take $\hbar = 1$. $D = 2.87$ GHz is the temperature-dependent zero-field splitting, and $g_S = 1.80$ MHz/G is the gyromagnetic ratio for the electron spin. The magnetic field taken parallel to the NV center axis (z) is denoted as $\vec{B} = (0, 0, B_z)$. The spin-1 operator, $\vec{\hat{S}} = (\hat{S}_x, \hat{S}_y, \hat{S}_z)$, is defined as

$$\hat{S}_x = \frac{\hbar}{\sqrt{2}} \begin{bmatrix} 0 & 1 & 0 \\ 1 & 0 & 1 \\ 0 & 1 & 0 \end{bmatrix}; \tag{3.10}$$

$$\hat{S}_y = \frac{\hbar}{\sqrt{2}} \begin{bmatrix} 0 & -i & 0 \\ i & 0 & -i \\ 0 & i & 0 \end{bmatrix}; \tag{3.11}$$

$$\hat{S}_z = \hbar \begin{bmatrix} 1 & 0 & 0 \\ 0 & 0 & 0 \\ 0 & 0 & -1 \end{bmatrix}. \tag{3.12}$$

$\hat{S}_i$ is the spin matrix for the i^{th} NV center. Due to the Zeeman effect in the presence of a magnetic field, the electron spin ($S = 1$) is split into three states: $m_s = 0, 1, -1$, denoted as $|0\rangle$, $|1\rangle$ and $|-1\rangle$ (further details in Section 3.3.1). The initial state of the NV center is taken in the excited state $|-1\rangle$,

$$|\psi_0\rangle = \bigotimes_{i=1}^{N} |-1\rangle. \tag{3.13}$$

Then, each NV center undergoes a $\pi/2$ pulse, achieved by applying a rotation operator,

$$\mathrm{e}^{-i\frac{\pi}{2}\hat{S}_x}.$$

This pulse is experimentally generated by microwave drives [Mariani et al., 2020].

3.6.3 Spin Squeezing Generation

To describe the intricate dynamics and capture the squeezing effects in the Hamiltonian for two NV centers, a squeezing term is introduced [Wang and Sanders, 2003],

$$\hat{H}_{\mathrm{S}} = c_1 \left(\sum_{i=1}^{N} \hat{S}_{xi} \right)^2 , \tag{3.14}$$

where c_1 is the squeezing constant. The Hamiltonian (3.14) is referred to as a one-axis twisting Hamiltonian. The choice of x-axis twisting in the context of spin squeezing is strategic, as it allows for the manipulation of the noise cone, effectively narrowing the error ellipse of the spin. This, combined with the optimal ground state, enhances the precision of the magnetic field measurement by interplaying with the z-axis rotation induced by the magnetic field [Tóth et al., 2009].

The generation of this type of Hamiltonian in real setup has been discussed in the literature. It can be realized through phonon mediation, as evidenced by [Bennett et al., 2013] or produced in optical cavities [Borregaard et al., 2017]. In our specific protocol, we need to deactivate spin squeezing after a specific duration. A dynamic control method for NV center spin squeezing, as discussed by [Song et al., 2017], could potentially address the technical challenge.

Alternative approaches to generating spin squeezing have been proposed. One example involves using microwave fields in silicon-vacancy centers, which are similar to NV centers [Ma et al., 2021]. A universal method, introduced by [Huang et al., 2021b], is also applicable to NV centers. The method presents a generic scheme for creating spin squeezing in any non-squeezing systems through the use of periodic rotation pulses.

3.6.4 Open Quantum System Dynamics

We describe the open quantum system dynamics of the NV center by the following Lindblad master equation [Breuer et al., 2002],

$$\dot{\rho}(t) = -i\left[\hat{H}, \rho(t)\right] + \mathcal{D}_t(\rho(t)) + \mathcal{D}_d(\rho(t)), \tag{3.15}$$

where the unitary contribution to the dynamics, $\hat{H}$, is provided as follows,

- during free evolution by $\hat{H} = \hat{H}_0$,
- during spin squeezing by $\hat{H} = \hat{H}_0 + \hat{H}_\mathrm{S}$.

The NV center, while a robust quantum system, is inevitably influenced by the fluctuating states of nearby nuclear spins. These nuclear spins introduce a dynamic and unpredictable backdrop, contributing to the environmental noise that impacts the precision of measurements performed on the NV center. We assume very low temperatures relative to the NV center transition frequencies. Dephasing and thermalization are incorporated respectively through the dissipators as follows,

$$\mathcal{D}_d(\rho) = \sum_{i=1}^{N} \gamma_\mathrm{d} \left[\hat{S}_{zi}\rho(t)\hat{S}_{zi} - \rho(t)\right]; \tag{3.16}$$

$$\mathcal{D}_t(\rho) = \sum_{i=1}^{N} \gamma_t \left[\hat{S}_i^- \rho(t)\hat{S}_i^+ - \frac{1}{2}\left\{\hat{S}_i^+\hat{S}_i^-, \rho(t)\right\}\right], \tag{3.17}$$

where $\hat{S}_i^-$ is the lowering operator of the i^th NV center, and,

$$\hat{S}^- = \frac{1}{2}\left(\hat{S}_x - i\hat{S}_y\right). \tag{3.18}$$

We fix the thermalization rate, denoted by γ_t, at 20 μs, based on the literature [Abeywardana et al., 2014]. For the dephasing rate, γ_d, we will consider two scenarios: one where γ_d is 10% of the thermalization rate ($\gamma_d = 0.1\gamma_t$), and another where it is equal to the thermalization rate ($\gamma_d = \gamma_t$).

3.6.5 Spin Squeezing Parameter

The concept of spin squeezing is established by defining it as the condition where the variance of a spin component normal to the mean spin is smaller than the standard quantum limit. To quantify the extent of spin squeezing, we employ the spin squeezing parameter, as introduced by [Kitagawa and Ueda, 1993]. Kitagawa-Ueda spin squeezing brings quantum entanglement perspective (see Section 3.6.9) to the usual spin squeezing which is the reduction of spin noise in a certain direction at the cost of more noise in other directions. This criterion is given by

$$\xi^2 = \frac{4\left(\Delta \hat{J}^2_{n_\perp}\right)_{\min}}{N}, \tag{3.19}$$

where $n_\perp$ is an axis perpendicular to the mean-spin direction $\hat{n}$, N is the number of spins (in our case, $N = 2$), and $\hat{J}$ represents the collective spin operator.

Kitagawa-Ueda and other quantum correlations-based criteria of spin squeezing [Ma et al., 2011] are commonly defined for SU(2) or spin-1/2 atomic ensembles. Spin squeezing in SU(3) or spin-1 systems can be discussed in their SU(2) subgroups, such as isospin squeezing [Müstecaplıoğlu et al., 2002]. We follow a similar approach to characterize quantum correlations and spin squeezing within the manifold of $\{|0\rangle, |-1\rangle\}$. In general, spin squeezing can be optimized by rotating the coordinate frame and choosing the critical rotation angles. For simplicity, we only consider a fixed reference frame. Based on this manifold, and taking I_3 as the three-dimensional unit matrix, the spin matrices, $\hat{\sigma} = (\hat{\sigma}_x, \hat{\sigma}_y, \hat{\sigma}_z)$, are written as

$$\hat{\sigma}_x = |0\rangle\langle -1| + |-1\rangle\langle 0|, \tag{3.20}$$

$$\hat{\sigma}_y = i(|0\rangle\langle -1| - |-1\rangle\langle 0|), \tag{3.21}$$

$$\hat{\sigma}_z = |-1\rangle\langle -1| - |0\rangle\langle 0|, \tag{3.22}$$

and the collective spin, $\hat{J} = (\hat{J}_x, \hat{J}_y, \hat{J}_z)$, is defined as

$$\hat{J}_x = \frac{1}{2}(\hat{\sigma}_x \otimes I_3 + I_3 \otimes \hat{\sigma}_x), \tag{3.23}$$

$$\hat{J}_y = \frac{1}{2}(\hat{\sigma}_y \otimes I_3 + I_3 \otimes \hat{\sigma}_y), \tag{3.24}$$

$$\hat{J}_z = \frac{1}{2}(\hat{\sigma}_z \otimes I_3 + I_3 \otimes \hat{\sigma}_z). \tag{3.25}$$

To calculate spin squeezing, we calculate the mean spin squeezing direction $\hat{n}$ for the state,

$$\hat{n} = \frac{\left(\langle \hat{J}_x \rangle, \langle \hat{J}_y \rangle, \langle \hat{J}_z \rangle\right)}{|\langle \hat{J} \rangle|}. \tag{3.26}$$

And then, we take the minimal variance, $\left(\Delta \hat{J}^2_{n_\perp}\right)_{\min}$, in the perpendicular direction of $\hat{n}$. The presence of spin squeezing is characterized by $\xi^2 < 1$.

Given the initial state is oriented along the z-axis, when spin squeezing is applied, it reduces the variance in a specific direction, creating an ellipsoid shape that remains aligned with the z-axis. A $\pi/2$ pulse then shifts the spin into the x-y plane while preserving this variance ellipsoid. The effect of the magnetic field, B, is to precess the spin around the z-axis, and the x-axis twisting deforms the noise cone, effectively narrowing the spin's error ellipse. This sequence is illustrated in Figure 3.4.

3.6.6 Results

In our simulations, to quantify the precision, we employ the QuanEstimation toolbox in Python [Zhang et al., 2022] to calculate the QFI. Furthermore, for the results presented in this thesis, the magnetic field was fixed at $B = 50\,\mathrm{G}$, but similar outcome were obtained across a range of values from $5\,\mathrm{G}$ to $500\,\mathrm{G}$.

Initially, we investigate the typical Ramsey sequence for one and two NV centers, both starting in the initial state (3.13). Subsequently, after a $\pi/2$ pulse, we allow the system to undergo evolution through the free Hamiltonian H_0 for a duration of $T_{\mathrm{fr}} = 20\ \mu\mathrm{s}$, T_{fr} being the free evolution time. We choose this time taking into account the dissipative time that falls within the order of tenth of microseconds. To further enhance precision, we start again in the initial state (3.13). However, before the $\pi/2$ pulse and the free evolution, we introduce spin squeezing for the duration of T_{sq} which corresponds to the time it takes for the squeezing parameter to reach its minimum value. The two scenarios are illustrated in Figure 3.3.

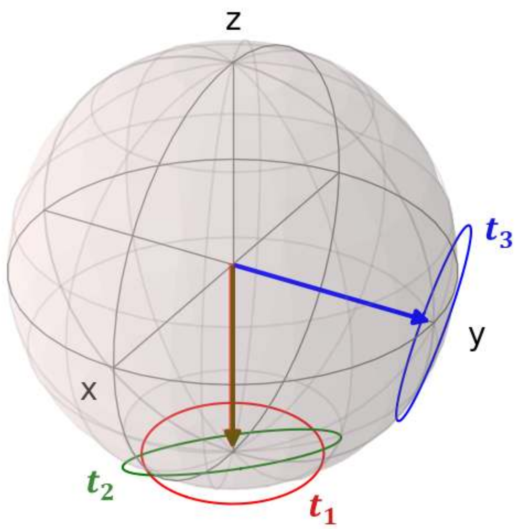

Figure 3.4: Illustration of the mean spin orientation and the variance of state preparation before the free evolution of the NV centers. At time t_1, the state is in its initial configuration (3.13) with homogeneous variance. At time t_2, the state reaches the end of the spin squeezing period, remaining aligned in the z-direction but with noise squeezed into an ellipse. Finally, at time t_3, a $\pi/2$ pulse is applied, shifting the state into the x-y plane.

3.6.7 Analysis with Spin-1 Formalism

Figure 3.5 compares one NV center without spin squeezing (blue), two NV centers without spin squeezing (red) and two NV centers with spin squeezing applied at varying strengths, specifically with squeezing constants of $c_1 = 0.25$ GHz (green) and $c_1 = 2.5$ GHz (cyan).

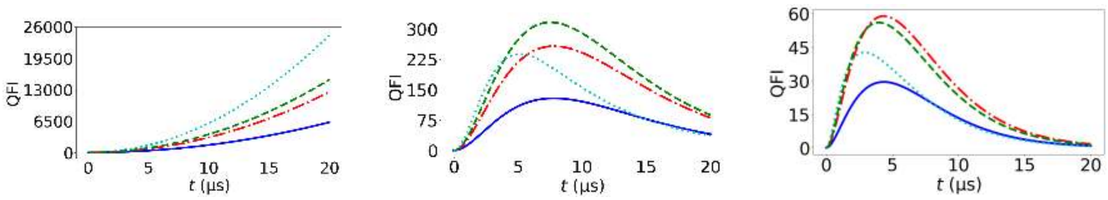

(a) (b) (c)

Figure 3.5: The Quantum Fisher Information (QFI) as a function of time, t, with $B = 50$ G for the spin-1 formalism. The curves represents the free evolution as follows: the solid blue curve corresponds to a single NV center, the dashed-dotted red curve corresponds to two NV centers, the pointed cyan curve represents two NV centers subjected to spin squeezing ($c_1 = 2.5$ GHz, $T_{\text{sq}} = 3$ ns), and the dashed green curve represents two NV centers subjected to spin squeezing ($c_1 = 0.25$ GHz, $T_{\text{sq}} = 30$ ns). The different scenarios are illustrated as: (a) without including any noise terms, (b) including thermalization and dephasing with $\gamma_t = 0.2$ MHz and $\gamma_d = 0.1\gamma_t$, and (c) including thermalization and dephasing with $\gamma_t = 0.2$ MHz and $\gamma_d = \gamma_t$.

Without spin squeezing

Figure 3.5a shows a twofold increase in the QFI when transitioning from one NV center (blue) to two NV centers (red). When environmental noise is introduced (Figures 3.5b and 3.5c), whether the QFI increases or decreases for one NV center, the twofold enhancement persists for two NV centers.

With spin squeezing

In the absence of noise (Figure 3.5a), the QFI is larger when spin squeezing is applied with squeezing constant, $c_1 = 0.25$ GHz (green). It increases further with a higher squeezing constant, $c_1 = 2.5$ GHz (cyan).

When environmental noise is introduced with $\gamma_{\text{d}} = 0.1\gamma_{\text{t}}$ (Figure 3.5b), spin squeezing remains beneficial (green), particularly at a lower squeezing constant, $c_1 = 0.25$ GHz.

This suggests that in the presence of noise, a higher squeezing constant does not necessarily lead to higher QFI. Instead, a low squeezing constant ($c_1 = 0.25$ GHz), which is sufficient enough to generate spin squeezing, is more advantageous. However, within the first 4 μs, a higher squeezing constant, $c_1 = 2.5$ GHz, provides more benefit (cyan).

Finally, Figure 3.5c shows that the advantage of squeezing is lost when the dephasing rate increases to $\gamma_{\mathrm{d}} = \gamma_{\mathrm{t}}$. While spin squeezing enhance magnetic sensing capabilities, they are also highly sensitive to environmental noise, particularly dephasing.

Analyzing the behavior of the QFI curves under such noise conditions is crucial. By identifying the time at which the QFI reaches its maximum, we can optimize experimental design and ensure measurements are performed at the peak sensitivity. Experimentally, we typically measure populations or $\langle \hat{S}_z \rangle$ values. However, it is important to note that while the QFI is calculated for the optimal Positive Operator-Valued Measure (POVM), specifically the eigenprojectors of the SLD, measuring $\hat{S}_z$ could potentially be suboptimal.

The effect of spin squeezing on the NV centers is further illustrated in Figure 3.6. The squeezing parameter, ξ^2, initially around 0.5 (below 1) at the beginning of free evolution, increases due to dephasing and thermalization during this period.

3.6.8 Analysis with Spin-1/2 Formalism

In this section, we examine the outcomes within the identical parameter scope for the spin-1/2 framework. This is achieved by concentrating on the dynamics of the states $|0\rangle$ and $|-1\rangle$. The Hamiltonian, in this context, is characterized as follows,

$$\hat{H}_0 = \sum_{i=1}^{N} \frac{\omega}{2} \hat{\sigma}_{zi}, \tag{3.27}$$

where $\omega = D - g_S B_z$ and $\hat{\sigma}_i = (\hat{\sigma}_{xi}, \hat{\sigma}_{yi}, \hat{\sigma}_{zi})$ are the Pauli matrices for the i^{th} NV center.

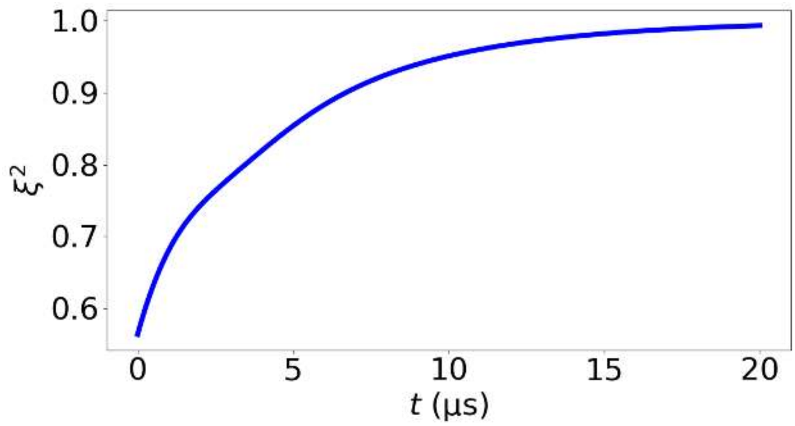

Figure 3.6: The squeezing parameter, ξ^2, for the spin-1 formalism, as a function of time, t, during the free evolution of two NV centers subjected to spin squeezing with $c_1 = 2.5$ GHz for a time of $T_{\rm sq} = 3$ ns, including thermalization and dephasing with $\gamma_t = 0.2$ MHz, $\gamma_d = 0.1\gamma_t$, and $B = 50$ G.

The parameters and open quantum system dynamics are kept same as in the spin-1 model. Eq. (3.16) and Eq. (3.17) are modified respectively to

$$\mathcal{D}_d(\rho) = \sum_{i=1}^{N} \gamma_{\rm d} \left[\hat{\sigma}_{zi}\rho(t)\hat{\sigma}_{zi} - \rho(t)\right]; \tag{3.28}$$

$$\mathcal{D}_t(\rho) = \sum_{i=1}^{N} \gamma_t \left[\hat{\sigma}_i^- \rho(t)\hat{\sigma}_i^+ - \frac{1}{2}\left\{\hat{\sigma}_i^+\hat{\sigma}_i^-, \rho(t)\right\}\right], \tag{3.29}$$

where $\hat{\sigma}_i^\pm$ are the Pauli spin ladder operators for the $i^{\rm th}$ NV center. The spin squeezing Hamiltonian (3.14) is modified to

$$\hat{H}_{\rm S} = c_1 \left(\sum_{i=1}^{N} \hat{\sigma}_{xi}\right)^2. \tag{3.30}$$

The initial state of the NV center is taken in the excited state $|-1\rangle$. Then each NV center undergoes an $\pi/2$ pulse, achieved by applying a rotation operator,

$$\mathrm{e}^{-i\frac{\pi}{2}\hat{\sigma}_x}.$$

As in the spin-1 formalism, if spin squeezing is added, it is applied before the $\pi/2$ pulse. We then proceed to analyze the QFI under both scenarios (with and without squeezing), considering the presence and absence of noise.

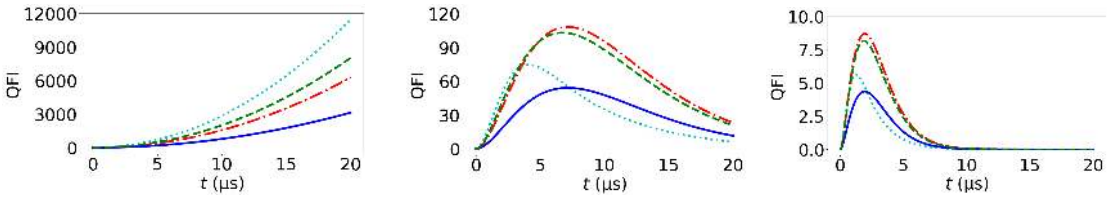

(a) (b) (c)

Figure 3.7: The Quantum Fisher Information (QFI) as a function of time, t, with $B = 50$ G for the spin-1/2 formalism. The curves represents the free evolution as follows: the solid blue curve corresponds to a single NV center, the dashed-dotted red curve corresponds to two NV centers, the pointed cyan curve represents two NV centers subjected to spin squeezing ($c_1 = 2.5$ GHz, $T_{\text{sq}} = 3$ ns), and the dashed green curve represents two NV centers subjected to spin squeezing ($c_1 = 0.25$ GHz, $T_{\text{sq}} = 30$ ns). The different scenarios are illustrated as: (a) without including any noise terms, (b) including thermalization and dephasing with $\gamma_t = 0.2$ MHz and $\gamma_d = 0.1\gamma_t$, and (c) including thermalization and dephasing with $\gamma_t = 0.2$ MHz and $\gamma_d = \gamma_t$.

In Figure 3.7a, we observe that without considering any noise channel, spin squeezing yields a higher QFI. However, in the presence of noise (Figure 3.7b and Figure 3.7c), the advantages of spin squeezing are lost even for small dephasing (Figure 3.7b), and Ramsey sequence without spin squeezing is more beneficial. Earlier in Figure 3.5b, for the qutrit case, we observed advantages even in the presence of dephasing. Therefore, the benefits of using qutrit sensors over qubit sensors are clearly evident.

3.6.9 Entanglement

Spin squeezing is closely tied to the creation of entanglement [Tóth et al., 2009, Sirsi, 2004, Vitagliano et al., 2014]. A previous study suggests that initial squeezing can aid in entanglement [Pradana and Chew, 2021]. Our results are consistent with this suggestion.

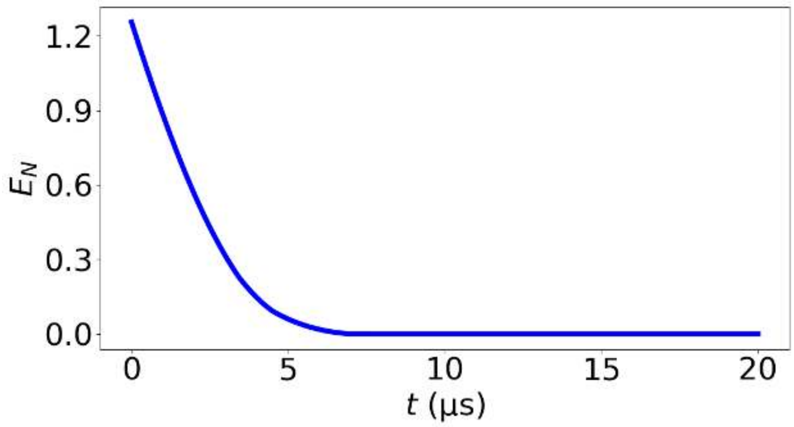

Figure 3.8: The logarithmic negativity, E_N, for the spin-1 formalism, as a function of time, t, during the free evolution of two NV centers subjected to spin squeezing with $c_1 = 2.5$ GHz for a time of $T_{\rm sq} = 3$ ns, including thermalization and dephasing with $\gamma_t = 0.2$ MHz, $\gamma_d = 0.1\gamma_t$, and $B = 50$ G. Entanglement appears when $E_N > 0$ at the start of free evolution which is right after the application of spin squeezing. Afterward, entanglement decreases due to noise.

For higher-dimensional systems than qubits, some entanglement measures exist. The logarithmic negativity (2.6) is related to the negativity and serves as a good indicator of the degree of entanglement in our system.

In Figure 3.8, we observe that the application of spin squeezing to the two NV centers system creates an entanglement between them. This entanglement is illustrated by an increase in the logarithmic negativity during the application of spin squeezing. During free evolution, this entanglement decreases due to environmental noise. Thus, the creation of spin squeezing in our spin-1 systems is accompanied by the creation of entanglement.

3.7 Integrating NV Centers with Responsive Hydrogels for High-Precision Biological Measurements

Responsive materials have captured the attention of researchers due to their vast potential in various fields, including tissue engineering, biological coatings, drug delivery, and biosensing [Petrini et al., 2020]. Among these, hydrogels stand out for their unique properties and exceptional compatibility with biological systems.

3.7.1 Hydrogels

Hydrogels are interesting due to the following characteristics [Hendrickson and Lyon, 2009].

- Highly adaptable in water: Hydrogels exhibit remarkable flexibility within watery environments. Their networks can be precisely adjusted both mechanically and chemically. This inherent biocompatibility makes them ideal candidates for a wide range of biological applications.

- Tunable and responsive: The behavior of hydrogel constructs can be finely tuned, with responsiveness being a crucial feature for bio-applications. By carefully selecting the building blocks (monomers and cross-linkers) during synthesis, hydrogels can be engineered to be inherently responsive to specific stimuli.

Common responsive hydrogels include thermo-responsive and pH-responsive types. Thermo-responsive hydrogels undergo dramatic changes in structure (phase transitions) at specific temperatures [Klouda and Mikos, 2008]. In contrast, pH-responsive hydrogels respond to changes in pH and salt content by altering their intermolecular electrostatic interactions, causing them to swell or shrink [Gupta et al., 2002].

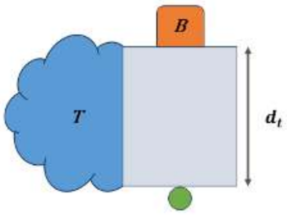

(a)

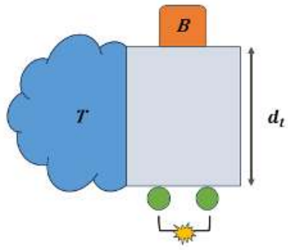

(b)

Figure 3.9: Schematic representation of the experimental setup: the blue cloud represents the biological system at temperature T, the gray box signifies the hydrogel with a thickness of d_t, the orange box denotes the static magnetic source B, and the green disc represents the NV center. (a) Configuration for a single NV center. (b) Configuration for two entangled NV centers, with entanglement symbolized by the yellow star.

3.7.2 Choosing The Right Bioresponsive Material

While thermo-responsive and pH-responsive hydrogels are beneficial for certain applications, selecting a bioresponsive material should be based on the specific biological stimulus, such as differences in redox potential, glucose level, antigen-antibody binding, enzyme-substrate interactions, and ionic strengths [Lu et al., 2016]. Appropriate stimuli-responsive mechanisms should be chosen according to the application, considering that stimuli-triggered responses can result in physical changes (such as swelling/shrinking or assembling/dissociating), chemical changes (such as degradation), or a combination of both.

To design effective hydrogels, we need to evaluate response efficacy (high selectivity, sensitivity, and spatiotemporal control) and translation potential (stability, biocompatibility, and scalability). In addition, selecting appropriate bioresponsive modalities based on application needs by using biomimetics or bioinspired approaches, and considering interactions between materials, devices, and the biological environment are crucial to refining design strategies.

3.7.3 Our Proposal

Our objective is to employ quantum sensing with NV centers to access biological information. Initially, we will focus on hydrogels due to their physical response to stimuli, though other materials may be considered in the future. The idea is to incorporate a hydrogel, whose thickness changes in response to the biological functions that we are interested in gauging.

As illustrated in Figure 3.9a, a magnetic source is positioned such that it is separated from the NV center by the hydrogel, which is in turn placed near our biological system, and hence influenced by it. When the biological system undergoes a change in function, the hydrogel undergoes a phase transition, resulting in a change in thickness. The NV center's ability to sense the change in magnetic field enables the determination of the system's temperature or other characteristics. The use of uncorrelated NV centers has already been discussed in the literature [Zhang et al., 2018]. Our objective is to advance this approach by utilizing correlated NV centers, focusing on two NV centers (Figure 3.9b).

As an example, if we want to measure, in an experiment, the temperature using a hydrogel as a transducer, it is feasible to conduct heating-cooling cycles at predetermined temperatures. This procedure allows for the construction of a calibration curve establishing the correlation between hydrogel thickness (d_t) and temperature (T) [Zhang et al., 2018]. This same method can be adapted for the biological function we want to access.

The preliminary results from Section 3.6 indicate that quantum correlations, such as spin squeezing, can enhance the accuracy of magnetic field sensing. Furthermore, integrating hydrogels may provide additional benefits by exploiting these quantum correlations to improve existing NV-center-based magnetic sensing techniques for biological functions. However, at this stage it is under investigation. Further inquiry is necessary to determine the feasibility of this scenario.

3.8 Conclusion

We have examined the potential of Nitrogen-Vacancy (NV) centers as quantum sensors for magnetic fields, elucidating various methodologies involving single and paired NV centers, using both qubit and qutrit models, and employing spin squeezing within Ramsey or Ramsey-type pulse sequence protocols. Throughout our investigation, we have analyzed the dynamics of Quantum Fisher Information (QFI) across these scenarios, utilizing the Lindblad master equation to model the spin system's evolution under dephasing and thermalizing noise.

Incorporating a spin squeezing step in magnetometric measurement and utilizing qutrit NV centers have demonstrated a precision increase relative to standard Ramsey magnetometry. However, the advantage of spin squeezing was notably sensitive to the dephasing environment. Our numerical analysis showed that, as dephasing increased, the advantages became marginal compared to standard methods. We also observed that moderate squeezing results in higher QFI compared to strong squeezing, which was only beneficial for a brief period of free evolution. Furthermore, by conducting the entire analysis using the spin-1/2 formalism and comparing it with the spin-1 formalism, we have demonstrated the advantages of utilizing a qutrit system over a qubit system.

Additionally, we have observed that spin squeezing was accompanied by the generation of entanglement, aligning with the general expectation of quantum entanglement as a metrological resource. However, further investigation would be needed to determine whether it was spin noise distribution or entanglement alone that caused the precision limit enhancement.

Our findings may contribute to the broader exploration of quantum technologies beyond qubits, where qutrits and higher-dimensional qubits (qudits) are increasingly considered, particularly in the context of quantum computing [Ogunkoya et al., 2024, Xu et al., 2024]. An intriguing question persists regarding the scalability of these advantages, especially regarding the utilization of NV center qutrit ensembles or the investigation of higher-level systems (qudits). These avenues pose exciting challenges for future studies, promising further insights.

Finally, we have proposed how to adapt magnetic sensing to various biological functions. While hydrogels are a promising avenue, we should also research other bioresponsive materials. This opens up exciting possibilities for NV centers in achieving precise and adaptable quantum sensing across biology and other domains.

Chapter 4

QUANTUM LIGHT AS A BIOLOGICAL PROBE

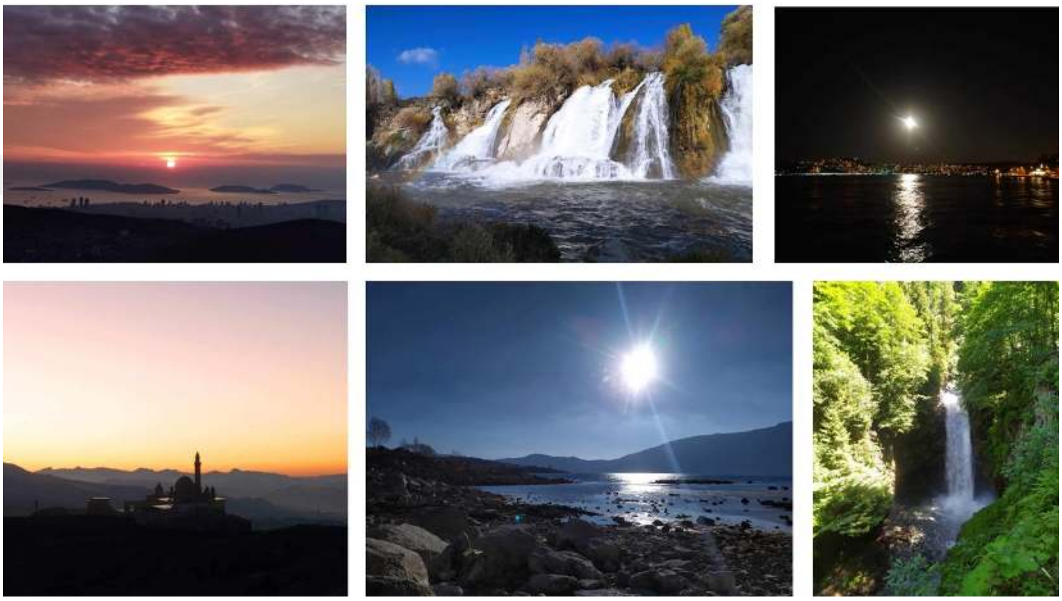

4.1 Introduction to Vision

The very origin of the field of Optics is the eye. “Optike” is a greek word which means look. Water was used by ancient Romans and Greeks to create lenses [Plantzos, 1997]. The history of lenses goes even further backwards in time [Calvo and Enoch, 2005]. However, there were many misconceptions about how the eye perceives what it sees. One of the probably most known theories originates partly from Plato who expressed in a poetic language the so-called emission theory based on fire which can be summarized as, the eyes emitting light rays generate the sensation that we refer as “seeing” [Darrigol, 2012].

A new era of experimental optics started when Alhazen [Lindberg, 1967] presented observations and experiments in the eleventh century that not only contradicts the emission theory but demonstrates the opposite, that is, light rays are reflected from every "visible" object and they travel in straight lines going in every possible direction and thus can enter the eye [Darrigol, 2012].

Actually, if one thinks about it, the eye being also a visible object itself, doesn't Alhazen's demonstrations also imply that light is reflected from every eye and that is, for example, how we perceive the colours of human eyes as blue eyes, brown eyes, etc? One can deduce that no theory is completely wrong or completely right and thanks to that, our knowledge resources as a human race keeps evolving through all these centuries until today where we now have quantum optics [Agarwal, 2012, Bachor and Ralph, 2019] and photonics [Saleh and Teich, 2019] as well established scientific fields of research. Quantum optics is a cross-pollination of the field of quantum physics and that of optics.

Quantum physics became prevalent in the nineteenth century with Max Plank's explanation of black-body radiation [Klein, 1961] which was soon confirmed in the following century by Albert Einstein's experiment on photoelectric effect [Einstein, 2016]. Since then, the concept of observation [Zeh, 1973, Bloch, 1967] or seeing reality has greatly been influenced by the continuous development of quantum theory [Park, 2012]. Do we "see" atoms and electrons or can we simply predict their instantaneous positions based on probability? Heisenberg [Busch et al., 2007] and Schrödinger [Duan, 2019], among many others, attempted to answer these questions with their contributions to the field. Schrödinger was also responsible for two key terms of this discussion, entanglement [Paneru et al., 2020] and coherent state [Zhang et al., 1990, Sanders, 1992] which would later give rise to research about squeezed states [Walls, 1983]. With the further advancement of quantum mechanics, the question revolved no more only around, "how do we see" but also "what do we see". Quantum optics deals with the interaction of light and matter [Mekhov and Ritsch, 2012] and that is the very essence of what happens when light enters the human eye [Holmes et al., 2018].

However, first one should ask, is seeing a classical or quantum process [Khoshbin-e Khoshnazar, 2014]? With respect to our topic, the main difference between classical and quantum that is necessary to point out is the level of uncertainty that is introduced along with the measurement of a quantum state unlike with that of a classical state which remains unaffected when recorded with utmost certainty. The change in properties of the quantum state during its measurement opens room to various counter-intuitive hypotheses and theories, some of them having been proven by experiment and others still debatable or falling into the category of philosophical science [Koch and Hepp, 2006]. As far as possible, we will only consider the empirical cases. Nevertheless, one is encouraged to stay tuned to research development which is slowly but surely touching upon the philosophical aspect [Rosen, 2021] and bridging the missing gaps [Cordero, 2019]. One such topic that this thesis deals with is entanglement [Brody, 2020].

Quantum entanglement [Horodecki et al., 2009] is such a phenomenon whereby two or more states are non-separable and non-local [Buscemi, 2012]. Two or more particles are said to be non-local if they behave in a connected way despite being far apart from each other. This is often referred to as "spooky action at a distance" [Hardy, 1998], a famous expression from A. Einstein. On the other side, if we have a system in which the state of all the particles cannot be individually separated, then this system is said to be non-separable. Empirical data for quantum entanglement is widely available and this is therefore a well established and well accepted concept in the scientific community [Plenio and Virmani, 2014]. In particular to the field of quantum optics, systems involving more than two photons have been successfully tested for the presence of quantum entanglement.

Despite all the advancements in quantum optics, the initial queries about sight have evolved but have not been solved. Nowadays, the visual threshold is being discussed and this has been taking place over a century [Hecht et al., 1941]. The question whether human can detect a single photon is a very interesting subject that is still being unearthed [Tinsley et al., 2016a]. Some research groups such as [Vivoli et al., 2016] have focused their research on whether human can or cannot detect entanglement. The investigation into the human visual system's sensitivity to the quantum properties of light and its impact on visual functions has been a long-standing area of interest [Bouman, 2012, Pugh, 2018]. In-vitro studies have shown that rod cells are capable of detecting individual photons [Rieke and Baylor, 1998, Yau et al., 1977, Baylor et al., 1979a, Baylor et al., 1979b, Baylor et al., 1984, Reingruber et al., 2013, Phan et al., 2014, Sim et al., 2012]. However, early psychophysical experiments in dark adaptation conditions suggested that while humans can detect a single photon in their retina, visual perception only becomes possible when a threshold of several photons is reached [Hecht et al., 1942, van der Velden, 1946, Barlow, 1956, Sakitt, 1972, Teich et al., 1982a, Prucnal and Teich, 1982, Teich et al., 1982b]. The earliest experimental estimate of this threshold is five to seven photons [Hecht et al., 1942]. Later studies revealed that the visual threshold and noise in the visual pathway are connected and it is crucial to take into account the dark counts, false positives and experimental uncertainties in general, in order to interpret and understand the data collected in the psychophysical experiments [Barlow, 1956, Sakitt, 1972, Teich et al., 1982a, Prucnal and Teich, 1982, Teich et al., 1982b, Barlow, 1977, Donner, 1992, Lillywhite, 1981, Field et al., 2005]. Recent research suggests that humans may have the ability to directly perceive a single photon with a probability greater than 50%, and that this efficiency increases with earlier photon absorption [Tinsley et al., 2016b].

These intriguing findings present the potential for the use of quantum technologies, particularly quantum metrology, in biometry [Loulakis et al., 2017, Kominis et al., 2022], the study of retinal circuits [Pedram et al., 2022], the diagnosis of visual and brain disorders [Archibald et al., 2009], and for exploring the boundaries of classical and quantum theories [Brunner et al., 2008]. The quantum parameter estimation theory can predict biometric signatures, such as variations in photodetection efficiency among individuals, and is secure against classical measurements [Loulakis et al., 2017]. The degeneration of retinal tissue has been identified as an early indicator of neurodegenerative diseases like Parkinson's, highlighting the need for more precise and sensitive quantum optical techniques for imaging the retina [Archibald et al., 2009]. [Berchera and Degiovanni, 2019a] investigated the use of sub-Poissonian, low-photon flux light for creating high-resolution images of the retina. It was also demonstrated that the retinal network can be treated as a convolutionary neural network and that its parameters can be estimated more accurately using sub-Poissonian quantum light distributions, such as Fock states [Pedram et al., 2022]. The advantages of quantum technologies have become increasingly significant with increased quantum entanglement.

Our aim is to determine if human subjects can perceive higher-dimensional, quantum entangled photons through psychophysical experiments, starting with the simpler case of bipartite entangled states before considering tripartite entangled states to understand the impact of psychophysical conditions.

[Brunner et al., 2008] proposed the detection of bipartite entangled states in a Bell experiment through the use of human eyes modeled as threshold photodetectors. However, they found that for a more accurate eye model that accounted for the smooth probability of seeing, postselection was necessary to verify the violation of the Bell inequality. [Sekatski et al., 2009] demonstrated that the violation of the Bell inequality could be confirmed without postselection by amplifying one photon of an entangled pair through stimulated emission.

[Vivoli et al., 2016] created an entanglement witness to assess the ability of the human eye to detect bipartite photonic entanglement. They proposed an interferometric setup that amplifies low photon numbers with coherent state generators before detection by the human eye. Building on this methodology, [Dodel et al., 2017] showed that it is possible to detect non-classical (sub-Poissonian) light states using human eyes as photodetectors.

[Sarenac et al., 2020a] experimentally demonstrated that human subjects can distinguish between two polarization-coupled Orbital Angular Momentum (OAM) states when viewing a structured light beam. More recently, it was demonstrated that human subjects can perceive different OAM modes created through Pancharatnam-Berry phases [Sarenac et al., 2022b].

We present a detection method for entangled optical states, both bipartite and tripartite. We use the bipartite interferometry setup and the bipartite entanglement witness of [Riccardi et al., 2020] to investigate whether humans can detect bipartite entanglement. Afterward, we extend the interferometer to measure tripartite W state entanglement witness [Bourennane et al., 2004] and find out whether human subjects can detect such multipartite entanglement.

In our photodetection scheme, we model human subjects as biological photodetectors and incorporate the noise due to photon loss in the eye and the additive noise due to false positive into the "probability of seeing" distributions. Our results suggest that the detection of entangled quantum light is possible for a range of noise levels and, more critically, the visual threshold.

Finally, we explore amplitude squeezing as an alternative approach for amplification [Sundar, 1996, Dantas et al., 1998], but we find that it does not improve performance in our specific setting. However, with further advancements in quantum optics and the potential to develop a perfect photon amplifier that could then be used instead of displacement operations in the future, our results could be improved significantly.

Overall, Chapter 4 expounds on the exciting potential of quantum light as a tool for probing biological systems. Section 4.2 lays the groundwork of understanding light from a quantum perspective and how with the help of statistics, it can be used as a metrological tool and thus be beneficial to applications in biology. Section 4.3 introduces the concept of entanglement witnesses, focusing on tripartite versions. It also briefly covers bipartite entanglement witnesses and some of the challenges of experimental implementation. Following this, Section 4.4 discusses the intriguing concept of ideal photon amplifiers, which can have significant implications across various fields. The chapter then presents novel research work in Section 4.5 about human eye's ability to detect entanglement in a psychophysical experiment. To wrap up, Chapter 4 concludes with a summary in Section 4.6.

4.2 Quantum Light and Metrology

4.2.1 Light from Quantum Perspective

While classical optics describes light as a continuous wave, the quantum theory suggests a more granular picture. The electromagnetic field, responsible for light propagation, can be quantized. This means the field can exist in discrete energy states represented by photons. Light, therefore, can be viewed as a collection of photons, each with a specific energy, E, and momentum, p, as described by the equations:

$$E = h\nu, \quad \text{and} \quad p = \frac{h}{\lambda}, \tag{4.1}$$

where h is Planck's constant, ν is the frequency, and λ is the wavelength of light [Gerry and Knight, 2023].

When two light beams overlap, they can interfere, leading to constructive or destructive interactions depending on their relative phases. In classical optics, interference relies on the well-defined phases of the waves. The quantum nature of light introduces a new layer of complexity. Photons can exhibit wave-like interference even if they arrive at the detector one at a time. This phenomenon, known as quantum interference, requires a high degree of coherence between the photons.

Coherent photons essentially maintain a fixed phase relationship, allowing for constructive or destructive interference.

Furthermore, the quantum theory of light also encompasses the concept of entanglement, where the quantum states of individual photons can become interlinked, such that the state of one photon instantly influences the state of another, regardless of the distance separating them. This entanglement leads to non-classical correlations between photons that are fundamental to many quantum optics experiments and applications, such as quantum cryptography and quantum computing [Zeilinger, 2007, Schimpf et al., 2021, O'brien, 2007].

To quantize the field, the classical description of the electromagnetic field in terms of its vector potential, $\mathbf{A}(\mathbf{r}, t)$, is expanded in terms of plane wave solutions,

$$\mathbf{A}(\mathbf{r}, t) = \sum_{\mathbf{k},\lambda} \left(\mathbf{e}_{\mathbf{k},\lambda} A_{\mathbf{k},\lambda} e^{i(\mathbf{k}\cdot\mathbf{r}-\omega t)} + \text{c.c.} \right), \tag{4.2}$$

where $\mathbf{k}$ is the wave vector, λ represents the polarization state, ω is the angular frequency, $\mathbf{e}_{\mathbf{k},\lambda}$ is the polarization vector, $A_{\mathbf{k},\lambda}$ are the mode amplitudes, and c.c. stands for complex conjugate. To quantize the field, these mode amplitudes are replaced by operators. The field becomes a sum over quantized modes,

$$\mathbf{A}(\mathbf{r}, t) = \sum_{\mathbf{k},\lambda} \sqrt{\frac{\hbar}{2\epsilon_0 V \omega}} \left(\mathbf{e}_{\mathbf{k},\lambda} \hat{a}_{\mathbf{k},\lambda} e^{i(\mathbf{k}\cdot\mathbf{r}-\omega t)} + \mathbf{e}^*_{\mathbf{k},\lambda} \hat{a}^\dagger_{\mathbf{k},\lambda} e^{-i(\mathbf{k}\cdot\mathbf{r}-\omega t)} \right), \tag{4.3}$$

where $\hat{a}_{\mathbf{k},\lambda}$ and $\hat{a}^\dagger_{\mathbf{k},\lambda}$ are the annihilation and creation operators respectively, $\hbar$ is the reduced Planck's constant, ϵ_0 is the vacuum permittivity, and V is the quantization volume. These operators obey the following commutation relations,

$$\left[\hat{a}_{\mathbf{k},\lambda}, \hat{a}^\dagger_{\mathbf{k}',\lambda'}\right] = \delta_{\mathbf{k},\mathbf{k}'} \delta_{\lambda,\lambda'}, \tag{4.4}$$

$$\left[\hat{a}_{\mathbf{k},\lambda}, \hat{a}_{\mathbf{k}',\lambda'}\right] = \left[\hat{a}^\dagger_{\mathbf{k},\lambda}, \hat{a}^\dagger_{\mathbf{k}',\lambda'}\right] = 0. \tag{4.5}$$

The quantized field Hamiltonian can then be written as

$$\hat{H} = \sum_{\mathbf{k},\lambda} \hbar\omega \left(\hat{a}^\dagger_{\mathbf{k},\lambda} \hat{a}_{\mathbf{k},\lambda} + \frac{1}{2} \right), \tag{4.6}$$

where the term $\frac{1}{2}$ represents the zero-point energy of the field.

The creation operator $\hat{a}^\dagger_{\mathbf{k},\lambda}$ adds a photon to the mode $(\mathbf{k}, \lambda)$, and the annihilation operator $\hat{a}_{\mathbf{k},\lambda}$ removes a photon from the mode. This formalism is crucial for describing the interaction of light with matter, such as in the processes of absorption and emission of photons by atoms and molecules. The spontaneous and stimulated emission processes, which are fundamental to laser operation, can be understood through the action of these operators [Mandel and Wolf, 1995].

In summary, the quantum perspective on light not only incorporates the granular nature of photons but also unveils a rich array of phenomena such as quantum interference, entanglement, and the quantization of the electromagnetic field. These concepts form the bedrock of modern quantum optics and have profound implications for technology and our understanding of fundamental physics.

4.2.2 Sub-Poissonian Light

Light sources typically exhibit Poissonian statistics, meaning the number of emitted photons follows a random distribution with a variance equal to the mean. However, a fascinating class of light sources known as sub-Poissonian light sources defies this classical behavior. These sources emit light with a variance less than the mean, leading to a more controlled and well-defined photon emission pattern.

To quantify the degree of sub-Poissonian character, we utilize the second-order coherence function, also known as the Glauber correlation function, $g^{(2)}(\tau)$ [Glauber, 1963]. This function describes the probability of detecting two photons separated by a time delay, τ. For a perfectly coherent (ideal) source with single photons emitted in a well-defined state, $g^{(2)}(0) = 0$. This indicates that there is no chance of detecting two photons simultaneously ($\tau = 0$). In contrast, a classical Poissonian source has $g^{(2)}(0) = 1$, reflecting the random nature of photon emission. Sub-Poissonian sources lie between these extremes, with $0 < g^{(2)}(0) < 1$. The lower the value of $g^{(2)}(0)$, the stronger the sub-Poissonian character.

The quest for sub-Poissonian light has led to the development of various quantum light sources [Klauder and Sudarshan, 2006, Garrison and Chiao, 2008]:

- Lasers below threshold: Lasers typically operate above the threshold, generating a large number of photons with Poissonian statistics. However, operating a laser slightly below the threshold can lead to sub-Poissonian light emission due to the suppression of spontaneous emission processes [Kovalenko et al., 2023].

- Squeezed states: Through specific techniques like parametric down-conversion, light can be manipulated into "squeezed states" where the uncertainty in one quadrature (e.g., amplitude or phase) is reduced at the expense of the other. This squeezing can lead to sub-Poissonian light in one quadrature [Teich and Saleh, 1989].

- Single-photon sources (Ideal single-photon sources): Exactly one photon is emitted per excitation event. This represents the ultimate form of sub-Poissonian light with $g^{(2)}(0) = 0$. While achieving perfect efficiency is challenging, sources like cavity-enhanced spontaneous parametric down-conversion [Christ et al., 2013, Couteau, 2018] and single-photon emitters based on quantum dots [Sapienza et al., 2015, Senellart et al., 2017] come close to this ideal model.

By harnessing sub-Poissonian light sources, researchers in quantum optics [Gerry and Knight, 2023, Davidovich, 1996] unlock new possibilities in areas like:

- Quantum Information Processing: Precise control over photon number fluctuations is crucial for reliable quantum communication and computation [Giacobino et al., 1989]. Sub-Poissonian sources offer superior fidelity compared to classical light sources.

- High-Precision Metrology: The reduced noise level of sub-Poissonian light allows for enhanced sensitivity in interferometric measurements, leading to more accurate sensors and instruments [Berchera and Degiovanni, 2019b, Vahlbruch et al., 2007].

Techniques like interferometry can be used to create entangled light, which is a special type of quantum light and follows the sub-Poissonian distribution. Two or more photons are linked in a way that their properties, such as polarization, are correlated. Interferometry can manipulate the interaction of these photons, leading to a situation where a measurement of one photon instantly determines the state of the others. These possibilities allow scientists to devise scenarios using entangled light to probe biological systems with higher precision.

4.2.3 Applications in Biology

Light has always been a principal tool for probing the environment. The simple act of seeing involves our eyes as light sensors to observe the surroundings. Over time, various methods have been developed to probe biological systems with greater precision and detail.

Polarization techniques have been crafted for decades in biological and clinical research [He et al., 2021]. These techniques quantify the variation of light caused by objects, making them useful due to their non-invasive and sensitive nature. Applications of polarized light include cancer detection, cell studies, and more [Le Gratiet et al., 2021, Tuniyazi et al., 2021, Peyvasteh et al., 2021].

The optical microscope, which uses visible light and a system of lenses to produce magnified images of small objects, is a fundamental tool in biological research [Webb, 1996]. Advances in microscopy, such as Two-Photon Microscopy, have significantly enhanced our ability to observe cells and tissues, including applications in neuroscience [Helmchen and Denk, 2005, Rubart, 2004, Svoboda and Yasuda, 2006]. Fluorescence microscopy has also provided detailed insights into biological systems [Yuste, 2005]. Currently, the exploration of quantum light is opening new possibilities for achieving even greater precision. For example, entanglement-enhanced microscopy is being investigated for its potential to provide highly detailed images [Ono et al., 2013]. The use of OAM light to probe vision [Sarenac et al., 2020b, Sarenac et al., 2022b, Gerry and Knight, 2023, Pedram et al., 2024b] or tissues [Ono et al., 2013] is also being explored.

Quantum polarimetry is another promising area of biophysics [Pedram et al., 2024a]. For instance, polarization-entangled photon pairs are used to gauge living microorganisms in microfluidic environments [Besaga et al., 2024], and photon entanglement is employed to examine monolayer cultures of mammalian cells [Zhang et al., 2024a]. Quantum imaging of biological organisms through spatial and polarization entanglement is also being researched [Zhang et al., 2024b]. Moreover, spectroscopy with entangled photons has potential biological applications [Eshun et al., 2022].

Entanglement appears to be a key quantum aspect in all of these undertakings. Various properties of light, such as its polarization and spatial characteristics, can be entangled. Squeezed light is also being explored for biological systems, with applications in tracking and sensing [Lawrie et al., 2019, Xu et al., 2019b].

In summary, the progression from classical to quantum light techniques is paving the way for unprecedented insights into biological systems, pushing the boundaries of what could be achieved in biomedical research.

4.3 Entanglement Witness

Entanglement witnesses are a class of observables that are used to detect the presence of entanglement in quantum systems. They are called witnesses because they provide evidence of entanglement without revealing the entangled state itself. They are observables that allow the detection of entanglement in quantum systems.

An entanglement witness for n-partite entanglement is an observable that yields a positive expectation value for states exhibiting $(n-1)$-partite entanglement, while producing a negative expectation value for n-partite entangled states. Witnesses offer sufficient criteria for detecting entanglement and distinguishing between the various classes of multipartite entangled states [Chruściński and Sarbicki, 2014].

A general framework for deriving multipartite witness operators and breaking them into observables that are locally measurable has been established [Tóth and Gühne, 2005]. This method demonstrates how local projective measurements, even in multipartite systems, can be used to implement these witness operators in experimental contexts.

A general witness operator that detects genuine multipartite entanglement of a pure state, ψ, in the presence of noise, is defined as

$$W = \alpha \mathbb{1} - |\psi\rangle \langle\psi| , \tag{4.7}$$

with $\mathbb{1}$ being the identity operator, and α being given by

$$\alpha = \max_{\phi \in B} | \langle\phi| |\psi\rangle |^2, \tag{4.8}$$

where B is the set of biseparable states, ϕ. For any biseparable state ρ_B, this approach ensures that $\mathrm{Tr}(W |\psi\rangle \langle\psi|) < 0$ and that $\mathrm{Tr}(W\rho_B) = 0$. Therefore, it is evident that multipartite entanglement is carried by the state ψ when the observable W has a negative expectation value. Explicitly maximizing the overlap with any biseparable state can make determining α a challenging process.

For the experimental implementation of the witness, it is essential to decompose it into multiple local von Neumann (or projective) measurements. Each observable, which serves as the basis for the relevant von Neumann measurement, can be measured with a single setting (Section 4.5.2) of the measuring devices. To achieve "optimal" results, the number of projective measurements in the decomposition should be minimized.

4.3.1 Tripartite Entanglement Witness

For example, if we consider the tripartite entanglement state, W state,

$$|\mathrm{W}\rangle = \frac{1}{\sqrt{3}}(|001\rangle + |010\rangle + |001\rangle), \tag{4.9}$$

the entanglement witness becomes

$$W_1 = \frac{2}{3}\mathbb{1} - |\mathrm{W}\rangle \langle\mathrm{W}| . \tag{4.10}$$

In both completely separable and biseparable states, its expectation value is positive. As a result, it recognizes all states that fall into the W class and the GHZ class, the two classes of states that have true tripartite entanglement, but it does not differentiate between them. The largest squared overlap between the W state and biseparable states is represented by the factor 2/3. The witness may be reformulated as follows, in terms of Pauli matrices,

$$\begin{aligned} W_1 = \frac{1}{24}[&17 \cdot \mathbb{1} \otimes \mathbb{1} \otimes \mathbb{1} + 7 \cdot \sigma_z \otimes \sigma_z \otimes \sigma_z \\ &+ 3 \cdot (\sigma_z \otimes \mathbb{1} \otimes \mathbb{1} + \mathbb{1} \otimes \mathbb{1} \otimes \sigma_z + \mathbb{1} \otimes \sigma_z \otimes \mathbb{1}) \\ &+ 5 \cdot (\sigma_z \otimes \sigma_z \otimes \mathbb{1} + \sigma_z \otimes \mathbb{1} \otimes \sigma_z + \mathbb{1} \otimes \sigma_z \otimes \sigma_z) \\ &- (\mathbb{1} + \sigma_x + \sigma_z) \otimes (\mathbb{1} + \sigma_x + \sigma_z) \otimes (\mathbb{1} + \sigma_x + \sigma_z) \\ &- (\mathbb{1} + \sigma_z - \sigma_x) \otimes (\mathbb{1} + \sigma_z - \sigma_x) \otimes (\mathbb{1} + \sigma_z - \sigma_x) \\ &- (\mathbb{1} + \sigma_y + \sigma_z) \otimes (\mathbb{1} + \sigma_y + \sigma_z) \otimes (\mathbb{1} + \sigma_y + \sigma_z) \\ &- (\mathbb{1} + \sigma_z - \sigma_y) \otimes (\mathbb{1} + \sigma_z - \sigma_y) \otimes (\mathbb{1} + \sigma_z - \sigma_y)]. \end{aligned} \tag{4.11}$$

Finding such a decomposition and proving its optimality is technically demanding as illustrated by [Gühne and Hyllus, 2003].

4.3.2 Distinguishing Between Two Classes of Tripartite Entanglement

We may look at an additional witness, W_2, that, using the same set of local data, can identify true tripartite entanglement and discriminate between the W and GHZ states.

$$W_2 = \frac{1}{2}\mathbb{1} - |\overline{\text{GHZ}}\rangle \langle\overline{\text{GHZ}}|, \tag{4.12}$$

where

$$|\overline{\text{GHZ}}\rangle = \frac{1}{2}(|\overline{000}\rangle + |\overline{111}\rangle), \tag{4.13}$$

with

$$\begin{aligned} |\overline{0}\rangle &= \frac{1}{2}(|0\rangle + i\,|1\rangle); \\ |\overline{1}\rangle &= -\frac{1}{2}(|0\rangle - i\,|1\rangle). \end{aligned}$$

This witness is built in a somewhat different way from the previous ones. In this case, the greatest squared overlap between $|\overline{\mathrm{GHZ}}\rangle$ and any biseparable state is represented by 1/2. Besides, given that 3/4 is the largest overlap between $|\overline{\mathrm{GHZ}}\rangle$ and any W state, the following operator is a GHZ witness,

$$W_{\mathrm{GHZ}} = \frac{3}{4}\mathbb{1} - |\overline{\mathrm{GHZ}}\rangle \langle\overline{\mathrm{GHZ}}| \,. \tag{4.14}$$

Indeed, it has a negative expectation value for states in the GHZ class, but a positive value for states in the W state class. Thus, if $\mathrm{Tr}(\rho W_2) < 0$, we may demonstrate with the witness W_2 that a state ρ is fully tripartite entangled. The state ρ does not belong to the W state class if $\mathrm{Tr}(\rho W_2) < 1/4$. W_2 can be decomposed as

$$\begin{aligned} W_2 = \frac{1}{16}[&6 \cdot \mathbb{1} \otimes \mathbb{1} \otimes \mathbb{1} + 4 \cdot \sigma_z \otimes \sigma_z \otimes \sigma_z \\ &- 2 \cdot (\sigma_y \otimes \sigma_y \otimes \mathbb{1} + \sigma_y \otimes \mathbb{1} \otimes \sigma_y + \mathbb{1} \otimes \sigma_y \otimes \sigma_y) \\ &- (\sigma_x + \sigma_z) \otimes (\sigma_x + \sigma_z) \otimes (\sigma_x + \sigma_z) \\ &- (\sigma_z - \sigma_x) \otimes (\sigma_z - \sigma_x) \otimes (\sigma_z - \sigma_x)]. \end{aligned} \tag{4.15}$$

4.3.3 Bipartite Entanglement Witness

Furthermore, we can get similar decompositions for bipartite entanglement with a minimal number of local von Neumann measurements. The following witness is a general witness for a two-dimension system,

$$\begin{aligned} W_3 = \frac{1}{4}[&\mathbb{1} \otimes \mathbb{1} + \sigma_z \otimes \sigma_z + \left(a^2 - b^2\right) \sigma_y \otimes \sigma_y \\ &+ 2ab(\mathbb{1} \otimes \sigma_z + \sigma_z \otimes \mathbb{1}) + \left(a^2 - b^2\right) \sigma_x \otimes \sigma_x], \end{aligned} \tag{4.16}$$

with a and b being real numbers.

4.3.4 Is Entanglement Witness Experimentally Feasible?

Entanglement witnesses have been proposed as a tool for detecting and characterizing entanglement in quantum systems [Gühne, 2004, Chruściński and Sarbicki, 2014, Lewenstein et al., 2000]. Many different types of entanglement witnesses have been developed, each optimized for different applications and types of entangled states [Hyllus and Eisert, 2006, Jungnitsch et al., 2011, Bae et al., 2020].

While these theoretical constructions have been useful for understanding the nature of entanglement and developing algorithms for quantum information processing, their experimental implementation remains a significant challenge.

In our particular case, we are interested in using entanglement witnesses for experimental detection of multipartite entanglement. We want to design a witness operator that can be measured using local projective measurements, making it feasible to implement in a realistic laboratory setting. This requires finding an optimal decomposition of the witness operator into a set of local observables, each of which can be measured with a single setting of the measuring devices. By designing an experimentally feasible entanglement witness, we can probe and understand the entanglement properties of multipartite quantum systems in the laboratory, which has important implications for the development of quantum technologies.

4.4 Ideal Photon Amplifiers

In quantum optics, researchers have investigated the idea of an ideal photon number amplifier. This device aims to take an input state containing n photons and amplify it to an output state with G photons, where G is greater than 1. Both linear and non-linear amplification methods have been scrutinized in the literature [Ho and Yuen, 1994, D Ariano, 1992, Caves et al., 2012, Propp and van Enk, 2019].

Linear amplification increases the number of photons proportionally, maintaining the phase relationships between them. However, it often introduces noise and does not perfectly preserve the quantum properties of the photons.

Non-linear amplification, on the other hand, relies on processes where the amplification rate depends on specific properties of the input photons, such as their number or intensity. This means that the amplification is not a simple proportional increase but is influenced by the initial state of the photons. This approach allows for more precise control and can better preserve the quantum characteristics of the input state. Due to these advantages, non-linear amplification has shown greater promise for achieving an ideal photon number amplifier.

Consider that a mode refers to a particular quantized state of the electromagnetic field, defined by specific frequency and spatial distribution. Given $\hat{a}^\dagger$ and $\hat{a}$ are respectively the creation and annihilation operators for bosonic mode amplitude a, and $\hat{b}^\dagger$ and $\hat{b}$ are respectively the creation and annihilation operators for an independent auxiliary bosonic mode b. As stated by [Propp and van Enk, 2019], the standard approach to describing linear quantum amplification is through Caves' relation,

$$\hat{a}_{\text{out}} = \sqrt{G}\hat{a}_{\text{in}} + \sqrt{G-1}\hat{b}^\dagger_{\text{in}}. \tag{4.17}$$

This relation creates an output field, $\hat{a}_{\text{out}}$, which is a combination of the input field amplitude, $\hat{a}_{\text{in}}$, multiplied by $\sqrt{G}$ and an additional term, $\hat{b}_{\text{in}}$, the input field of mode b, multiplied by $\sqrt{G-1}$. The presence of mode b introduces extra noise, even if it is in a vacuum state, affecting the output field. The variance expression showing the impact of this extra noise on the amplified field is

$$\sigma^2_{(\hat{a}^\dagger\hat{a})_{\text{out}}} = G\Delta n_a^2 + (G-1)^2\Delta n_b^2 + G(G-1)(2\bar{n}_a\bar{n}_b + \bar{n}_a + \bar{n}_b + 1), \tag{4.18}$$

where $\bar{n}_a = \left\langle \left(\hat{a}^\dagger\hat{a}\right)_{\text{in}} \right\rangle$ and $\bar{n}_a^2 + \Delta\bar{n}_a^2 = \left\langle \left(\hat{a}^\dagger\hat{a}\right)^2_{\text{in}} \right\rangle$. We obtain similar expressions for mode b.

Non-linear amplification involves transferring energy from an input mode with n photons to a second reservoir, resulting in ideal noiseless amplification of a photon number state. The second reservoir starts with zero excitations and ends up containing Gn excitations if the input field had n photons. In the Heisenberg picture, the ideal coupling to a reservoir mode b, resulting in an output mode with no additional amplification noise, can be expressed as

$$\hat{b}^\dagger_{\text{out}}\hat{b}_{\text{out}} = \hat{b}^\dagger_{\text{in}}\hat{b}_{\text{in}} + G\hat{a}^\dagger_{\text{in}}\hat{a}_{\text{in}}, \tag{4.19}$$

which gives as variance,

$$\sigma^2_{(\hat{b}^\dagger\hat{b})_{\text{out}}} = \Delta n_b^2 + G^2\Delta n_a^2. \tag{4.20}$$

The number fluctuations in the auxiliary mode are not amplified, particularly if the input field is in a number state with zero fluctuation. In a more realistic scenario where reservoirs consist of many modes (for example G modes), the number fluctuations in the output mode are a combination of the amplified fluctuations from both the input and reservoir modes,

$$\sigma^2_{(\hat{b}^\dagger\hat{b})_{\text{out}}} = G\Delta n_b^2 + G^2\Delta n_a^2. \tag{4.21}$$

Here, noise is amplified, although the amplification is significantly lower compared to the linear case. The amplification of noise is a common feature in both linear and non-linear amplification methods. However, the non-linear approach has the advantage of conditional coupling, which can reduce noise under certain conditions.

4.5 Human Eye Detection of Bipartite and Tripartite Entanglement in Psychophysical Experiments

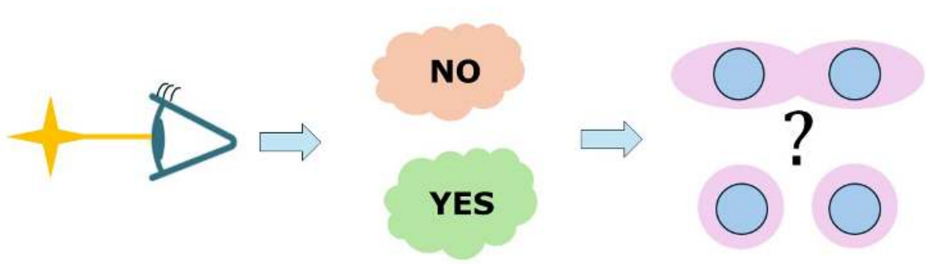

This section is derived from my publication [Gassab et al., 2024a].

4.5.1 Initial State and Amplification

We focus our analysis to a Bell state for the bipartite case and a W state for the tripartite case assuming that they have been produced by the interferometric setups of [Vivoli et al., 2016] and [Bourennane et al., 2004] respectively and horizontal polarization components are probed by human eyes in place of photodetectors.

The usage of bipartite entanglement and tripartite entanglement start respectively with the states,

$$|\psi_1\rangle = \frac{1}{\sqrt{2}}(|HV\rangle + |VH\rangle); \tag{4.22}$$

$$|\psi_2\rangle = \frac{1}{\sqrt{3}}(|HHV\rangle + |HVH\rangle + |VHH\rangle), \tag{4.23}$$

where H stands for horizontal polarization and V for vertical polarization.

We choose to represent the starting states in terms of the creation operator, $\hat{a}^\dagger$, applied to the vacuum as follows,

$$|\psi_1\rangle = \frac{1}{\sqrt{2}}\left(\hat{a}_H^{\dagger 1}\hat{a}_V^{\dagger 2} + \hat{a}_V^{\dagger 1}\hat{a}_H^{\dagger 2}\right)|0\rangle\,; \tag{4.24}$$

$$|\psi_2\rangle = \frac{1}{\sqrt{3}}\left(\hat{a}_H^{\dagger 1}\hat{a}_H^{\dagger 2}\hat{a}_V^{\dagger 3} + \hat{a}_H^{\dagger 1}\hat{a}_V^{\dagger 2}\hat{a}_H^{\dagger 3} + \hat{a}_V^{\dagger 1}\hat{a}_H^{\dagger 2}\hat{a}_H^{\dagger 3}\right)|0\rangle\,, \tag{4.25}$$

with the superscripts (1,2,3) corresponding to the branches in the interferometric setup (see Figure 4.1) and the subscripts (H,V) corresponding to the horizontal and vertical polarization.

The human visual threshold cannot resolve single photons, or two or three-photons. After the photons go through the polarization analyzers complex, a coherent light is mixed with the entangled photons so that the mean photon number is coherently amplified above the visual threshold. Theoretically, this amplification means applying to the horizontal polarized photons a displacement operator,

$$\hat{D}(\alpha) = \mathrm{e}^{\alpha\hat{a}^\dagger - \alpha^*\hat{a}}, \tag{4.26}$$

where α is the displacement parameter; $\hat{a}^\dagger$ and $\hat{a}$ are respectively the photon creation and annihilation operators.

The measurement in the vacuum state and single-photon subspace yields two outcomes (termed "no see" and "see") and is represented as a Positive Operator-Valued Measure (POVM) on the Bloch sphere. The measurement direction depends on the displacement's amplitude and phase, enabling effective measurements, particularly along the x-axis. The method capitalizes on the partial overlap in photon number space due to the displacement operation. In our case the main role of the displacement operator is to increase the number of photons to a level above the human visual threshold when a photon is present. Conversely, in the absence of photons, the amplification remains below the threshold. This approach effectively boosts the contrast between "yes" and "no" cases, making photon detection more robust and accurate.

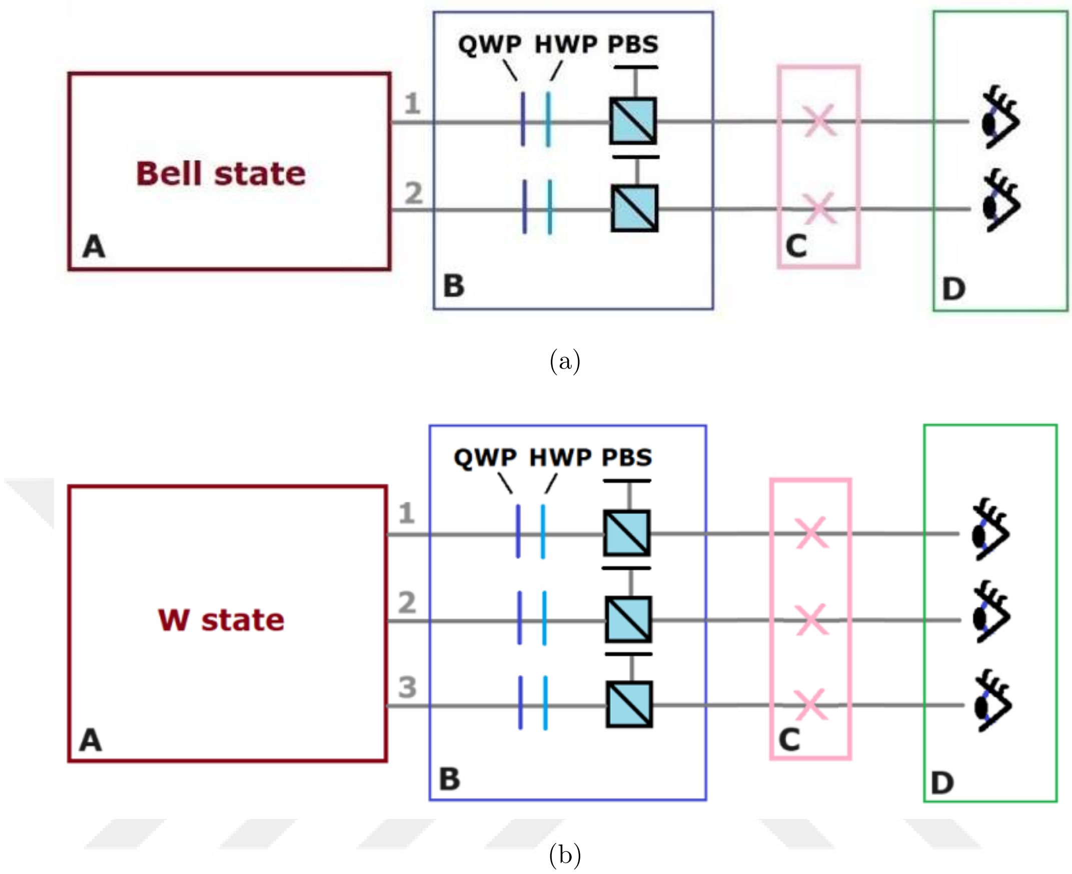

Figure 4.1: A schematic representation of the setup for human eye detection of bipartite and tripartite entanglement in psychophysical experiments. The red boxes (labeled by A) are schematic representation of the interferometric entanglement generation setups. Upper (a) and lower (b) panels are respectively for the bipartite and tripartite cases. The blue boxes (labeled by B) represent the polarization analyzers complexes, which includes a Quarter Wave Plate (QWP), a Half Wave Plate (HWP) and a Polarized Beam Splitter (PBS). The pink boxes (labeled by C) represent the coherent amplification processes. The green boxes (labeled by D) represent the detection part of the horizontal polarization by the human eye. A horizontal black line appears at one of the outputs of the PBS to illustrate the beam being blocked. The numbers 1,2 and 3 correspond to the branches in the interferometric setup.

4.5.2 Polarization Analyzers

The polarization analyzers complex consists of a Quarter Wave Plate (QWP), a Half Wave Plate (HWP) and a Polarized Beam Splitter (PBS). Considering the unitary transformation operator as defined in Eq. (2) of [Hou et al., 2015] as

$$U(\theta, \delta) = \begin{pmatrix} \cos^2\theta + e^{i\delta}\sin^2\theta & \frac{1}{2}(1 - e^{i\delta}\sin 2\theta) \\ \frac{1}{2}(1 - e^{i\delta}\sin 2\theta) & \sin^2\theta + e^{i\delta}\cos^2\theta \end{pmatrix}, \tag{4.27}$$

the QWP is represented by $U(q, \frac{\pi}{2})$ and the HWP by $U(p, \pi)$ where q and p are real numbers. In each interferometric branch, the creation operators for horizontal and vertical polarization are modified by the application of the unitary operators,

$$U\left(q, \frac{\pi}{2}\right)\, U(p, \pi) \begin{pmatrix} \hat{a}^\dagger_H \\ \hat{a}^\dagger_V \end{pmatrix} = \begin{pmatrix} \hat{a}^{\dagger\prime}_H \\ \hat{a}^{\dagger\prime}_V \end{pmatrix}, \tag{4.28}$$

with $\hat{a}^{\dagger\prime}_H$ and $\hat{a}^{\dagger\prime}_V$ being the modified creation operators after going through the polarization analyzer. Equivalently, the polarization analyzers complex transforms the polarization operator σ_z as follows,

$$\sigma_z \mapsto r(q, p).\sigma, \tag{4.29}$$

in which $\sigma = (\sigma_x, \sigma_y, \sigma_z)$ is the row vector of Pauli spin-1/2 operators, and $r(q, p)$ is a column vector given by

$$r(q, p) = \begin{pmatrix} \sin(2q)\cos(4p - 2q) \\ \sin(4p - 2q) \\ \cos(2q)\cos(4p - 2q) \end{pmatrix}, \tag{4.30}$$

where p and q are chosen in such a way to be able to obtain the appropriate polarization analyzer setting. For example, if we need to measure σ_y, then we take $q = 0$ and $p = \pi/8$ which gives

$$r\left(0, \frac{\pi}{8}\right) = \begin{pmatrix} 0 \\ 1 \\ 0 \end{pmatrix}. \tag{4.31}$$

In a real experimental scenario, the PBS in the polarizer analyzer complex separates the vertically and horizontally polarized photons as illustrated by the box B in Figure 4.1. At this point, it is worth noting that, when performing computational simulations, the polarized photons are already separated by the two tensor products of the creation operator representing the horizontal and vertical polarization in each interferometric branch.

Next, the horizontal polarization are amplified (box C of Figure 4.1), and transmitted to and detected by the human eye (box D of Figure 4.1). The schematic representation of the full setup is shown in Figure 4.1.

4.5.3 Entanglement Witness Derivation

To decide whether or not our state is entangled (multipartite entangled), we need an entanglement witness. In the quantum information and quantum optics literature there exists a plethora of entanglement witnesses. We choose two specific witnesses that can be implemented in an experimental setup, one for the bipartite entanglement witness [Riccardi et al., 2020], and the other for the tripartite entanglement witness [Bourennane et al., 2004]. If the expectation value of either of the entanglement witness is strictly negative, we can deduce that we have an entangled or multipartite entangled state.

The entanglement witness for bipartite entanglement and multipartite entanglement can be decomposed into a number of local von Neumann measurements,

$$W_1 = \frac{1}{4}[\mathbb{1} \otimes \mathbb{1} + \sigma_z \otimes \sigma_z - \sigma_y \otimes \sigma_y - \sigma_x \otimes \sigma_x]; \tag{4.32}$$

$$\begin{aligned} W_2 = \frac{1}{16}&[6 \cdot \mathbb{1} \otimes \mathbb{1} \otimes \mathbb{1} + 4 \cdot \sigma_z \otimes \sigma_z \otimes \sigma_z \\ &- 2 \cdot (\sigma_y \otimes \sigma_y \otimes \mathbb{1} + \sigma_y \otimes \mathbb{1} \otimes \sigma_y + \mathbb{1} \otimes \sigma_y \otimes \sigma_y) \\ &- (\sigma_x + \sigma_z) \otimes (\sigma_x + \sigma_z) \otimes (\sigma_x + \sigma_z) \\ &- (\sigma_z - \sigma_x) \otimes (\sigma_z - \sigma_x) \otimes (\sigma_z - \sigma_x)]. \end{aligned} \tag{4.33}$$

These measurements correspond to different combinations of Pauli matrices.

Therefore, the witnesses can be simply expressed as

$$W = \sum_{k=1}^{S} M_k, \tag{4.34}$$

where the observable M_k corresponds to the k^{th} combination of Pauli matrices appearing in the witnesses and S denotes the number of different settings needed. Actually, the different combination of Pauli matrices are generated thanks to the polarization analyzer as presented in Eq. (4.29). In our analysis, we need $S = 3$ different settings for Bell state detection and $S = 5$ different settings for W state. For example, when looking at the witness (4.32) for Bell state, we need three setups of the polarization analyzers to recover the witness, which means having in Eq. (4.29) $q = 0$, $p = 0$ for $\sigma_z \otimes \sigma_z$, $q = 0$, $p = \pi/8$ for $\sigma_y \otimes \sigma_y$ and $q = \pi/8$, $p = 0$ for $\sigma_x \otimes \sigma_x$. For each setting, we calculate the probabilities of the different states before the detection and we generate these states in the simulation according to their probabilities.

4.5.4 Detection by Human Eye or Photodetector

Subsequently, the detection is realized by a human eye or by a perfect photodetector.

- If the human receives an H polarized photon, the human will see light with the probability of seeing, P_{see} (4.44).

- If the human eye does not receive any photon (that is, the photons were in V polarization and hence not transmitted to the eye), then the probability of seeing, P_{see}, will not be zero due to the amplification process and the person will see light with a different value of the probability.

- If we use a perfect photodetector in place of a human eye, the probability of detection will be 1 for H polarization and 0 for V polarization.

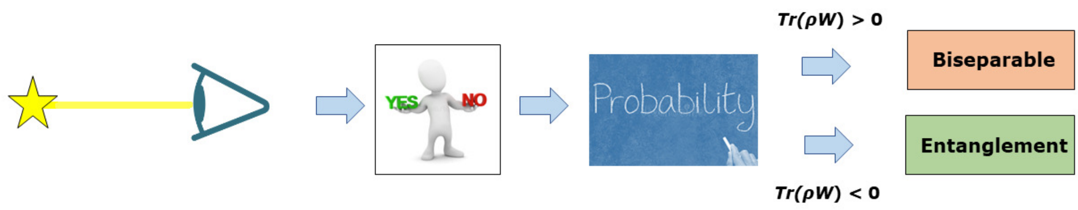

Figure 4.2: Simplified representation of the detection method. The light source is represented by a yellow star. The light coming into the human eye is represented by the solid yellow line. Then, the human subject answers by yes or no according to whether he/she sees or does not see the light. After N simulations of the experiment, we calculate the probabilities needed in the different witnesses (4.32) and (4.33). From these probabilities, we can calculate the expectation value of the entanglement witness and conclude if the human subject can differentiate between entangled and non-entangled light or multipartite and biseparable light.

Thus, according to the simultaneous responses of the human eyes or the output of the photodetectors, we can construct four different probabilities for the Bell state,

$$P(HH), P(HV), P(VH), P(VV),$$

corresponding to the photonic states with the polarizations,

$$HH, HV, VH, VV,$$

and eight different probabilities for the W state,

$$P(HHH), P(HHV), P(HVH), P(HVV),$$
$$P(VHH), P(VHV), P(VVH), P(VVV),$$

corresponding to the photonic states with the polarizations,

$$HHH, HHV, HVH, HVV, VHH, VHV, VVH, VVV.$$

From these probabilities, for different setup, we can calculate the expectation value of the witness after N simulations as

$$\begin{aligned}\langle W\rangle &= \sum_k \mathrm{Tr}(M_k\rho) \\ &= \sum_k \sum_{l_1,\ldots,l_n=V,H} d^{(k)}_{l_1,\ldots,l_n} P^{(k)}(l_1,\ldots,l_n),\end{aligned} \tag{4.35}$$

where ρ is the density matrix of the state. l_n corresponds to the polarization of the photon in the interferometric branch n such that $n=2$ for the Bell state and $n=3$ for the W state. $d^{(k)}_{l_1,\ldots,l_n}$ are real weight coefficients taken from the witnesses (4.32) and (4.33) and k is the setting of the polarization analyzer. $P^{(k)}(l_1,\ldots,l_n)$ are the probabilities of the different possible outputs given by the human or photodetector.

In our setup, we employ perfect photodetectors. However, it is important to acknowledge the quantum efficiency of typical photodetectors in practical scenarios, where their performance remains consistently high [Shen et al., 2022]. Although there may be minor detrimental effects on the overall witness measurement, these are anticipated to be minimal.

Finally, we can conclude whether or not the human eye can detect bipartite entangled state or multipartite entanglement. Indeed after calculating the expectation value of the witness, given that we know that we have sent a Bell state or a W state to the human eye, if it is negative ($\langle W\rangle < 0$), we can conclude that we have entanglement or multipartite entanglement. The general strategy is summarized in Figure 4.2.

4.5.5 Probability of Seeing

To simulate the human response, we need to define the probability of seeing. The probability of seeing will depend on the input light coming to the eye. The occurrence of a no-seeing event with unit efficiency can be associated with

$$\hat{P}^{K,\eta=1}_{\mathrm{ns}} = \sum_{m=0}^{K-1} |m\rangle\langle m|\,, \tag{4.36}$$

where K is the human visual threshold and η is the quantum efficiency.

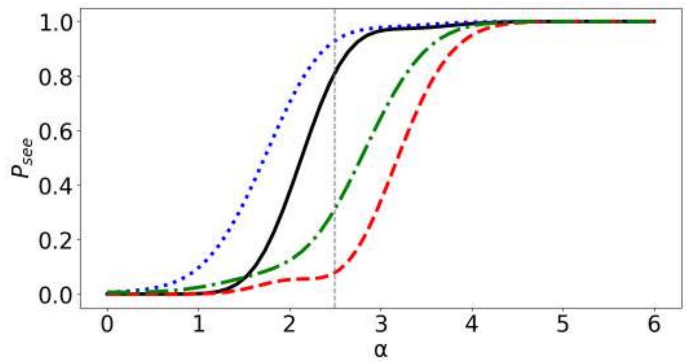

Figure 4.3: Probability of seeing, P_{see} (4.44), as a function of the coherence parameter α of the coherent amplification. The solid black line represents P_{see} for the state $|1'\rangle$ and the dashed red line represents P_{see} for the state $|0'\rangle$. The dotted blue line represents P_{see} for the state $|1'\rangle$ with additive noise $D = 2$ and the dashed dotted green line represents P_{see} for the state $|0'\rangle$ with additive noise $D = 2$. The threshold K is taken as 7 and $\eta = 0.08$. The dashed vertical gray line is given for $\alpha = 2.5$.

To model non-unit efficiency, we can introduce a beam-splitter interaction between the detected mode A and an unoccupied ancillary mode C. These modes are described by the bosonic operators a, $a^\dagger$, and c, $c^\dagger$ respectively. The beam splitter operator, U_{BS}, can be expressed as

$$U_{BS}\left|0\right\rangle_c = C_L = \mathrm{e}^{\tan\gamma\, ac^\dagger}\mathrm{e}^{\ln(\cos\gamma)a^\dagger a}\left|0\right\rangle_c, \tag{4.37}$$

with $\cos^2\gamma = \eta$. The no-seeing operator is defined as

$$\hat{P}_{\text{ns}}^{K,\eta=1} = C_L^\dagger \sum_{m=0}^{K-1} |m\rangle\langle m|\, C_L. \tag{4.38}$$

The no-seeing probability is eventually given by the operator,

$$\hat{P}_{\text{ns}}^{K,\eta} = \frac{\eta^K}{(K-1)!}\frac{d^{K-1}}{d(1-\eta)^{K-1}}\left[\frac{(1-\eta)^{\hat{a}^\dagger\hat{a}}}{\eta}\right]. \tag{4.39}$$

Then, the probability of no-seeing after coherent amplification is calculated as

$$
\begin{aligned}
P_{\text{ns}}^{K,\eta} &= \langle n| \hat{D}(\alpha)^{\dagger} \hat{P}_{ns}^{K,\eta} \hat{D}(\alpha) |n\rangle \\
&= \frac{\eta^K}{(K-1)!} \frac{d^{K-1}}{d(1-\eta)^{K-1}} \left[\frac{\mathrm{e}^{-\eta|\alpha|^2} p_n^{\alpha}(\eta)}{\eta} \right],
\end{aligned} \tag{4.40}
$$

where

$$
p_n^{\alpha}(\eta) = \langle n| \mathrm{e}^{-\eta\alpha\hat{a}^{\dagger}} (1-\eta)^{\hat{a}^{\dagger}\hat{a}} \mathrm{e}^{-\eta\alpha^{*}\hat{a}} |n\rangle , \tag{4.41}
$$

with n being the number of horizontal polarized photon in the interferometric branch before the amplification process (0 or 1).

Although eye-based measurements are incapable of assessing the z-axis, they exhibit a level of comparability to single photon detectors when it comes to conducting measurements along the x-axis. When the state is amplified via coherent amplification, human or any detector is no longer interrogated with respect to amplified $|0\rangle$ and $|1\rangle$ states but with respect to amplified $|0+1\rangle$ and $|0-1\rangle$ states. So, instead of differentiating between the states $|1\rangle$ and $|0\rangle$ we differentiate between the states,

$$
|1'\rangle = \frac{1}{\sqrt{2}}(|0\rangle + |1\rangle); \tag{4.42}
$$

$$
|0'\rangle = \frac{1}{\sqrt{2}}(|0\rangle - |1\rangle). \tag{4.43}
$$

This improves the distinguishability between these two states by the human eye. Using the states $|0'\rangle$ and $|1'\rangle$ for $|n\rangle$ in Eq. (4.41), we can compute the probability (4.40) and use

$$
P_{\text{see}} = 1 - P_{\text{ns}}^{K,\eta}, \tag{4.44}
$$

as the probability of seeing in our simulation. In Figure 4.3, the probability of seeing for state $|1'\rangle$ corresponding to the presence of a horizontal polarized photon and $|0'\rangle$ corresponding to the absence of photon are represented. The threshold, K, is varied up to 7 and the efficiency, η, is equal to 0.08. Based on Figure 4.3, we choose for the rest of the calculations the displacement parameter, $\alpha = 2.5$, in order to get the best distinguishability between the states $|0'\rangle$ and $|1'\rangle$.

4.5.6 Noise Addition

To have a more faithful simulation, we consider an additive noise. We use a generic model, in which a parameter, D, is added to the average photon number, $|\alpha|^2$, appearing in the probability of seeing. D represents the dark noise which takes into account false positive responses by the subjects. Since there is no experimental data for the parameter, D, in such low photon number, we consider arbitrary values between 0 and 5. Introducing noise has the potential to diminish the distinction between states with and without a photon.

As illustrated in Figure 4.3, it becomes evident that for both larger and smaller values of α, the probabilities associated with the presence and absence of a photon converge, diminishing their distinguishability. The simulation is run N times to calculate the probabilities needed. This means that we send the entangled or multipartite state N times and we receive the response of either the human eye or the photodetector.

While our work primarily embodies the noise scenarios unique to psychophysical experimental conditions and their effects, it is worth noting that error correction techniques have been a significant area of research in quantum information science [Devitt et al., 2013, Sivak et al., 2023]. These techniques aim to correct measurement operator errors and enhance the reliability of quantum systems.

4.5.7 Results

In the case of one human eye and an ideal photodetector, the expectation values of the entanglement witness, for the bipartite case and for different thresholds according to the number of runs of the simulation, are plotted as shown in Figure 4.4. We also investigate the effect of additive noise in the probability of seeing on our results.

When looking at Figure 4.4a, we see that for K superior to 4 we get a negative value for the witness. So, one human eye and an ideal photodetector can be used to detect entangled state in the case of bipartite entanglement. For K inferior to 4, the witness is positive. This may be due to the fact that the displacement operator has been optimized for $K = 7$.

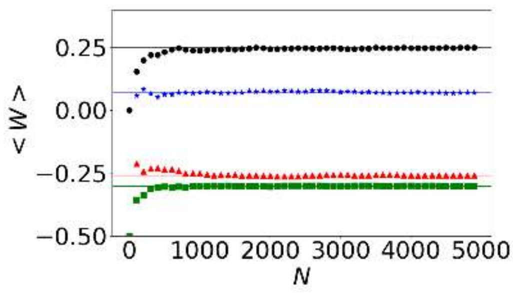

(a)

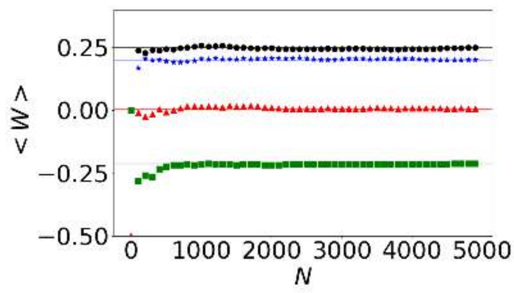

(b)

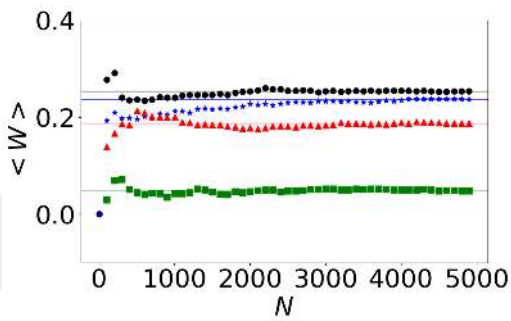

(c)

Figure 4.4: Results for the expectation values $\langle W \rangle$ of the Bell state witness (4.32) with respect to the number of runs N and for different values of the human vision threshold K. The black circles, the blue star, the red triangle, and the green square represent $K = 1$, $K = 3$, $K = 5$, $K = 7$ respectively. The markers on the graph are represented every hundred steps. For each threshold, the horizontal solid lines represent the last value of the witness expectation values. The probability of seeing is evaluated for $\eta = 0.08$. In these graphs, a human eye and an ideal photodetector have been used. $\langle W \rangle$ is plotted for the additive noise (a) $D = 0$, (b) $D = 2$, and (c) $D = 5$.

When adding noise, as shown in Figures 4.4b and 4.4c, the entanglement detection becomes less probable according to the amount of noise. For $D = 2$, the detection is possible only for $K = 7$ and becomes impossible for $D \geq 5$. When considering two human eyes for the detection of Bell state, entanglement detection is possible without noise and for additive noise corresponding to $D < 3$.

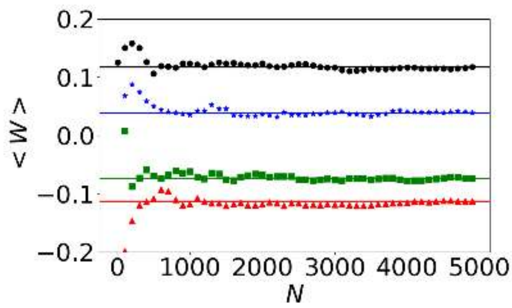

(a)

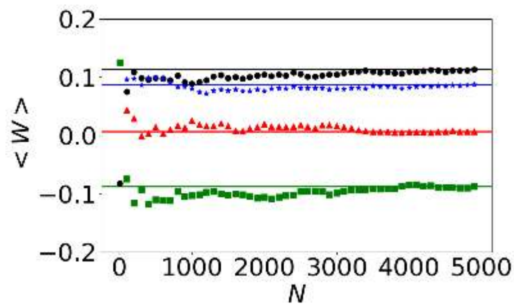

(b)

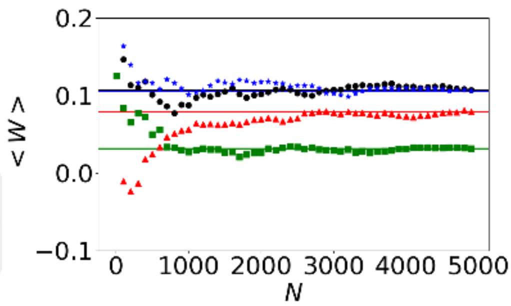

(c)

Figure 4.5: Results for the expectation values $\langle W \rangle$ of the W state witness (4.33) with respect to the number of runs N and for different values of the human vision threshold K. The black circles, the blue star, the red triangle, and the green square represent $K = 1$, $K = 3$, $K = 5$, $K = 7$ respectively. The markers on the graph are represented every hundred steps. For each threshold, the horizontal solid lines represent the last value of the witness expectation values. The probability of seeing is evaluated for $\eta = 0.08$. In these graphs, a human eye and two ideal photodetectors have been used. $\langle W \rangle$ is plotted for the additive noise (a) $D = 0$, (b) $D = 2$, and (c) $D = 5$.

In Figure 4.5 we consider the case of one human eye as photodetector and two ideal photodetectors. The results are very similar to the Bell state case. The multipartite detection is possible if we consider an additive noise strictly inferior to $D = 5$.

However, when considering two human eyes and one ideal photodetector, or three human eyes, the detection of multipartite entanglement becomes critical. For two human eyes and one ideal photodetector, multipartite detection is possible only for limited cases, that is, for a noise strictly inferior to $D = 2$, and only for a threshold $K = 5$. For three human eyes, the value of the witness is positive regardless of the value of the threshold and without additive noise.

The feasibility of using humans as photodetectors to resolve single photons and entangled pairs of photons has already been shown in experiments in the literature. Our scheme do not improve the detection efficiency of humans in this regard, but contributes partly to answer the critical question of what are the limits of human photodetectors to detect higher dimensional entanglement in realistic psychophysical experimental conditions. We find that the additional noise in such experiments seriously hinder the resolution of even a tripartite entangled state and we determine how the experiments should be designed with combination of coherent amplifiers, artificial detectors and humans to determine the tripartite entanglement with acceptable success rates.

4.5.8 Amplification via Amplitude Squeezing

We have seen that an amplification scheme is necessary to increase the average photon number pre-measurement above the detection threshold. Previous studies have achieved this through coherent amplification techniques, such as the displacement operator [Vivoli et al., 2016], stimulated emission [Sekatski et al., 2009], and optical parametric amplification [Spagnolo et al., 2011]. However, these methods also result in an increase in photon number fluctuations.

We examine the noise generated by the application of a displacement operator, a squeezing operator and then both of them to create an amplitude squeezing.

The general expression for mean photon number, $\bar{N}$, and the photon number variance, $V(\hat{N})$, are given by

$$\bar{N} = \langle \hat{a}^\dagger \hat{a} \rangle, \tag{4.45}$$

$$V(\hat{N}) = \langle \hat{N}^2 \rangle - \langle \hat{N} \rangle^2, \tag{4.46}$$

where $\hat{N} = \hat{a}^\dagger \hat{a}$.

Noise due to the displacement operator

We apply a displacement operator to $|n\rangle$ as follows,

$$|n, \alpha, z\rangle = \hat{D}(\alpha) |n\rangle . \tag{4.47}$$

Figures 4.6a and 4.6b illustrate the mean number of photons, photon number variance, and standard deviation for the cases $n = 0$ and $n = 1$ after the application of the displacement operator. These values are plotted as functions of the real displacement parameter. As anticipated, when $n = 0$, the variance and expectation value are identical. Additionally, the variance increases significantly with increasing displacement parameter, reaching up to 28 for $r = 3$.

Noise due to the squeezing operator

We apply a squeezing operator to $|n\rangle$ as follows,

$$|n, \alpha, z\rangle = \hat{S}(z) |n\rangle . \tag{4.48}$$

Figures 4.6c and 4.6d illustrate the mean number of photons, photon number variance, and standard deviation for the cases $n = 0$ and $n = 1$ after the application of the squeezing operator. These values are plotted as functions of the real squeezing parameter, z. We can see that for quadrature squeezing the variance is even larger than in the coherent case, going up to 100 for $z = 1.5$. This is expected because the quadrature squeezing does not squeeze the photon number.

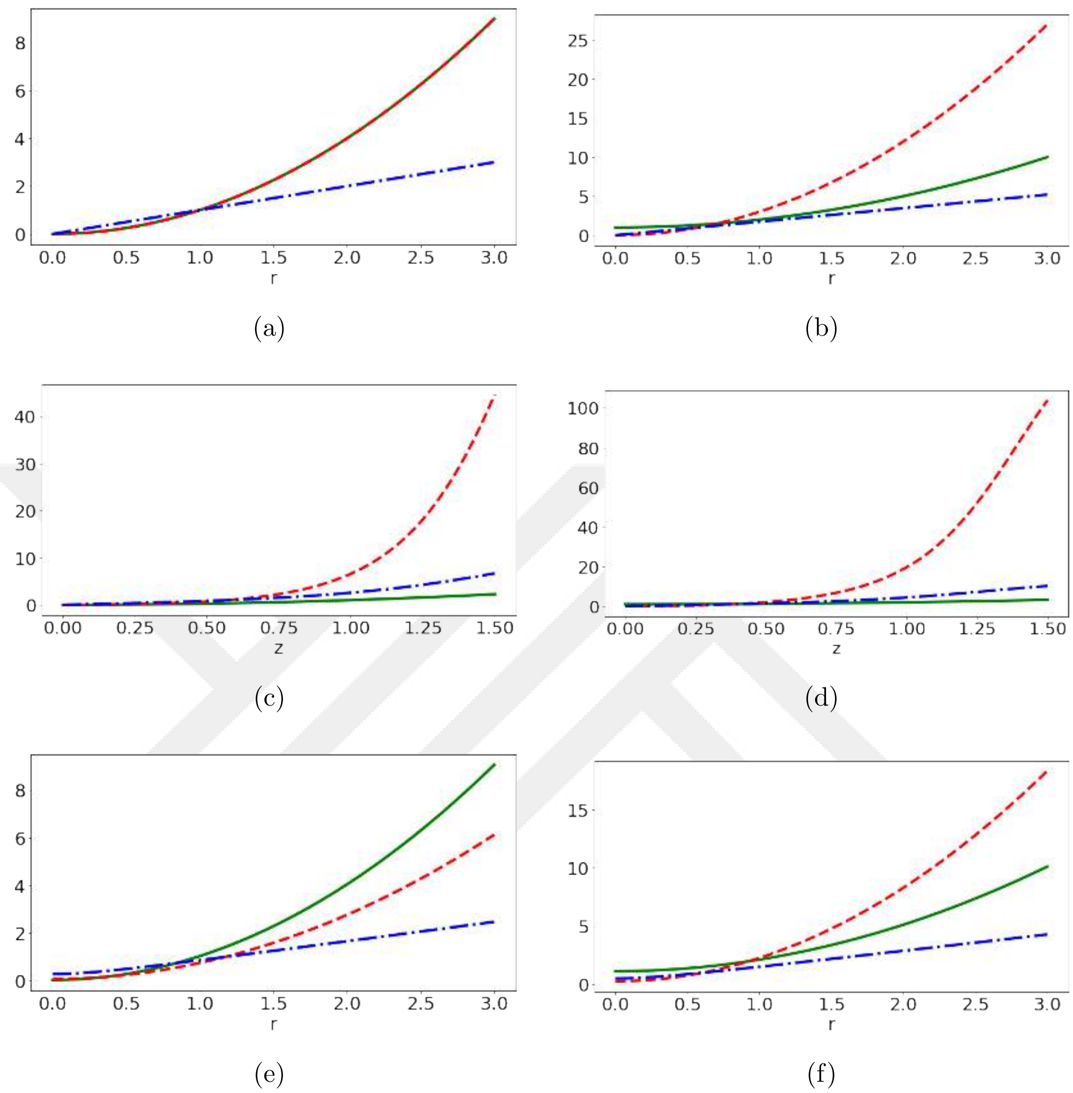

Figure 4.6: Statistics of different amplification methods. The solid green curve represents the mean photon number, while the dashed red curve and the dashed-dotted blue curve depict the variance and standard deviation of the photon number respectively. (a) and (b) correspond to the application of the displacement operator plotted against the displacement parameter, r, for $n = 0$ and $n = 1$, respectively. (c) and (d) correspond to the application of the squeezing operator plotted against the squeezing parameter, z, for $n = 0$ and $n = 1$ respectively. (e) and (f) illustrate amplitude squeezing for different values of r, which represents the modulus of the displacement (coherence) parameter, for $n = 0$ and $n = 1$ respectively. The phase of the squeezing parameter is set to $s = 0.2$ with $\theta = \phi - \frac{\pi}{2}$, and the phase of the displacement parameter is $\phi = \pi$.

Noise due to amplitude squeezing

To minimize the noise, we propose the use of amplitude squeezing. The application of amplitude squeezing utilizes both the displacement operator, $\hat{D}$, and the squeezing operator, $\hat{S}$, such that the amplitude squeezing operator acting on the input state can be written as

$$|n, \alpha, z\rangle = \hat{D}(\alpha)\hat{S}(z)\,|n\rangle\,, \tag{4.49}$$

where

$$\hat{D}(\alpha) = \mathrm{e}^{\alpha\hat{a}^\dagger - \alpha^*\hat{a}}; \tag{4.50}$$

$$\hat{S}(z) = \mathrm{e}^{\frac{1}{2}\left(z^*\hat{a}^2 - z\hat{a}^{\dagger 2}\right)}. \tag{4.51}$$

Here, we have two complex numbers:

- the displacement parameter, $\alpha = re^{i\phi}$,
- the squeezing parameter, $z = se^{i\theta}$.

Amplitude squeezing appears for specific values of the phases ϕ and θ. Indeed, the expression of the mean photon number and the photon number variance can be derived for amplitude squeezed state as follows,

$$\langle\hat{N}\rangle = |\alpha|^2 + (2n+1)\sinh^2(r) + n; \tag{4.52}$$

$$\begin{aligned} V(\hat{N}) = |\alpha|^2(2n+1)&\left[\mathrm{e}^{2r}\cos^2\left(\theta - \frac{\phi}{2}\right) + \mathrm{e}^{-2r}\sin^2\left(\theta - \frac{\phi}{2}\right)\right] \\ &+ (n^2+n+1)2\sinh^2(r)\cosh^2(r). \end{aligned} \tag{4.53}$$

The photon number fluctuations reduce at the cost of increasing phase noise, consistent with the phase-number Heisenberg uncertainty relation. Figures 4.6e and 4.6f illustrate the mean number of photons and photon number variance and standard deviation after the application of amplitude squeezing. We can see that in this case the variance is reduced (reaching 18) compared to coherent amplification.

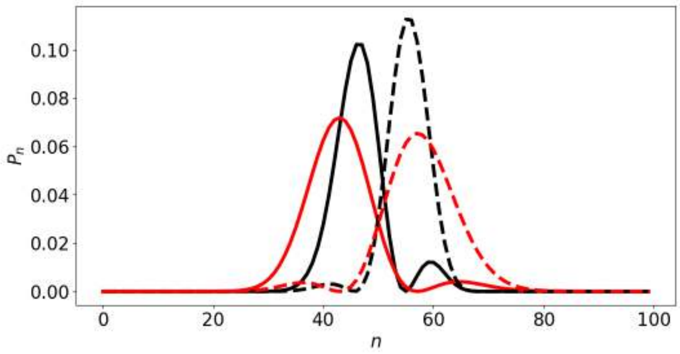

Figure 4.7: Probability distribution, P_n, according to the photon number n. The red dotted curve corresponds to the case of applying a displacement operator to $|0'\rangle$. The solid red curve corresponds to the case of applying a displacement operator to $|1'\rangle$. The black dotted curve corresponds to the case of applying amplitude squeezing to $|0'\rangle$ and the solid red curve corresponds to the case of applying amplitude squeezing to $|1'\rangle$. The modulus of the displacement (coherence) parameter is taken as $r = \sqrt{50}$. The modulus and the phase of the squeezing parameter are $s = 0.5$ and $\theta = 0$ respectively. The phase of the displacement parameter is taken as $\phi = 0$.

However, despite the reduction in variance and distribution narrowing, choosing amplitude squeezing over displacement does not improve the distinguishability between scenarios with and without photons (see Figure 4.7). While it decreases variance, it simultaneously amplifies dark counts, rendering it an unreliable option for amplification and complicating the process of entanglement witnessing.

Envisaging a superior amplification method compared to displacing the state or using amplitude squeezing is crucial for achieving better distinguishability between the one-photon and zero-photon states. The key requirement for entanglement witnessing is the ability to clearly distinguish the absence of photons when they are not present and their presence when they are.

Ideal photon amplifiers, discussed in Section 4.4, offer the potential for maintaining a zero-photon state with minimal noise and amplifying the one-photon state beyond a specified threshold. While the experimental implementation may pose challenges, striving for the realization of ideal photon amplifiers represents a promising direction for future advancements.

4.6 Conclusion

We investigated the conditions for detecting multipartite quantum entanglement using the human eye in psychophysical experiments. The coherent amplification technique was generalized from detecting entanglement in a bipartite entangled Bell state to a tripartite entangled W state. We utilized entanglement witnesses that could be measured using polarization analyzers in the interferometric setup. To evaluate the entanglement witnesses, we simulated human responses by modifying the probability of seeing to include the additive noise in the retina. In so doing, we were able to simulate false positives in psychophysical experiments.

4.6.1 The Different Scenarios

When the additive noise was neglected, our results showed that the detection of the entangled photons in the Bell state was possible using one human eye and one ideal photodetector, or with two human eyes as photodetectors, for threshold values $K > 4$. However, when the intrinsic retinal noise (D) was added to the simulation, the detection became more challenging but was still achievable depending on the noise level. In the case of the W state scenario, the detection was not possible with three human eyes even without noise addition, but by replacing one or two human eyes with perfect photodetectors, multipartite detection became possible. As with the Bell state, adding noise to the simulation resulted in a deterioration of the detection, but it was still feasible if the noise remained below a certain threshold.

4.6.2 The Three Critical Factors

In conclusion, the possibility of using the human eye as a photodetector to detect entanglement appeared to be dependent on three critical factors: the order (dimensionality) of entanglement, the retinal noise, D, and the human visual threshold, K. Detection of higher-dimensional entanglement was more difficult by only human eyes, but it would be possible if:

- high-efficiency photodetectors could be used together with human eyes;
- D could be smaller than a few photons ($D \sim 5$);
- the signal could be coherently and optimally amplified for a given visual threshold.

While the efficiency of the photodetector model of the human eye was another biometric factor that severely limited entanglement detection, it was kept as a constant in the present work, and its small variations were assumed to have no significant impact on the conclusion of the possibility of detection of entanglement. Guided by the ranges of influence of significant biometric factors discussed here, interrogation strategies and the design of psychophysical experiments could be optimized to use higher-dimensional entangled states to probe the human visual system with the potential benefits of quantum metrology.

4.6.3 Alternative Approach

We explored ways to improve the amplification process, beginning with amplitude squeezing. However, our observations indicated that this method would worsen the distinguishability between photon and non-photon states by elevating dark counts. Given this context, we looked into various alternative amplification approaches documented in the literature. It appeared that the application of non-linear amplification would align more closely with the ideal photon amplifier scenario, presenting the potential to effectively alleviate noise-related challenges.

The aim was to primarily inquire into the fascinating and fundamental aspects of utilizing the human eye for detecting quantum entanglement, similar to the pioneering work on Bell states. Beyond its scientific curiosity, this research could yield practical benefits. Indeed, our findings on applying scaled multipartite quantum entanglement in psychophysical experiments might open doors for quantum-based approaches to investigating aspects of human psychology and vision.

4.6.4 Orbital Angular Momentum States?

We utilized entangled states in the horizontal (H) and vertical (V) polarization basis for photodetection. In recent years a novel research direction emerged in which structured light with left (L) and right (R) circularly polarized states were used for human vision experiments. In this line of work, the researchers successfully utilized R and L polarization coupled with Orbital Angular Momentum (OAM) states, that had an azimuthal phase dependence, to trigger the entoptic vision of the human subject in which the number of visible azimuthal fringes became proportional to the difference in the OAM values [Sarenac et al., 2020b, Sarenac et al., 2022a]. Utilizing OAM structured light showed promise as humans were able to distinguish OAM states with high accuracy and it was argued that one could use such states for diagnosis of macular degeneration, as the number of observed fringes would be different between healthy and unhealthy subjects [Pushin et al., 2023, Pushin et al., 2024].

Although using such states could be an interesting research direction to investigate entanglement sensitivity of the human visual system, challenges would exist in adapting such techniques to our proposed experimental scheme. To see entoptic phenomena, peripheral vision would need to be activated which would usually require a much brighter light source than what scotopic vision would require for activation. Therefore, for our scotopic vision based proposal, we could choose the simpler case of H and V entangled light sources with wavelengths around the peak wavelength of human rod cell's absorption curves between 495 nm and 505 nm [Tinsley et al., 2016b].

4.6.5 The Way Forward

The intersection of quantum mechanics and biology, particularly in vision, presents an interesting direction. Quantum biology's role in vision suggests a subtle, yet profound, connection where quantum mechanics may influence how we perceive light. This means we may view both light and the eye itself through a quantum perspective [Lambert et al., 2013, Fleming et al., 2011]. Such an understanding could contribute to technical advancements from neuroscience to medicine, in which the visual system is the subject of investigation.

Quantum tomography is an indispensable tool of quantum sciences and technologies [Mauro D. Ariano et al., 2003, Cramer et al., 2010, Heinosaari et al., 2013, Mohseni et al., 2008, Altepeter et al., 2003, Lundeen et al., 2009, Pedram et al., 2024c] which can bridge this gap. A recent study showed that quantum process tomography methods could be applied to the human visual system to reconstruct the visual perception model using Bayesian statistics [van der Reep et al., 2023]. Light pulses with Poissonian photon statistics were used. Using quantum entangled sources of light it may be possible to come up with, and validate, a finer perception model using fewer number of trials.

This "quantum vision" project opens up new avenues, as illustrated above, with numerous possibilities for expanding our model both theoretically and experimentally. This paves the way for fundamental questions about the connection between the brain and our visual sensors, while also offering practical applications in medicine.

Chapter 5

GENERAL CONCLUSION

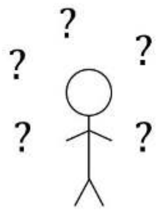

5.1 Summary

In conclusion, while the three main chapters of this thesis might have seemed diverse, they all elaborated on similar disciplines from different perspectives. Chapter 2 examined how geometry and symmetry, which are prevalent in biology, influenced the preservation of quantum information. This suggested that biological systems might be adopting specific configurations to utilize quantum properties for measurement and communication. Chapter 3 shifted the focus to probing biological systems, using quantum sensors such as Nitrogen-Vacancy centers and applying quantum correlations to enhance their efficacy as biological probes. Chapter 4 dealt with a complex biological system — the human eye and its connection to the brain — investigating how this biological sensor could detect entangled light. In this chapter, metrology was studied from the perspective of light.

5.2 The Journey

My four-year journey as a PhD student has been an enriching learning experience. I have discovered that learning is a lifelong process. Every project you start opens up ten new ones; it is a never-ending process and there is always more to discover. Coming from the French academic system, it was interesting to learn about a new system and to immerse myself in a new culture. I have not only learned a new culture but also a new language. It has not always been easy, but stepping out of my comfort zone has been the most enriching decision of my life.

5.3 Reflection on Physics

My reflection on quantum physics is that, for me, quantum is not an adjective; we should not say: this is quantum, this is classical. Quantum and classical physics are just tools to explore the universe. Sometimes, a classical tool is sufficient according to what you want to study, explain, but sometimes taking the "glasses" of quantum physics to look at your system might unlock some aspect that could explain your observation more completely. However, even these "glasses" could be upgraded because they may not explain everything yet.

Physics excels at building upon existing knowledge through refinement and expansion. However, it is crucial to maintain a balance. While a strong foundation in established models is essential, we must also prioritize fresh perspectives. An over-reliance on existing frameworks can restrict creativity, hindering the escalation of potentially groundbreaking new approaches.

5.4 The Journey Continues...

A PhD involves more than research; it encompasses communication, organization, and teaching. Writing is not the sole challenge; it is about mastering various skills. For instance, managing multiple projects simultaneously has taught me time management and prioritization.

Choosing to complete my PhD is a significant decision. We can never fully grasp any subject, but the journey itself shapes us. Participating in conferences, public talks, and teaching has highlighted my growth. Success is not solely about results, it is about personal development.

I have also learned more about myself and discovered that everyone manages their PhD differently. I used to stress about not knowing everything, but now I realize it is not a shame or a problem. I do not need to know everything and it is okay if I forget something because, at the end of the day, we are here to learn.

5.5 Connection to The Brain

If you look at the thesis from my perspective, a common point is present: the brain. It is linked to Chapter 2 via the "Quantum Brain" proposal, but also to Chapter 3 since we could perhaps use NV centers to probe the brain. Finally, in Chapter 4, the concept of vision is directly linked to the brain, where even without light, the brain can generate the perception of light.

On top of that, the brain was linked to the thesis due to the simple and amusing fact that it was what I used to write and study everything presented here. I also aimed to stimulate brains and make the thesis more attractive. How? If you look at the beginning of each chapter, I used photographs — these photographs were chosen by my own brain. They were selected at a specific time when my brain was in a certain mindset and environment. Thus, the choice of photographs for each chapter was directly linked to how I was thinking at that particular moment in my life based on my experiences. If I had to do it again now, my perspective has changed, and I might choose different photographs.

Why do I mention all this? Because it is fascinating that each person will try to make connections based on their own experiences, and every link they make will be unique to them. The purpose is to stimulate the brain, making the thesis original and personal. At the end of the day, a thesis is a personal research journey. In Chapter 6, I provide a personal reflection on the brain and my aspirations for future research.

Chapter 6

FUTURE PERSPECTIVES

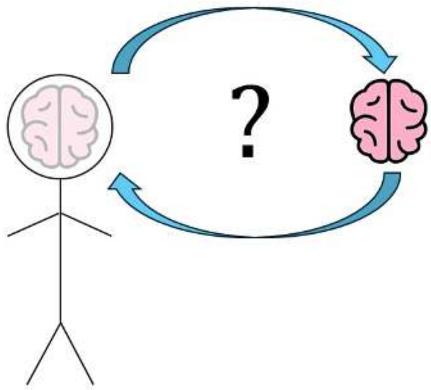

This chapter is an amalgamation of some future plausible publications, some of which are being drafted already [Gassab et al., 2024d, Gassab et al., 2024c, Gassab, 2024].

6.1 The Intertwining Relationship Between Biology and Quantum Physics

In this thesis it is interesting to look at the intersection of biology and quantum physics through multiple pathways:

1. "Quantum in biology" refers to quantum effects in biological systems;
2. "Quantum for biology" is the use of quantum technology for biological assessment;
3. "Biology for quantum" draws inspiration from biological systems to build quantum technologies.

Chapter 2 looks into the Posner cluster, examining the potential presence of quantum physics within biological systems, aligning with the first point above. Chapter 3 addresses the second point by using quantum physics to measure biological functions. Finally, Chapter 4 relates to the third point by investigating how the human eye might detect entanglement, suggesting the possibility of employing biological systems to measure quantum properties such as entanglement.

The intertwining of biology and quantum physics is just at the beginning of its growth. It offers possibilities in many different ways. One way leads toward using technology to probe biology, and another leads to using biology to develop technology. The latter could help us to understand the fundamental functions in biology. By looking through the lens of quantum physics, we may gain insights into one of the most mysterious biological systems that currently you are using to read this text and that impacts everything we do. This is the brain!

The current trend is that, when we cannot understand how biology functions with the classical laws of physics, we intend to look at it through the perspective of quantum physics. Indeed, everything is made up of fundamental particles that, for now, can only be explained by quantum mechanics. It is interesting how what we are made up of and what is around us is at the essence governed by quantum mechanics, but in biology, since the system is too complex and too warm, it often does not make sense to many that quantum mechanics could explain its behavior. If we think about it carefully, the quantum nature at the essence is still present nonetheless.

6.2 The Brain

What scientists want to understand is how the brain is working. First, it was thought that the brain was just like a computer [Newell et al., 1972], but it can do things that are not doable by a computer as yet, and some call it "consciousness" [Hameroff and Penrose, 2014, McFadden, 2020]. This term is very famous and usually not liked because it is not well defined, and as a matter of fact, it is used to explain something that we do not understand. It is not solving any issue.

Several theories in neuroscience try to look into the origins of consciousness at a quantum level. Orchestrated Objective Reduction (Orch OR), conceptualized by [Hameroff and Penrose, 1996, Hameroff and Penrose, 2014, Hameroff, 2007] since the early 1990s, posits that consciousness emerges from quantum processes within neurons. The Conscious Electromagnetic Information (CEMI) Field Theory from [McFadden, 2002, McFadden, 2020] offers another perspective, suggesting that consciousness is embedded within and influenced by the brain's electromagnetic field. [Fisher, 2015, Weingarten et al., 2016] draw parallels between quantum computing and brain function, proposing that the brain may operate akin to a quantum computer.

6.2.1 Mind or Brain?

When we prompt Gemini (formerly known as Bard, a large language model designed by Google): "What is brain, and what is mind?", the following is the output as of July 1, 2024:

> "The brain and mind are two closely related concepts, but they are fundamentally different things.
>
> Brain: The brain is a physical organ located in your head. It's the most complex organ in the human body and is made up of billions of nerve cells called neurons. The brain is responsible for everything you do, from thinking and feeling to controlling your muscles and organs.
>
> Mind: The mind is a bit more mysterious. It's not a physical thing like the brain, but rather an idea or concept that refers to all your mental processes, including:
>
> Thoughts, Feelings, Memories, Perceptions, Consciousness.
>
> We can think of the brain as the hardware and the mind as the software. The brain is the physical organ that allows the mind to exist."

Since in the lab, no accurate distinction has been made yet between the brain and the mind, and whether the mind really exists, or how it should be physically defined, hereon, when we refer to the brain, it may also refer to the above current global definition of the mind.

When we look at how our own brain works, it is probably different for everyone. It is very hard to study an interface by using the interface itself, that is, the brain. However, when we look over people around us, and ourselves, we may see that the brain likes new things. It likes being triggered and learning something it does not know, especially when it makes sense in the life of the person. For instance, we go on vacation and get relief from our routine.

It is very interesting to see how our society is based on norms and regulations that our brain may not like. The brain likes to be creative; it likes to learn and to be a researcher. However, at the same time, the society imposes rules and templates that are expected to be followed. Although the brain may feel reassured by norms, by remaining in the comfort zone, we may be going against what is one of the plausible true natures of the brain, which is adaptability.

In my view, by repeating the same task or action, or even the same thinking, we create pathways in the brain or block them. It has been shown that a repetition of stimuli reduces neural activities [Grill-Spector et al., 2006]. We become more machine-like because we restrict ourselves to performing specific tasks.

6.2.2 Brain Plasticity

The ability of the brain to adapt is linked to the plasticity of the brain. It is well known that our interaction with the world rewires our brain [Johansen-Berg, 2007, Kolb and Whishaw, 1998]. When one loses or is deficient of a particular sense, the brain adapts and makes the other sense(s) stronger [Bavelier and Neville, 2002, Voss, 2013, Gougoux et al., 2004, Levänen and Hamdorf, 2001, Sadato et al., 1996]. It has also been shown that when one of the brain hemispheres is removed, the other hemisphere can adapt to take care of the functions that were once run by the absent hemisphere [Pulsifer et al., 2004, Shimizu, 2005, Jutila et al., 2014, Boatman et al., 1999].

This demonstrates that the brain is very efficient with change. Yet, we are scared of change even though our brain is made for it. But then, which part of our brain makes us scared? Most of the time, the balance of this fear and ability to change is studied for cases of disabilities caused by accidents and injuries [Livneh, 2001, Kennedy and Evans, 2001, Keatley et al., 2023, Horgan and MacLachlan, 2004, Tedeschi and Calhoun, 1996]. It sums up to what goes on in the head of the patient. Are they motivated enough to attempt to move their paralyzed body parts, or are they drowned in the fear of never being able to walk or move again [Maclean et al., 2000, Craig et al., 2009, Wiles et al., 2002]?

6.2.3 Effects of Electric Signals On The Brain and In The Brain

Indeed, our thoughts and repetitive ways of thinking probably have an impact on the wiring structure of the brain [Draganski et al., 2004, Fox et al., 2005, Hölzel et al., 2011, DeRubeis et al., 2008, Kandel, 2001]. It has been shown how electrical signals can shape [Li et al., 2019] and influence [Ravikumar et al., 2019] the material world. So, it should make sense how electrical information from the sensors in our body could shape the brain. But what about the thoughts? Is there an external sensor (outside the brain) that gives the brain information to "think"? Suppose that one is able to deactivate all the external senses discussed at the beginning of Chapter 3, and just think. Will the person be able to process information and even have new information? If it is possible, then which interaction helps to do so? Which electrical field originating from the brain and triggering this mechanism of thinking makes the person aware of oneself?

6.2.4 Stress

Stress often has a direct correlation with thinking. It has been addressed how neuroplasticity is affected by stress [Nordman et al., 2023, Radley and Morrison, 2005]. Stress blocks the thinking ability of the brain.

This stress is also constructed by the brain when it evaluates a situation as "stressful", which we can technically translate as an unrealizable situation. Stress appears when we are not in control of a situation and we are scared about the future. It is like, in some sense, blocking our thoughts toward a negative outcome. The statements in the previous sentences are based on a self-reflection.

Like every research in science, the appealing part is to find out where this mechanism of responding to stress comes from. When we are a child, we do not stress much [Lupien et al., 2009]. We just play to learn [Gopnik and Wellman, 2012]. We do not block our brain from learning [Knudsen, 2004]. Eventually, we grow up and we block this process of learning and adaptability and get stuck in what we think we know already [Hensch, 2005]. This leads to cognitive rigidity and reduced performance in adults [Beilock and Carr, 2005]. Such social behavior is well studied in developmental psychology [Diamond, 2013], educational sector [Hirsh-Pasek, 2009], and now thankfully in neuroscience too [Hamilton, 2024, Procopio et al., 2024, Luk and Christodoulou, 2024].

$$\text{Playing} + \text{Having Fun} = \text{Learning - Stress.} \tag{6.1}$$

How is all this related to physics and biology, and hence maybe to quantum mechanics? Without interdisciplinary research, we may never figure it out. Actually, it is all happening in the brain. This is where physics, chemistry and biology meet with all other sciences.

We should try to look at the physical level how it works and then we will be able to understand. When a baby is just born, its brain did not yet get full exposure to the surrounding environment. We have sensors in our entire body that send signals to the brain. By receiving electric signals from the sensors, the brain is shaped in a certain way and develops automated mechanisms that we need like walking, talking, eating, etc.

What about breathing? In the field of respiratory physiology, it is still not clear how the first breath of the baby is prompted.

Ongoing research into the specific neural and hormonal mechanisms involved tend to focus on the stress hormones known as catecholamines and the activation of chemoreceptors that detect changes in blood gases [Lagercrantz and Bistoletti, 1977, Polin and Abman, 2011, Mortola, 2001]. If these hypotheses turn out to be true, we will be able to deduce that a condition such as stress that is considered deficient for an adult's health might have been beneficial at the birth stage.

6.2.5 Solutions to Stress and Brain Disorders

Like stress, brain processes may be another example of a two-sided coin. While some brain processes are at the origin of neurological disorders and hence, the root of many neurodegenerative diseases, other brain processes may hold the solutions to these health issues. For instance, cognitive restructuring can help to reduce stress which is at the origin of many brain disorders [Hofmann et al., 2012, Olatunji et al., 2007, Schnurr et al., 2007, Hollon and Beck, 1979, McEwen, 2007, Turner et al., 2007] such as depression, anxiety disorders, bipolar disorder, substance use disorders, Attention Deficit Hyperactivity Disorder (ADHD), Post-Traumatic Stress Disorder (PTSD), Obsessive-Compulsive Disorder (OCD), chronic pain syndromes, Irritable Bowel Syndrome (IBS), Alzheimer's disease and other dementias. By overriding stress blockage with the help of cognitive exercises such as:

1. Cognitive Behavioral Therapy (CBT) [Beck, 2020, Hofmann et al., 2012, Ellis, 2019],

2. Mindfulness-Based Stress Reduction (MBSR) [Kabat-Zinn, 2013, Chiesa and Serretti, 2009],

3. Gratitude Exercises [Emmons and McCullough, 2003, Wood et al., 2010],

4. Progressive Muscle Relaxation [Jacobsen, 1929, Bernstein et al., 2000],

5. Problem-Solving Therapy [Nezu et al., 2012, Bell and D'Zurilla, 2009],

the processing capacity of the brain such as adaptability and rewiring could be restored, and as a result, the effects of many of these diseases could be mitigated or even cured.

6.2.6 Can Quantum Physics Address Pathological Issues?

When examining the rewiring of the brain at a molecular level, the microtubule cytoskeleton is at the origin of this restructuring. Microtubules serve as the cell's skeleton, providing shape and form according to their function. Brain rewiring involves the creation of new dendrites, new synapses, and new connections, as well as the cessation of existing connections [Kapitein and Hoogenraad, 2015, Schmidt and Rathjen, 2010, Sakakibara et al., 2013].

However, this description does not explain how this process occurs. It merely attributes the phenomenon to microtubules. The critical question is: how do microtubules receive the information needed to rewire? It is unlikely that this process is purely chemical due to efficiency considerations. The integration of signals to produce specific changes at particular locations within the neuron remains an area of active research [Etienne-Manneville, 2010, Avila et al., 2003]. Understanding how these networks function as a whole to produce coordinated outcomes is a significant challenge.

It seems that microtubules not only receive information but are also aware of their surroundings, making the process efficient in both time and space. Quantum mechanics may explain this capability, suggesting the efficient transfer of information through quantum coherence and possibly entanglement [Kalra et al., 2023, Babcock et al., 2024]. Perhaps microtubules may be merely the messengers of a field connected to everything [Hameroff and Penrose, 1996]. Who knows?

6.2.7 Does Quantum Physics Have All The Answers?

Maybe quantum mechanics could help to resolve the diverse issues discussed above [Wu et al., 2024]. Or, maybe some other theory beyond quantum physics may come up. The following are theories related to the brain that have been studied in the past.

- **Information Processing Theory**: This theory treats the brain as a complex information processor, similar to a computer. It emphasizes the brain's ability to encode, store, retrieve, and process information [Newell et al., 1972].

- **Integrated Information Theory (IIT)**: IIT proposes that consciousness corresponds to the ability of a system to integrate information. This theory attempts to quantify consciousness by measuring the amount of integrated information in a system [Tononi, 2008].

- **Predictive Coding and Bayesian Brain Hypothesis**: This theory suggests that the brain constantly generates and updates a model of the environment based on incoming sensory information and prior knowledge, aiming to minimize prediction errors [Friston, 2010].

- **Connectome Theory**: This approach focuses on mapping and understanding the brain's structural and functional connectivity (connectome). It posits that the brain's network architecture plays a critical role in its function and behavior [Sporns et al., 2005].

- **Embodied Cognition**: The theory emphasizes the role of the body and its interactions with the environment in shaping the mind. It argues that cognitive processes are deeply rooted in the body's physical and sensory experiences [Barsalou, 2008].

- **Complex Systems Theory**: This theory advocates how the brain functions as a complex system with properties such as emergence, self-organization, and nonlinearity. It provides a framework for understanding how simple interactions at the micro level can lead to complex behaviors at the macro level [Bassett and Gazzaniga, 2011, Kelso, 1995].

- **Neural Darwinism (Theory of Neuronal Group Selection)**: Proposed by [Edelman, 1983], this theory suggests that the development and functioning of the brain involve a process of selection among neuronal groups, analogous to natural selection.

Some of these theories, despite being now obsolete, provide alternative frameworks for understanding the brain that are not dependent on quantum physics. Each offers unique insights and methodologies for comprehending brain function and cognition. Research should not be bounded by one particular theory. On the contrary, the more cross-fertilized the discipline is, the sweeter the fruit may be!

6.2.8 Outlook

The entire society, the problems in our society, the goodness of our society and our evaluation of what is good, what is bad, lie in our brain. By studying the brain and its processes, we will understand every discipline, and why they are shaped the way they are.

Science is derived from our observation of the world. At the beginning, there were no theories, but now, we have so many different theories based on two things:

1. the different interactions of the brain with the world,

2. putting all these interactions together in a language that is sane and makes sense to the intellect part of the brain.

Some theories like the Standard Model of particle physics work partially, explaining the three fundamental forces in the universe but not accounting for gravity.

Many such theories, since they have been major contributions for a long time to the field of physics, can block the brain from being open to think differently and create new theories that may possibly cover the missing aspects of the existing theories.

At the beginning, theories used to emerge from our observation of the world: the behavior of plants, animals, humans, the ocean and other natural phenomena around us. In my opinion, while numerous scientists, in fields like botany, forestry, zoology, and oceanography, still carry out much fieldwork, what is probably lacking nowadays is this kind of observation coming from scholars working in the lab, or dealing with purely theoretical topics in closed offices and having this belief that physics, chemistry, or biology can only be studied in an empirical way or using traditional laboratory setup. On the other side, we also have the extrapolation of theories or hypotheses that may lead to pseudo-science. For instance, string theory and consciousness are currently viewed with a mix of optimism and skepticism in the physics community. If we go back in time, the atom used to be considered as the smallest indivisible particle. Many a time, we will continue to make mistake along the way, isn't this a good thing?

For scientific knowledge to expand and grow healthily, we need to strive for the right balance in the right direction. This is not easily achievable. However, we should put our efforts together by increasing multidisciplinary collaborations across all fields of science to build scientific theories that are well understood across all domains and that every scientist can relate to in the language of their field. Before the establishment of quantum theory, did anyone imagine the possibility of such theories? Now that quantum mechanics is a well settled concept, are we envisaging a completely new theory to emerge from our brain? That would definitely drive the whole scientific community to develop new research strategies.

We should take a step back and re-consider what research really means and how it all started in the history of humankind. We should also make our own deductions from our observations, and not just accept things the way we are told or taught, or because it is working partially.

The basic action of judging that something is right or working may be biased based on information already present in the brain and this judgment is ruled by the brain. Our deductions and analysis may not always be correct, but it will make us think, it will generate new pathways in our brain and keep our inquisitive mind alive.

In the bigger scheme of things, that is, considering our insignificant existence on this earth and its position in the known universe with one trillion galaxies, we should assume one thing: we know almost nothing. We have barely scratched the door of quantum biology or any other science. We just know what our brain shows us. So, by acknowledging the current brain limitations and future possibilities, we can probably unlock our understanding of its functionalities, and eventually comprehend our make and reality with a broader perspective. The brain is also the best example to improve tomorrow's technology such as Artificial Intelligence (AI) [Farisco et al., 2024, Pyrkov et al., 2024]. This makes it the most exciting and difficult system to study but it will potentially be the crucial key for the next discoveries.

Chapter 7

DISSEMINATION OF RESEARCH

7.1 Publications

- Gassab, L., Pusuluk, O., Müstecaplıoğlu, Ö. E. (2024). Geometrical optimization of spin clusters for the preservation of quantum coherence. *Physical Review A*, 109(1), 012424.

- Gassab, L., Pedram, A., Müstecaplıoğlu, Ö. E. (2024). Conditions on detecting tripartite entangled state in psychophysical experiments. *The European Physical Journal Plus*, 139(5), 379.

- Gassab, L., Müstecaplıoğlu, Ö. E. (2024.) Spin Squeezing Enhanced Quantum Magnetometry with Nitrogen-Vacancy Center Qutrits. *arXiv preprint*, arXiv:2406.15324.

- Gassab, L., Pusuluk, O., Müstecaplıoğlu, Ö. E. Quantum Models of Consciousness from a Quantum Information Science Perspective. *In preparation.*

- Gassab, L., Pusuluk, O., Xie, C., Kominis, I., Müstecaplıoğlu, Ö. E. Beyond the Nexus: Quantum and Biology Intertwined. *In preparation.*

- Pedram, A., Besaga, V.R., Gassab, L., Setzpfandt, F., Müstecaplıoğlu, Ö. E. (2024). Quantum Estimation of the Stokes Vector Rotation for a General Polarimetric Transformation, *arXiv preprint*, arXiv:2304.08258.

7.2 Conferences

- QuEBS 2022, poster presentation, June 6-10, 2022, Heraklion, Greece.
- LPHYS'22, oral presentation, July 18-22, 2022, online.
- KOBIT$|7\rangle$, oral presentation, February 2-3, 2023, Eskişehir, Türkiye.
- QuEBS 2023, oral presentation, June 26-30, 2023, University of Surrey, UK.
- Mini-Workshop on Quantum Thermodynamics, oral presentation, October 23-25, 2023, Koç University, Istanbul, Türkiye.
- ITAMP Winter school, poster presentation, February 18-24, Arizona, US.
- KOBIT$|8\rangle$, poster presentation, April 25-26, 2024, Gebze, Türkiye.

7.3 Events

- Public talk on Youtube with QTürkiye, January 16, 2021, online.
- Science Fair, poster presentation, May 31, 2023, Koç university, Türkiye.
- Science Fair, Quantum Theme Park, October 18, 2023, Koç university, Türkiye.
- Quantum Theme Park, January 12, 2024, Notre Dame Dion, Türkiye.
- Koç School Science Fair, February 13, 2024, Koç school, Türkiye.
- Science Fair, poster presentation, May 22, 2024, Koç university, Türkiye.

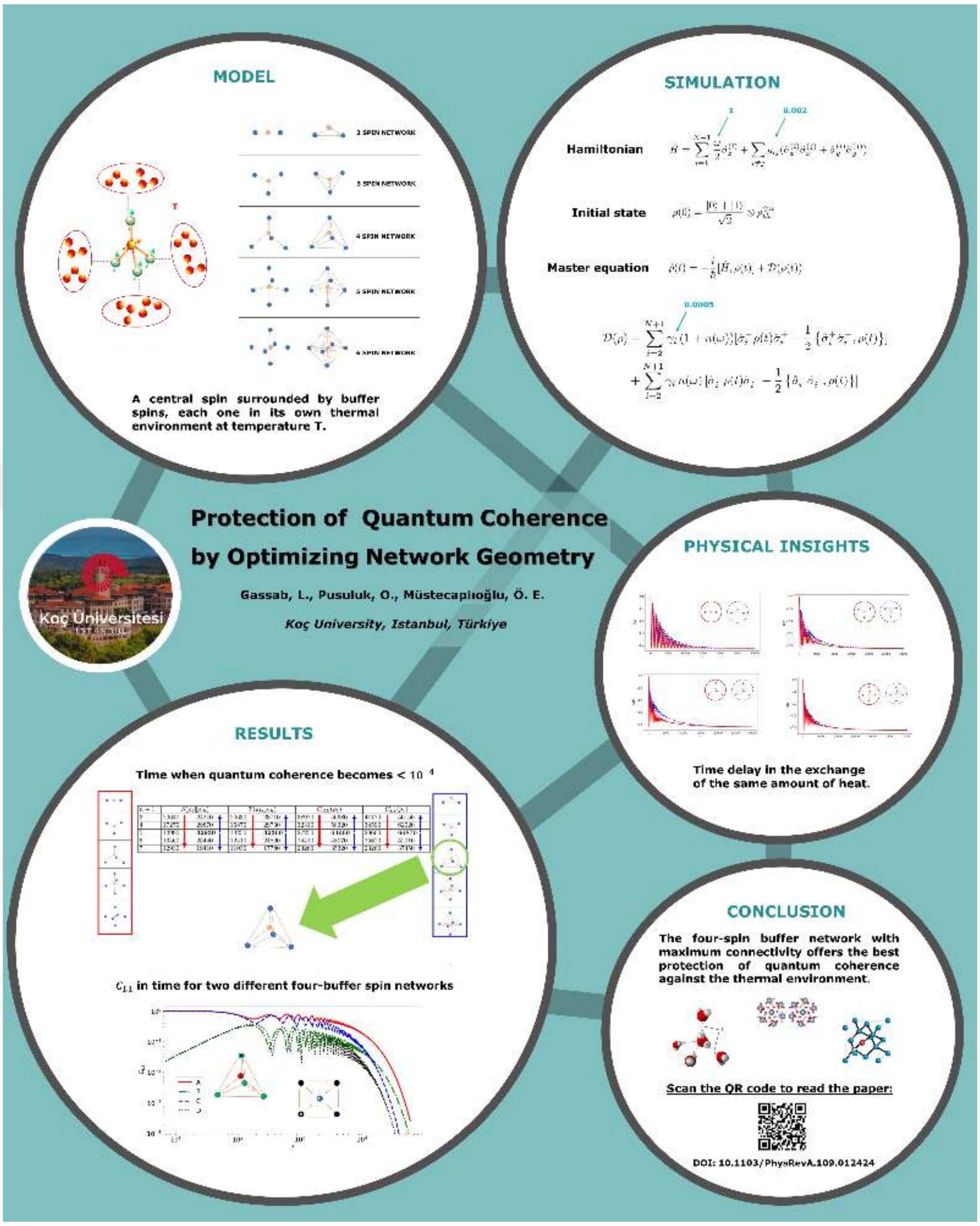
MODEL
2 SPIN NETWORK
3 SPIN NETWORK
4 SPIN NETWORK
5 SPIN NETWORK
6 SPIN NETWORK
A central spin surrounded by buffer spins, each one in its own thermal environment at temperature T.
SIMULATION
Hamiltonian
Initial state
Master equation
Protection of Quantum Coherence by Optimizing Network Geometry
Gassab, L., Pusuluk, O., Müstecaplıoğlu, Ö. E.
Koç University, Istanbul, Türkiye
Koç Üniversitesi
PHYSICAL INSIGHTS
Time delay in the exchange of the same amount of heat.
RESULTS
Time when quantum coherence becomes < 10⁻⁴
C_{11} in time for two different four-buffer spin networks
CONCLUSION
The four-spin buffer network with maximum connectivity offers the best protection of quantum coherence against the thermal environment.
Scan the QR code to read the paper:
DOI: 10.1103/PhysRevA.109.012424

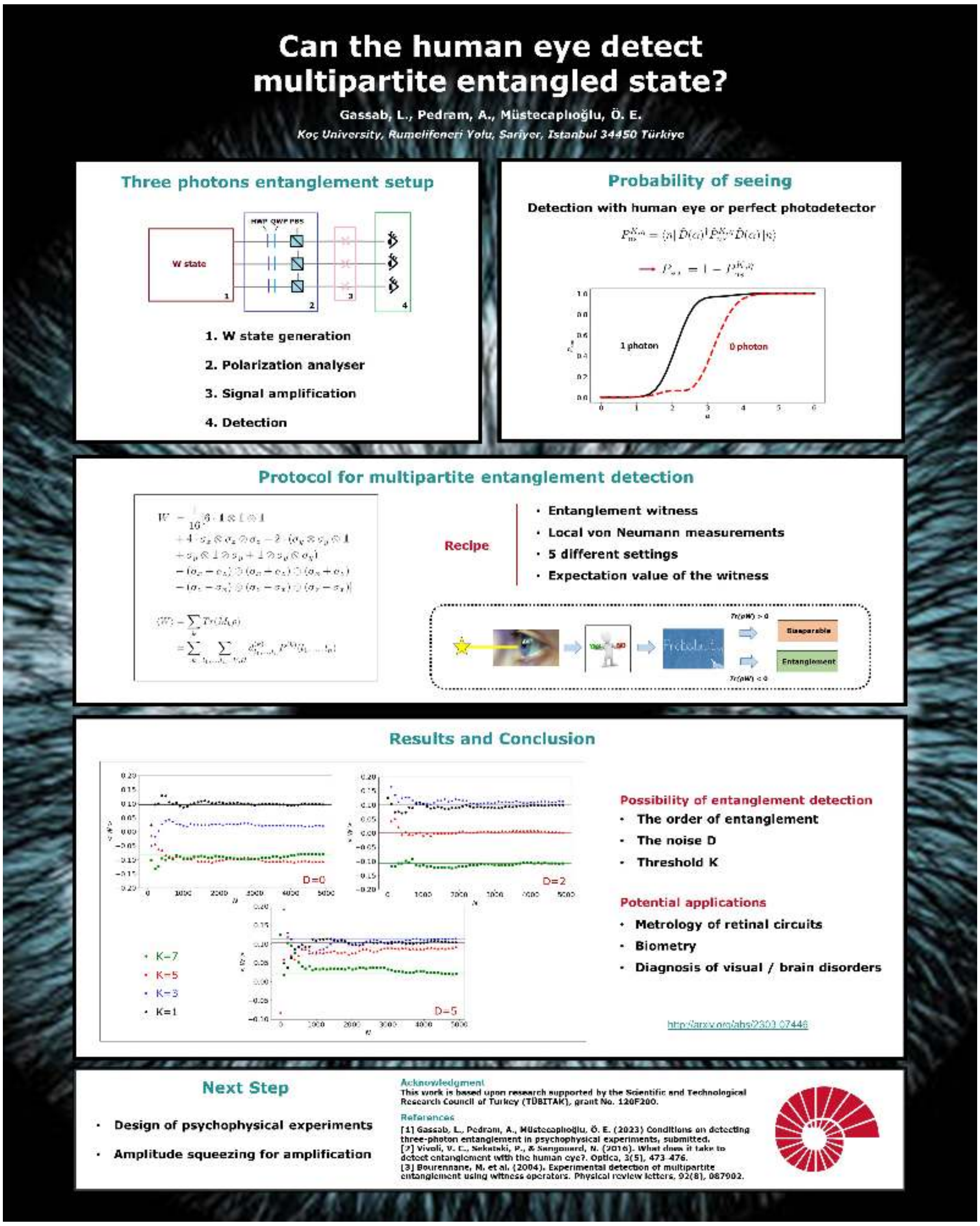
Can the human eye detect multipartite entangled state?
Gassab, L., Pedram, A., Müstecaplıoğlu, Ö. E.
Koç University, Rumelifeneri Yolu, Sarıyer, Istanbul 34450 Türkiye
Three photons entanglement setup
W state
1. W state generation
2. Polarization analyser
3. Signal amplification
4. Detection
Probability of seeing
Detection with human eye or perfect photodetector
1 photon
0 photon
Protocol for multipartite entanglement detection
Recipe
Entanglement witness
Local von Neumann measurements
5 different settings
Expectation value of the witness
Biseparable
Entanglement
Results and Conclusion
D=0
D=2
D=5
K=7
K=5
K=3
K=1
Possibility of entanglement detection
The order of entanglement
The noise D
Threshold K
Potential applications
Metrology of retinal circuits
Biometry
Diagnosis of visual / brain disorders
Next Step
Design of psychophysical experiments
Amplitude squeezing for amplification
Acknowledgment
This work is based upon research supported by the Scientific and Technological Research Council of Turkey (TÜBITAK), grant No. 120F200.
References
[1] Gassab, L., Pedram, A., Müstecaplıoğlu, Ö. E. (2023) Conditions on detecting three-photon entanglement in psychophysical experiments, submitted.
[2] Vivoli, V. C., Sekatski, P., & Sangouard, N. (2016). What does it take to detect entanglement with the human eye? Optica, 3(5), 473-476.
[3] Bourennane, M. et al. (2004). Experimental detection of multipartite entanglement using witness operators. Physical review letters, 92(8), 087902.

BIBLIOGRAPHY

[Abeywardana et al., 2014] Abeywardana, C., Stepanov, V., Cho, F. H., and Takahashi, S. (2014). Magnetic resonance spectroscopy using a single nitrogen-vacancy center in diamond. In *Quantum and Nonlinear Optics III*, volume 9269, pages 27–33. SPIE.

[Acosta and Hemmer, 2013] Acosta, V. and Hemmer, P. (2013). Nitrogen-vacancy centers: Physics and applications. *MRS bulletin*, 38(2):127–130.

[Adams et al., 2023] Adams, B., Sinayskiy, I., Agarwal, S., and Petruccione, F. (2023). Entanglement and coherence in pure and doped posner molecules. *arXiv preprint arXiv:2310.13484*.

[Agarwal, 2012] Agarwal, G. S. (2012). *Quantum optics*. Cambridge University Press.

[Aiello et al., 2022] Aiello, C. D., Abendroth, J. M., Abbas, M., Afanasev, A., Agarwal, S., Banerjee, A. S., Beratan, D. N., Belling, J. N., Berche, B., Botana, A., et al. (2022). A chirality-based quantum leap. *ACS nano*, 16(4):4989–5035.

[Altepeter et al., 2003] Altepeter, J. B., Branning, D., Jeffrey, E., Wei, T. C., Kwiat, P. G., Thew, R. T., O'Brien, J. L., Nielsen, M. A., and White, A. G. (2003). Ancilla-assisted quantum process tomography. *Phys. Rev. Lett.*, 90:193601.

[Anderson and Johnnesson, 2006] Anderson, J. B. and Johnnesson, R. (2006). *Understanding information transmission*. John Wiley & Sons.

[Archibald et al., 2009] Archibald, N. K., Clarke, M. P., Mosimann, U. P., and Burn, D. J. (2009). The retina in Parkinson's disease. *Brain*, 132(5):1128–1145.

[Ash, 2012] Ash, R. B. (2012). *Information theory.* Courier Corporation.

[Avila et al., 2003] Avila, J., DOMiNGUEZ, J., and Diaz-Nido, J. (2003). Regulation of microtubule dynamics by microtubule-associated protein expression and phosphorylation during neuronal development. *International Journal of Developmental Biology*, 38(1):13–25.

[Babcock et al., 2024] Babcock, N., Montes-Cabrera, G., Oberhofer, K., Chergui, M., Celardo, G., and Kurian, P. (2024). Ultraviolet superradiance from mega-networks of tryptophan in biological architectures. *The Journal of Physical Chemistry B.*

[Bachor and Ralph, 2019] Bachor, H.-A. and Ralph, T. C. (2019). *A guide to experiments in quantum optics.* John Wiley & Sons.

[Bae et al., 2020] Bae, J., Chruściński, D., and Hiesmayr, B. C. (2020). Mirrored entanglement witnesses. 6(1):15.

[Bahri et al., 2015] Bahri, Y., Vosk, R., Altman, E., and Vishwanath, A. (2015). Localization and topology protected quantum coherence at the edge of hot matter. *Nature Communications*, 6(1):7341.

[Baiesi et al., 2017] Baiesi, M., Orlandini, E., Seno, F., and Trovato, A. (2017). Exploring the correlation between the folding rates of proteins and the entanglement of their native states. *Journal of Physics A: Mathematical and Theoretical*, 50(50):504001.

[Balasubramanian et al., 2014] Balasubramanian, G., Lazariev, A., Arumugam, S. R., and Duan, D.-w. (2014). Nitrogen-vacancy color center in diamond—emerging nanoscale applications in bioimaging and biosensing. *Current opinion in chemical biology*, 20:69–77.

[Balasubramanian et al., 2009] Balasubramanian, G., Neumann, P., Twitchen, D., Markham, M., Kolesov, R., Mizuochi, N., Isoya, J., Achard, J., Beck, J., Tissler, J., et al. (2009). Ultralong spin coherence time in isotopically engineered diamond. *Nature materials*, 8(5):383–387.

[Bar-Gill et al., 2013] Bar-Gill, N., Pham, L. M., Jarmola, A., Budker, D., and Walsworth, R. L. (2013). Solid state electronic spin coherence time approaching one second. *Nature communications*, 4(1):1743.

[Barlow, 1977] Barlow, H. (1977). Retinal and central factors in human vision limited by noise. *Vertebrate photoreception*, 337:C358.

[Barlow, 1956] Barlow, H. B. (1956). Retinal noise and absolute threshold. *J. Opt. Soc. Am.*, 46(8):634–639.

[Barry et al., 2020] Barry, J. F., Schloss, J. M., Bauch, E., Turner, M. J., Hart, C. A., Pham, L. M., and Walsworth, R. L. (2020). Sensitivity optimization for nv-diamond magnetometry. *Reviews of Modern Physics*, 92(1):015004.

[Barsalou, 2008] Barsalou, L. W. (2008). Grounded cognition. *Annu. Rev. Psychol.*, 59(1):617–645.

[Bass and Doser, 2024] Bass, S. D. and Doser, M. (2024). Quantum sensing for particle physics. *Nature Reviews Physics*, pages 1–11.

[Bassett and Gazzaniga, 2011] Bassett, D. S. and Gazzaniga, M. S. (2011). Understanding complexity in the human brain. *Trends in cognitive sciences*, 15(5):200–209.

[Baumgratz et al., 2014] Baumgratz, T., Cramer, M., and Plenio, M. B. (2014). Quantifying coherence. *Physical review letters*, 113(14):140401.

[Bavelier and Neville, 2002] Bavelier, D. and Neville, H. J. (2002). Cross-modal plasticity: where and how? *Nature Reviews Neuroscience*, 3(6):443–452.

[Baylor et al., 1979a] Baylor, D. A., Lamb, T. D., and Yau, K. W. (1979a). The membrane current of single rod outer segments. *The Journal of Physiology*, 288(1):589–611.

[Baylor et al., 1979b] Baylor, D. A., Lamb, T. D., and Yau, K. W. (1979b). Responses of retinal rods to single photons. *The Journal of Physiology*, 288(1):613–634.

[Baylor et al., 1984] Baylor, D. A., Nunn, B. J., and Schnapf, J. L. (1984). The photocurrent, noise and spectral sensitivity of rods of the monkey macaca fascicularis. *The Journal of Physiology*, 357(1):575–607.

[Beck, 2020] Beck, J. S. (2020). *Cognitive behavior therapy: Basics and beyond*. Guilford Publications.

[Begzjav and Agarwal, 2021] Begzjav, T. K. and Agarwal, G. S. (2021). Squeezing of spin-1 quantum states via a one-axis twisting hamiltonian. *Physical Review A*, 104(2):023706.

[Beilock and Carr, 2005] Beilock, S. L. and Carr, T. H. (2005). When high-powered people fail: Working memory and "choking under pressure" in math. *Psychological science*, 16(2):101–105.

[Bell and D'Zurilla, 2009] Bell, A. C. and D'Zurilla, T. J. (2009). Problem-solving therapy for depression: a meta-analysis. *Clinical psychology review*, 29(4):348–353.

[Benabdallah et al., 2021] Benabdallah, F., Zad, H. A., Daoud, M., and Ananikian, N. (2021). Dynamics of quantum correlations in a qubit-qutrit spin system under random telegraph noise. *Physica Scripta*, 96(12):125116.

[Bennett, 1982] Bennett, C. H. (1982). The thermodynamics of computational review. *International Journal of Theoretical Physics*, 21:905–940.

[Bennett et al., 2013] Bennett, S. D., Yao, N. Y., Otterbach, J., Zoller, P., Rabl, P., and Lukin, M. D. (2013). Phonon-induced spin-spin interactions in diamond nanostructures: Application to spin squeezing. *Phys. Rev. Lett.*, 110:156402.

[Berchera and Degiovanni, 2019a] Berchera, I. R. and Degiovanni, I. P. (2019a). Quantum imaging with sub-poissonian light: challenges and perspectives in optical metrology. *Metrologia*, 56(2):024001.

[Berchera and Degiovanni, 2019b] Berchera, I. R. and Degiovanni, I. P. (2019b). Quantum imaging with sub-poissonian light: challenges and perspectives in optical metrology. *Metrologia*, 56(2):024001.

[Bernstein et al., 2000] Bernstein, D. A., Borkovec, T. D., and Hazlett-Stevens, H. (2000). *New directions in progressive relaxation training: A guidebook for helping professionals.* Praeger Publishers/Greenwood Publishing Group.

[Besaga et al., 2024] Besaga, V. R., Ott, F., Meyer-Zedler, T., and Setzpfandt, F. (2024). Application of polarization-entangled photon pairs for studying the density of microorganisms. In *Quantum Technologies 2024*, volume 12993, pages 54–57. SPIE.

[Bigelow, 2001] Bigelow, N. (2001). Squeezing entanglement. *Nature*, 409(6816):27–28.

[Bloch, 1967] Bloch, I. (1967). Some relativistic oddities in the quantum theory of observation. *Physical Review*, 156(5):1377.

[Bluvstein et al., 2019] Bluvstein, D., Zhang, Z., McLellan, C. A., Williams, N. R., and Jayich, A. C. B. (2019). Extending the quantum coherence of a near-surface qubit by coherently driving the paramagnetic surface environment. *Physical Review Letters*, 123(14):146804.

[Boatman et al., 1999] Boatman, D., Freeman, J., Vining, E., Pulsifer, M., Miglioretti, D., Minahan, R., Carson, B., Brandt, J., and McKhann, G. (1999). Language recovery after left hemispherectomy in children with late-onset seizures. *Annals of Neurology: Official Journal of the American Neurological Association and the Child Neurology Society*, 46(4):579–586.

[Boretti et al., 2019] Boretti, A., Rosa, L., Blackledge, J., and Castelletto, S. (2019). Nitrogen-vacancy centers in diamond for nanoscale magnetic resonance imaging applications. *Beilstein journal of nanotechnology*, 10(1):2128–2151.

[Born M, 1925] Born M, J. P. (1925). Zur quantenmechanik. *Zeitschrift für Physik*, 34:858–888.

[Borregaard et al., 2017] Borregaard, J., Davis, E., Bentsen, G. S., Schleier-Smith, M. H., and Sørensen, A. S. (2017). One-and two-axis squeezing of atomic ensembles in optical cavities. *New Journal of Physics*, 19(9):093021.

[Bouman, 2012] Bouman, M. A. (2012). *History and present status of quantum theory in vision*. Sensory Communication. The MIT Press.

[Bourennane et al., 2004] Bourennane, M., Eibl, M., Kurtsiefer, C., Gaertner, S., Weinfurter, H., Gühne, O., Hyllus, P., Bruß, D., Lewenstein, M., and Sanpera, A. (2004). Experimental detection of multipartite entanglement using witness operators. *Physical review letters*, 92(8):087902.

[Bramwell and Gingras, 2001] Bramwell, S. T. and Gingras, M. J. (2001). Spin ice state in frustrated magnetic pyrochlore materials. *Science*, 294(5546):1495–1501.

[Brandt, 1999] Brandt, H. E. (1999). Qubit devices and the issue of quantum decoherence. *Progress in Quantum Electronics*, 22(5-6):257–370.

[Brask et al., 2015] Brask, J. B., Chaves, R., and Kołodyński, J. (2015). Improved quantum magnetometry beyond the standard quantum limit. *Physical Review X*, 5(3):031010.

[Breuer et al., 2002] Breuer, H.-P., Petruccione, F., et al. (2002). *The theory of open quantum systems*. Oxford University Press on Demand.

[Brody, 2020] Brody, J. (2020). *Quantum entanglement*. MIT Press.

[Brunner et al., 2008] Brunner, N., Branciard, C., and Gisin, N. (2008). Possible entanglement detection with the naked eye. *Phys. Rev. A*, 78:052110.

[Buchmann et al., 2016] Buchmann, L., Schreppler, S., Kohler, J., Spethmann, N., and Stamper-Kurn, D. (2016). Complex squeezing and force measurement beyond the standard quantum limit. *Physical review letters*, 117(3):030801.

[Buffoni and Campisi, 2023] Buffoni, L. and Campisi, M. (2023). Cooperative quantum information erasure. *Quantum*, 7:961.

[Buscemi, 2012] Buscemi, F. (2012). All entangled quantum states are nonlocal. *Physical review letters*, 108(20):200401.

[Busch et al., 2007] Busch, P., Heinonen, T., and Lahti, P. (2007). Heisenberg's uncertainty principle. *Physics reports*, 452(6):155–176.

[Calvo and Enoch, 2005] Calvo, M. L. and Enoch, J. (2005). Introduction to the history of lenses and visual corrections: a reference to spain and the spanish colonies in the new world (xv-xvi c.). *Revista Cubana de Física*, 22(2):3–12.

[Cappellaro and Lukin, 2009] Cappellaro, P. and Lukin, M. D. (2009). Quantum correlation in disordered spin systems: Applications to magnetic sensing. *Physical Review A*, 80(3):032311.

[Caves et al., 2012] Caves, C. M., Combes, J., Jiang, Z., and Pandey, S. (2012). Quantum limits on phase-preserving linear amplifiers. *Physical Review A*, 86(6):063802.

[Chen and Jing, 2024] Chen, P. and Jing, J. (2024). Qubit-assisted quantum metrology. *arXiv preprint arXiv:2404.12649*.

[Chernobrod and Berman, 2005] Chernobrod, B. M. and Berman, G. P. (2005). Spin microscope based on optically detected magnetic resonance. *Journal of applied physics*, 97(1).

[Chiesa and Serretti, 2009] Chiesa, A. and Serretti, A. (2009). Mindfulness-based stress reduction for stress management in healthy people: a review and meta-analysis. *The journal of alternative and complementary medicine*, 15(5):593–600.

[Childress and Hanson, 2013] Childress, L. and Hanson, R. (2013). Diamond nv centers for quantum computing and quantum networks. *MRS bulletin*, 38(2):134–138.

[Chin et al., 2012] Chin, A., Huelga, S. F., and Plenio, M. B. (2012). Coherence and decoherence in biological systems: principles of noise-assisted transport and the origin of long-lived coherences. *Philosophical Transactions of the Royal Society A: Mathematical, Physical and Engineering Sciences*, 370(1972):3638–3657.

[Christ et al., 2013] Christ, A., Fedrizzi, A., Hübel, H., Jennewein, T., and Silberhorn, C. (2013). Parametric down-conversion. In *Experimental Methods in the Physical Sciences*, volume 45, pages 351–410. Elsevier.

[Chruściński and Sarbicki, 2014] Chruściński, D. and Sarbicki, G. (2014). Entanglement witnesses: construction, analysis and classification. *Journal of Physics A: Mathematical and Theoretical*, 47(48):483001.

[Chruściński and Sarbicki, 2014] Chruściński, D. and Sarbicki, G. (2014). Entanglement witnesses: construction, analysis and classification. *Journal of Physics A: Mathematical and Theoretical*, 47(48):483001.

[Cole and Hollenberg, 2009] Cole, J. H. and Hollenberg, L. C. (2009). Scanning quantum decoherence microscopy. *Nanotechnology*, 20(49):495401.

[Cordero, 2019] Cordero, A. (2019). *Philosophers look at quantum mechanics*, volume 406. Springer.

[Coto et al., 2021] Coto, R., Dinani, H. T., Norambuena, A., Chen, M., and Maze, J. R. (2021). Probabilistic magnetometry with a two-spin system in diamond. *Quantum Science and Technology*, 6(3):035011.

[Couteau, 2018] Couteau, C. (2018). Spontaneous parametric down-conversion. *Contemporary Physics*, 59(3):291–304.

[Cover et al., 1991] Cover, T. M., Thomas, J. A., et al. (1991). Entropy, relative entropy and mutual information. *Elements of information theory*, 2(1):12–13.

[Craddock et al., 2014] Craddock, T. J. A., Friesen, D., Mane, J., Hameroff, S., and Tuszynski, J. A. (2014). The feasibility of coherent energy transfer in microtubules. *Journal of the Royal Society Interface*, 11(100):20140677.

[Craig et al., 2009] Craig, A., Tran, Y., and Middleton, J. (2009). Psychological morbidity and spinal cord injury: a systematic review. *Spinal cord*, 47(2):108–114.

[Cramer et al., 2010] Cramer, M., Plenio, M. B., Flammia, S. T., Somma, R., Gross, D., Bartlett, S. D., Landon-Cardinal, O., Poulin, D., and Liu, Y.-K. (2010). Efficient quantum state tomography. *Nature Communications*, 1(1):149.

[Cristiano et al., 2015] Cristiano, R., Ejrnaes, M., Casaburi, A., Zen, N., and Ohkubo, M. (2015). Superconducting nano-strip particle detectors. *Superconductor Science and Technology*, 28(12):124004.

[Croucher et al., 2018] Croucher, T., Wright, J., Carvalho, A. R., Barnett, S. M., and Vaccaro, J. A. (2018). Information erasure. *Thermodynamics in the Quantum Regime: Fundamental Aspects and New Directions*, pages 713–730.

[D Ariano, 1992] D Ariano, G. (1992). Hamiltonians for the photon-number-phase amplifiers. *Physical Review A*, 45(5):3224.

[Dantas et al., 1998] Dantas, C., Almeida, N. G. d., and Baseia, B. (1998). Statistical properties of the squeezed displaced number states. *Brazilian journal of physics*, 28:462–469.

[Darrigol, 2012] Darrigol, O. (2012). *A history of optics from Greek antiquity to the nineteenth century*. OUP Oxford.

[Davidovich, 1996] Davidovich, L. (1996). Sub-poissonian processes in quantum optics. *Reviews of Modern Physics*, 68(1):127.

[Degen et al., 2017a] Degen, C. L., Reinhard, F., and Cappellaro, P. (2017a). Quantum sensing. *Reviews of Modern Physics*, 89:035002.

[Degen et al., 2017b] Degen, C. L., Reinhard, F., and Cappellaro, P. (2017b). Quantum sensing. *Reviews of modern physics*, 89(3):035002.

[DeMille et al., 2024] DeMille, D., Hutzler, N. R., Rey, A. M., and Zelevinsky, T. (2024). Quantum sensing and metrology for fundamental physics with molecules. *Nature Physics*, pages 1–9.

[DeRubeis et al., 2008] DeRubeis, R. J., Siegle, G. J., and Hollon, S. D. (2008). Cognitive therapy versus medication for depression: treatment outcomes and neural mechanisms. *Nature Reviews Neuroscience*, 9(10):788–796.

[Devitt et al., 2013] Devitt, S. J., Munro, W. J., and Nemoto, K. (2013). Quantum error correction for beginners. *Reports on Progress in Physics*, 76(7):076001.

[Diamond, 2013] Diamond, A. (2013). Executive functions. *Annual review of psychology*, 64(1):135–168.

[Dodel et al., 2017] Dodel, A., Mayinda, A., Oudot, E., Martin, A., Sekatski, P., Bancal, J.-D., and Sangouard, N. (2017). Proposal for witnessing non-classical light with the human eye. *Quantum*, 1:7.

[Doherty et al., 2013] Doherty, M. W., Manson, N. B., Delaney, P., Jelezko, F., Wrachtrup, J., and Hollenberg, L. C. (2013). The nitrogen-vacancy colour centre in diamond. *Physics Reports*, 528(1):1–45.

[Doherty et al., 2014] Doherty, M. W., Struzhkin, V. V., Simpson, D. A., McGuinness, L. P., Meng, Y., Stacey, A., Karle, T. J., Hemley, R. J., Manson, N. B., Hollenberg, L. C., et al. (2014). Electronic properties and metrology applications of the diamond nv- center under pressure. *Physical review letters*, 112(4):047601.

[Donner, 1992] Donner, K. (1992). Noise and the absolute thresholds of cone and rod vision. *Vision Research*, 32(5):853–866.

[Dooley et al., 2016] Dooley, S., Yukawa, E., Matsuzaki, Y., Knee, G. C., Munro, W. J., and Nemoto, K. (2016). A hybrid-systems approach to spin squeezing using a highly dissipative ancillary system. *New Journal of Physics*, 18(5):053011.

[Draganski et al., 2004] Draganski, B., Gaser, C., Busch, V., Schuierer, G., Bogdahn, U., and May, A. (2004). Changes in grey matter induced by training. *Nature*, 427(6972):311–312.

[Duan, 2019] Duan, L. (2019). Creating schrödinger-cat states. *Nature Photonics*, 13(2):73–74.

[Duan and Guo, 1997] Duan, L.-M. and Guo, G.-C. (1997). Preserving coherence in quantum computation by pairing quantum bits. *Physical Review Letters*, 79(10):1953.

[Edelman, 1983] Edelman, G. (1983). *The theory of neuronal group selection.* Los Alamos National Laboratory.

[Einstein, 2016] Einstein, A. (2016). 7 on the quantum theory of radiation. *The Old Quantum Theory: The Commonwealth and International Library: Selected Readings in Physics*, page 167.

[El-khatib et al., 2021] El-khatib, A. M., Elsafi, M., Sayyed, M., Abbas, M., and El-Khatib, M. (2021). Impact of micro and nano aluminium on the efficiency of photon detectors. *Results in Physics*, 30:104908.

[Ellis, 2019] Ellis, A. (2019). Early theories and practices of rational emotive behavior therapy and how they have been augmented and revised during the last three decades. *Advances in REBT: Theory, practice, research, measurement, prevention and promotion*, pages 1–21.

[Elzerman et al., 2004] Elzerman, J., Hanson, R., Willems van Beveren, L., Witkamp, B., Vandersypen, L., and Kouwenhoven, L. P. (2004). Single-shot read-out of an individual electron spin in a quantum dot. *nature*, 430(6998):431–435.

[Emmons and McCullough, 2003] Emmons, R. A. and McCullough, M. E. (2003). Counting blessings versus burdens: an experimental investigation of gratitude and subjective well-being in daily life. *Journal of personality and social psychology*, 84(2):377.

[Eshun et al., 2022] Eshun, A., Varnavski, O., Villabona-Monsalve, J. P., Burdick, R. K., and Goodson, T. (2022). Entangled photon spectroscopy. *Accounts of Chemical Research*, 55(7):991–1003.

[Etienne-Manneville, 2010] Etienne-Manneville, S. (2010). From signaling pathways to microtubule dynamics: the key players. *Current opinion in cell biology*, 22(1):104–111.

[Faizi and Ahansaz, 2019] Faizi, E. and Ahansaz, B. (2019). Protection of quantum coherence in an open v-type three-level atom through auxiliary atoms. *Physica Scripta*, 94(11):115102.

[Fano, 1949] Fano, R. M. (1949). *The transmission of information*, volume 65. Massachusetts Institute of Technology, Research Laboratory of Electronics ....

[Farisco et al., 2024] Farisco, M., Baldassarre, G., Cartoni, E., Leach, A., Petrovici, M. A., Rosemann, A., Salles, A., Stahl, B., and van Albada, S. J. (2024). A method for the ethical analysis of brain-inspired ai. *Artificial Intelligence Review*, 57(6):1–27.

[Field et al., 2005] Field, G. D., Sampath, A. P., and Rieke, F. (2005). Retinal processing near absolute threshold: From behavior to mechanism. *Annual Review of Physiology*, 67(1):491–514.

[Fisher et al., 2004] Fisher, B., Fels, S., MacLean, K., Munzner, T., and Rensink, R. (2004). Seeing, hearing, and touching: putting it all together. In *ACM SIGGRAPH 2004 Course Notes*, pages 8–es.

[Fisher, 2015] Fisher, M. P. (2015). Quantum cognition: The possibility of processing with nuclear spins in the brain. *Annals of Physics*, 362:593–602.

[Fleming et al., 2011] Fleming, G. R., Scholes, G. D., and Cheng, Y.-C. (2011). Quantum effects in biology. *Procedia Chemistry*, 3(1):38–57.

[Fox et al., 2005] Fox, M. D., Snyder, A. Z., Vincent, J. L., Corbetta, M., Van Essen, D. C., and Raichle, M. E. (2005). The human brain is intrinsically organized into dynamic, anticorrelated functional networks. *Proceedings of the National Academy of Sciences*, 102(27):9673–9678.

[Friston, 2010] Friston, K. (2010). The free-energy principle: a unified brain theory? *Nature reviews neuroscience*, 11(2):127–138.

[Garrison and Chiao, 2008] Garrison, J. and Chiao, R. (2008). *Quantum optics*. OUP Oxford.

[Gassab, 2024] Gassab, L. (2024). What goes on in the brain? *in preparation*.

[Gassab and Müstecaplıoğlu, 2024] Gassab, L. and Müstecaplıoğlu, E. (2024). Spin squeezing enhanced quantum magnetometry with nitrogen-vacancy center qutrits.

[Gassab et al., 2024a] Gassab, L., Pedram, A., and Müstecaplıoğlu, Ö. E. (2024a). Conditions on detecting tripartite entangled state in psychophysical experiments. *The European Physical Journal Plus*, 139(5):379.

[Gassab et al., 2024b] Gassab, L., Pusuluk, O., and Müstecaplıoğlu, Ö. E. (2024b). Geometrical optimization of spin clusters for the preservation of quantum coherence. *Physical Review A*, 109(1):012424.

[Gassab et al., 2024c] Gassab, L., Pusuluk, O., and Müstecaplıoğlu, Ö. E. (2024c). Quantum models of consciousness from a quantum information science perspective. *in preparation*.

[Gassab et al., 2024d] Gassab, L., Pusuluk, O., Xie, C., Kominis, I., and Müstecaplıoğlu, Ö. E. (2024d). Beyond the nexus: Quantum and biology intertwined. *in preparation*.

[Gaudin, 1976] Gaudin, M. (1976). Diagonalization of a class of spin hamiltonians. *J. Phys.(Paris);(France)*, 37(10).

[Gentile et al., 2017] Gentile, T. R., Nacher, P., Saam, B., and Walker, T. (2017). Optically polarized he 3. *Reviews of modern physics*, 89(4):045004.

[Gerry and Knight, 2023] Gerry, C. C. and Knight, P. L. (2023). *Introductory quantum optics*. Cambridge university press.

[Giacobino et al., 1989] Giacobino, E., Fabre, C., and Leuchs, G. (1989). Communication by squeezed light. *Physics World*, 2(2):31.

[Gillespie and Robinson, 2005] Gillespie, R. J. and Robinson, E. A. (2005). Models of molecular geometry. *Chemical Society Reviews*, 34(5):396–407.

[Gisin et al., 2002] Gisin, N., Ribordy, G., Tittel, W., and Zbinden, H. (2002). Quantum cryptography. *Review of Modern Physics*, 74:145–195.

[Glauber, 1963] Glauber, R. J. (1963). Coherent and incoherent states of the radiation field. *Physical Review*, 131(6):2766.

[Gopnik and Wellman, 2012] Gopnik, A. and Wellman, H. M. (2012). Reconstructing constructivism: causal models, bayesian learning mechanisms, and the theory theory. *Psychological bulletin*, 138(6):1085.

[Gordon, 1962] Gordon, J. P. (1962). Quantum effects in communications systems. *Proceedings of the IRE*, 50(9):1898–1908.

[Gordon, 1964] Gordon, J. P. (1964). " noise at optical frequencies: Information theory," in quantum electronics and coherent light. *Proc. Int. School Phys.'Enrico Fermi,'Course XXXI, 1964*.

[Gossuin et al., 2010] Gossuin, Y., Hocq, A., Gillis, P., and Lam, V. Q. (2010). Physics of magnetic resonance imaging: from spin to pixel. *Journal of Physics D: Applied Physics*, 43(21):213001.

[Gougoux et al., 2004] Gougoux, F., Lepore, F., Lassonde, M., Voss, P., Zatorre, R. J., and Belin, P. (2004). Pitch discrimination in the early blind. *Nature*, 430(6997):309–309.

[Graham et al., 2024] Graham, S., Newman, A., Stephen, C., Edmonds, A., Twitchen, D., Markham, M., and Morley, G. (2024). A vector diamond magnetometer in a moving vehicle. *arXiv preprint arXiv:2401.16090*.

[Gray, 2011] Gray, R. M. (2011). *Entropy and information theory.* Springer Science & Business Media.

[Grill-Spector et al., 2006] Grill-Spector, K., Henson, R., and Martin, A. (2006). Repetition and the brain: neural models of stimulus-specific effects. *Trends in cognitive sciences*, 10(1):14–23.

[Grinolds et al., 2013] Grinolds, M. S., Hong, S., Maletinsky, P., Luan, L., Lukin, M. D., Walsworth, R. L., and Yacoby, A. (2013). Nanoscale magnetic imaging of a single electron spin under ambient conditions. *Nature Physics*, 9(4):215–219.

[Gross, 2012] Gross, C. (2012). Spin squeezing, entanglement and quantum metrology with bose–einstein condensates. *Journal of Physics B: Atomic, Molecular and Optical Physics*, 45(10):103001.

[Gühne and Hyllus, 2003] Gühne, O. and Hyllus, P. (2003). Investigating three qubit entanglement with local measurements. *International Journal of Theoretical Physics*, 42:1001–1013.

[Güldeste and Bulutay, 2023] Güldeste, E. T. and Bulutay, C. (2023). Wavelet-based ramsey magnetometry enhancement of a single nv center in diamond. *arXiv preprint.*

[Gumerov et al., 2022] Gumerov, V. M., Andrianova, E. P., Matilla, M. A., Page, K. M., Monteagudo-Cascales, E., Dolphin, A. C., Krell, T., and Zhulin, I. B. (2022). Amino acid sensor conserved from bacteria to humans. *Proceedings of the National Academy of Sciences*, 119(10):e2110415119.

[Gupta et al., 2002] Gupta, P., Vermani, K., and Garg, S. (2002). Hydrogels: from controlled release to ph-responsive drug delivery. *Drug discovery today*, 7(10):569–579.

[Gühne, 2004] Gühne, O. (2004). Detecting quantum entanglement: entanglement witnesses and uncertainty relations.

[Hameroff and Penrose, 1996] Hameroff, S. and Penrose, R. (1996). Orchestrated reduction of quantum coherence in brain microtubules: A model for consciousness. *Mathematics and computers in simulation*, 40(3-4):453–480.

[Hameroff and Penrose, 2014] Hameroff, S. and Penrose, R. (2014). Consciousness in the universe: A review of the orch ortheory. *Physics of life reviews*, 11(1):39–78.

[Hameroff, 2007] Hameroff, S. R. (2007). The brain is both neurocomputer and quantum computer. *Cognitive Science*, 31(6):1035–1045.

[Hamilton, 2024] Hamilton, A. (2024). The neuroscience of play. In *Seriously Therapeutic Play with LEGO®*, pages 31–48. Routledge.

[Hanks et al., 2017] Hanks, M., Trupke, M., Schmiedmayer, J., Munro, W. J., and Nemoto, K. (2017). High-fidelity spin measurement on the nitrogen-vacancy center. *New Journal of Physics*, 19(10):103002.

[Hardy, 1998] Hardy, L. (1998). Spooky action at a distance in quantum mechanics. *Contemporary physics*, 39(6):419–429.

[Haroche, 2013] Haroche, S. (2013). Controlling photons in a box and exploring the quantum to classical boundary. *Annalen der Physik*, 525.

[Hart et al., 2021] Hart, C. A., Schloss, J. M., Turner, M. J., Scheidegger, P. J., Bauch, E., and Walsworth, R. L. (2021). N-v–diamond magnetic microscopy using a double quantum 4-ramsey protocol. *Physical Review Applied*, 15(4):044020.

[Hart et al., 2012] Hart, E., Sóbester, A., Djidjeli, K., Molinari, M., Thomas, K., and Cox, S. (2012). A geometry optimization framework for photonic crystal design. *Photonics and Nanostructures-Fundamentals and Applications*, 10(1):25–35.

[Hartley, 1928] Hartley, R. V. (1928). Transmission of information 1. *Bell System technical journal*, 7(3):535–563.

[Hasselbach et al., 2000] Hasselbach, K., Veauvy, C., and Mailly, D. (2000). Microsquid magnetometry and magnetic imaging. *Physica C: Superconductivity*, 332(1-4):140–147.

[Hayashi, 2006] Hayashi, M. (2006). *Quantum information*. Springer.

[Hayashi, 2016] Hayashi, M. (2016). *Quantum information theory*. Springer.

[Hazenberg and van Lier, 2016] Hazenberg, S. J. and van Lier, R. (2016). Touching and hearing unseen objects: Multisensory effects on scene recognition. *i-Perception*, 7(4):2041669516664530.

[He et al., 2021] He, C., He, H., Chang, J., Chen, B., Ma, H., and Booth, M. J. (2021). Polarisation optics for biomedical and clinical applications: a review. *Light: Science & Applications*, 10(1):194.

[Hecht et al., 1941] Hecht, S., Shlaer, S., and Pirenne, M. H. (1941). Energy at the threshold of vision. *Science*, 93(2425):585–587.

[Hecht et al., 1942] Hecht, S., Shlaer, S., and Pirenne, M. H. (1942). Energy, quanta, and vision . *Journal of General Physiology*, 25(6):819–840.

[Heinosaari et al., 2013] Heinosaari, T., Mazzarella, L., and Wolf, M. M. (2013). Quantum tomography under prior information. *Communications in Mathematical Physics*, 318(2):355–374.

[Helmchen and Denk, 2005] Helmchen, F. and Denk, W. (2005). Deep tissue two-photon microscopy. *Nature methods*, 2(12):932–940.

[Helstrom, 1967] Helstrom, C. W. (1967). Detection theory and quantum mechanics (ii). *Inf. Control.*, 13:156–171.

[Hendrickson and Lyon, 2009] Hendrickson, G. R. and Lyon, L. A. (2009). Bioresponsive hydrogels for sensing applications. *Soft Matter*, 5(1):29–35.

[Hensch, 2005] Hensch, T. K. (2005). Critical period mechanisms in developing visual cortex. *Current topics in developmental biology*, 69:215–237.

[Hill and Wootters, 1997] Hill, S. A. and Wootters, W. K. (1997). Entanglement of a pair of quantum bits. *Physical review letters*, 78(26):5022.

[Hiller-Sturmhöfel and Bartke, 1998] Hiller-Sturmhöfel, S. and Bartke, A. (1998). The endocrine system: an overview. *Alcohol health and research world*, 22(3):153.

[Hirsh-Pasek, 2009] Hirsh-Pasek, K. (2009). A mandate for playful learning in preschool: Applying the scientific evidence.

[Ho and Yuen, 1994] Ho, S.-T. and Yuen, H. P. (1994). Scheme for realizing a photon number amplifier. *Optics letters*, 19(1):61–63.

[Hofmann et al., 2012] Hofmann, S. G., Asnaani, A., Vonk, I. J., Sawyer, A. T., and Fang, A. (2012). The efficacy of cognitive behavioral therapy: A review of meta-analyses. *Cognitive therapy and research*, 36:427–440.

[Hollon and Beck, 1979] Hollon, S. D. and Beck, A. T. (1979). Cognitive therapy of depression. *Cognitive-behavioral interventions: Theory, research, and procedures*, pages 153–203.

[Holmes et al., 2018] Holmes, R. M., Victora, M. M., Wang, R. F., and Kwiat, P. G. (2018). Testing the limits of human vision with quantum states of light: past, present, and future experiments. In *Advanced Photon Counting Techniques XII*, volume 10659, pages 9–15. SPIE.

[Hölzel et al., 2011] Hölzel, B. K., Carmody, J., Vangel, M., Congleton, C., Yerramsetti, S. M., Gard, T., and Lazar, S. W. (2011). Mindfulness practice leads to increases in regional brain gray matter density. *Psychiatry research: neuroimaging*, 191(1):36–43.

[Hong et al., 2013] Hong, S., Grinolds, M. S., Pham, L. M., Le Sage, D., Luan, L., Walsworth, R. L., and Yacoby, A. (2013). Nanoscale magnetometry with nv centers in diamond. *MRS bulletin*, 38(2):155–161.

[Horgan and MacLachlan, 2004] Horgan, O. and MacLachlan, M. (2004). Psychosocial adjustment to lower-limb amputation: a review. *Disability and rehabilitation*, 26(14-15):837–850.

[Horodecki et al., 2009] Horodecki, R., Horodecki, P., Horodecki, M., and Horodecki, K. (2009). Quantum entanglement. *Reviews of modern physics*, 81(2):865.

[Hotter et al., 2024] Hotter, C., Ritsch, H., and Gietka, K. (2024). Combining critical and quantum metrology. *Physical Review Letters*, 132(6):060801.

[Hou et al., 2019] Hou, Q., Yang, C., Chen, C., An, J., Yang, W., and Feng, M. (2019). Preservation of quantum correlation between nitrogen-vacancy-center ensembles by squeezed-reservoir engineering. *Physical Review A*, 100(3):032302.

[Hou et al., 2015] Hou, Z., Xiang, G., Dong, D., Li, C.-F., and Guo, G.-C. (2015). Realization of mutually unbiased bases for a qubit with only one wave plate: theory and experiment. *Opt. Express*, 23(8):10018–10031.

[Huang et al., 2021a] Huang, K.-Q., Zhao, W.-L., and Li, Z. (2021a). Effective protection of quantum coherence by a non-hermitian driving potential. *Physical Review A*, 104(5):052405.

[Huang et al., 2021b] Huang, L., Chen, F., Li, X., Li, Y., Lü, R., and Liu, Y. (2021b). Dynamic synthesis of heisenberg-limited spin squeezing, npj quantum inf.

[Hyllus and Eisert, 2006] Hyllus, P. and Eisert, J. (2006). Optimal entanglement witnesses for continuous-variable systems. *New Journal of Physics*, 8(4):51.

[Ishizaki and Fleming, 2012] Ishizaki, A. and Fleming, G. R. (2012). Quantum coherence in photosynthetic light harvesting. *Annu. Rev. Condens. Matter Phys.*, 3(1):333–361.

[Jacobsen, 1929] Jacobsen, E. (1929). Progressive relaxation.

[Jelezko and Wrachtrup, 2006] Jelezko, F. and Wrachtrup, J. (2006). Single defect centres in diamond: A review. *physica status solidi (a)*, 203(13):3207–3225.

[Jibu et al., 1994] Jibu, M., Hagan, S., Hameroff, S. R., Pribram, K. H., and Yasue, K. (1994). Quantum optical coherence in cytoskeletal microtubules: implications for brain function. *Biosystems*, 32(3):195–209.

[Johansen-Berg, 2007] Johansen-Berg, H. (2007). Structural plasticity: rewiring the brain. *Current Biology*, 17(4):R141–R144.

[Johansson et al., 2012] Johansson, J. R., Nation, P. D., and Nori, F. (2012). Qutip: An open-source python framework for the dynamics of open quantum systems. *Computer Physics Communications*, 183(8):1760–1772.

[Jungnitsch et al., 2011] Jungnitsch, B., Moroder, T., and Gühne, O. (2011). Entanglement witnesses for graph states: General theory and examples. *Physical Review A*, 84(3):032310.

[Jutila et al., 2014] Jutila, L., Äikiä, M., Immonen, A., Mervaala, E., Alafuzoff, I., and Kälviäinen, R. (2014). Long-term memory performance after surgical treatment of unilateral temporal lobe epilepsy (tle). *Epilepsy research*, 108(7):1228–1237.

[Kabat-Zinn, 2013] Kabat-Zinn, J. (2013). *Full catastrophe living, revised edition: how to cope with stress, pain and illness using mindfulness meditation.* Hachette uK.

[Kalra et al., 2023] Kalra, A. P., Benny, A., Travis, S. M., Zizzi, E. A., Morales-Sanchez, A., Oblinsky, D. G., Craddock, T. J., Hameroff, S. R., MacIver, M. B., Tuszynski, J. A., et al. (2023). Electronic energy migration in microtubules. *ACS Central Science*, 9(3):352–361.

[Kandel, 2001] Kandel, E. R. (2001). The molecular biology of memory storage: a dialogue between genes and synapses. *Science*, 294(5544):1030–1038.

[Kapitein and Hoogenraad, 2015] Kapitein, L. C. and Hoogenraad, C. C. (2015). Building the neuronal microtubule cytoskeleton. *Neuron*, 87(3):492–506.

[Keatley et al., 2023] Keatley, E. S., Bombardier, C. H., Watson, E., Kumar, R. G., Novack, T., Monden, K. R., and Dams-O'Connor, K. (2023). Cognitive performance, depression, and anxiety 1 year after traumatic brain injury. *The Journal of head trauma rehabilitation*, 38(3):E195–E202.

[Kelso, 1995] Kelso, J. S. (1995). *Dynamic patterns: The self-organization of brain and behavior*. MIT press.

[Kennedy and Evans, 2001] Kennedy, P. and Evans, M. (2001). Evaluation of post traumatic distress in the first 6 months following sci. *Spinal Cord*, 39(7):381–386.

[Khoshbin-e Khoshnazar, 2014] Khoshbin-e Khoshnazar, M. (2014). Quantum superposition in the retina: evidences and proposals. *NeuroQuantology*, 12(1).

[Kingslake, 1989] Kingslake, R. (1989). *A history of the photographic lens*. Elsevier.

[Kirtley et al., 1995] Kirtley, J., Ketchen, M., Stawiasz, K., Sun, J., Gallagher, W., Blanton, S., and Wind, S. (1995). High-resolution scanning squid microscope. *Applied Physics Letters*, 66(9):1138–1140.

[Kitagawa and Ueda, 1993] Kitagawa, M. and Ueda, M. (1993). Squeezed spin states. *Physical Review A*, 47(6):5138.

[Kitching et al., 2011] Kitching, J., Knappe, S., and Donley, E. A. (2011). Atomic sensors–a review. *IEEE Sensors Journal*, 11(9):1749–1758.

[Klarer et al., 2014] Klarer, M., Arnold, M., Günther, L., Winter, C., Langhans, W., and Meyer, U. (2014). Gut vagal afferents differentially modulate innate anxiety and learned fear. *Journal of Neuroscience*, 34(21):7067–7076.

[Klauder and Sudarshan, 2006] Klauder, J. R. and Sudarshan, E. C. G. (2006). *Fundamentals of quantum optics*. Courier Corporation.

[Klein, 1961] Klein, M. J. (1961). Max planck and the beginnings of the quantum theory. *Archive for History of Exact Sciences*, 1:459–479.

[Klouda and Mikos, 2008] Klouda, L. and Mikos, A. G. (2008). Thermoresponsive hydrogels in biomedical applications. *European journal of pharmaceutics and biopharmaceutics*, 68(1):34–45.

[Knudsen, 2004] Knudsen, E. I. (2004). Sensitive periods in the development of the brain and behavior. *Journal of cognitive neuroscience*, 16(8):1412–1425.

[Koch and Hepp, 2006] Koch, C. and Hepp, K. (2006). Quantum mechanics in the brain. *Nature*, 440(7084):611–611.

[Kolb and Whishaw, 1998] Kolb, B. and Whishaw, I. Q. (1998). Brain plasticity and behavior. *Annual Review of Psychology*, 49(1):43–64.

[Kominis, 2020] Kominis, I. (2020). Quantum relative entropy shows singlet-triplet coherence is a resource in the radical-pair mechanism of biological magnetic sensing. *Physical Review Research*, 2(2):023206.

[Kominis et al., 2022] Kominis, I., Loulakis, M., and Müstecaplıoğlu, Ö. E. (2022). Quantum biometrics. *Recent Advances in Biometrics*, 131.

[Kovalenko et al., 2023] Kovalenko, A., Babjak, D., Lešundák, A., Podhora, L., Lachman, L., Obšil, P., Pham, T., Číp, O., Filip, R., and Slodička, L. (2023). Emergence of super-poissonian light from indistinguishable single-photon emitters. *Optica*, 10(4):456–463.

[Lagercrantz and Bistoletti, 1977] Lagercrantz, H. and Bistoletti, P. (1977). Catecholamine release in the newborn infant at birth. *Pediatric research*, 11(8):889–893.

[Lambert et al., 2013] Lambert, N., Chen, Y.-N., Cheng, Y.-C., Li, C.-M., Chen, G.-Y., and Nori, F. (2013). Quantum biology. *Nature Physics*, 9(1):10–18.

[Landauer, 1961] Landauer, R. (1961). Irreversibility and heat generation in the computing process. *IBM journal of research and development*, 5(3):183–191.

[Lawrie et al., 2019] Lawrie, B. J., Lett, P. D., Marino, A. M., and Pooser, R. C. (2019). Quantum sensing with squeezed light. *Acs Photonics*, 6(6):1307–1318.

[Le Gratiet et al., 2021] Le Gratiet, A., Bendandi, A., Sheppard, C. J., and Diaspro, A. (2021). Polarimetric optical scanning microscopy of zebrafish embryonic development using the coherency matrix. *Journal of Biophotonics*, 14(6):e202000494.

[Levänen and Hamdorf, 2001] Levänen, S. and Hamdorf, D. (2001). Feeling vibrations: enhanced tactile sensitivity in congenitally deaf humans. *Neuroscience letters*, 301(1):75–77.

[Lewenstein et al., 2000] Lewenstein, M., Kraus, B., Cirac, J. I., and Horodecki, P. (2000). Optimization of entanglement witnesses. *Physical Review A*, 62(5):052310.

[Li et al., 2019] Li, J., Wu, S., Kim, E., Yan, K., Liu, H., Liu, C., Dong, H., Qu, X., Shi, X., Shen, J., et al. (2019). Electrobiofabrication: electrically based fabrication with biologically derived materials. *Biofabrication*, 11(3):032002.

[Lillywhite, 1981] Lillywhite, P. (1981). Multiplicative intrinsic noise and the limits to visual performance. *Vision Research*, 21(2):291–296.

[Lindberg, 1967] Lindberg, D. C. (1967). Alhazen's theory of vision and its reception in the west. *Isis*, 58(3):321–341.

[Liu et al., 2020] Liu, J., Yuan, H., Lu, X.-M., and Wang, X. (2020). Quantum fisher information matrix and multiparameter estimation. *Journal of Physics A: Mathematical and Theoretical*, 53(2):023001.

[Liu et al., 2012] Liu, Y., Tan, J., Thomas, A., Ou-Yang, D., and Muzykantov, V. R. (2012). The shape of things to come: importance of design in nanotechnology for drug delivery. *Therapeutic delivery*, 3(2):181–194.

[Livneh, 2001] Livneh, H. (2001). Psychosocial adaptation to chronic illness and disability: A conceptual framework. *Rehabilitation counseling bulletin*, 44(3):151–160.

[Lloyd, 2011] Lloyd, S. (2011). Quantum coherence in biological systems. In *Journal of Physics-Conference Series*, volume 302, page 012037.

[Loulakis et al., 2017] Loulakis, M., Blatsios, G., Vrettou, C. S., and Kominis, I. K. (2017). Quantum biometrics with retinal photon counting. *Phys. Rev. Applied*, 8:044012.

[Lu et al., 2016] Lu, Y., Aimetti, A. A., Langer, R., and Gu, Z. (2016). Bioresponsive materials. *Nature Reviews Materials*, 2(1):1–17.

[Luk and Christodoulou, 2024] Luk, G. and Christodoulou, J. A. (2024). Cognitive neuroscience and education. In *Handbook of educational psychology*, pages 383–404. Routledge.

[Lundeen et al., 2009] Lundeen, J. S., Feito, A., Coldenstrodt-Ronge, H., Pregnell, K. L., Silberhorn, C., Ralph, T. C., Eisert, J., Plenio, M. B., and Walmsley, I. A. (2009). Tomography of quantum detectors. *Nature Physics*, 5(1):27–30.

[Luo, 2000] Luo, S. (2000). Quantum fisher information and uncertainty relations. *Letters in Mathematical Physics*, 53:243–251.

[Lupien et al., 2009] Lupien, S. J., McEwen, B. S., Gunnar, M. R., and Heim, C. (2009). Effects of stress throughout the lifespan on the brain, behaviour and cognition. *Nature reviews neuroscience*, 10(6):434–445.

[Ma et al., 2011] Ma, J., Wang, X., Sun, C.-P., and Nori, F. (2011). Quantum spin squeezing. *Physics Reports*, 509(2-3):89–165.

[Ma et al., 2021] Ma, Y.-H., Xu, Y., Ding, Q.-Z., and Chen, Y.-S. (2021). Preparation of spin squeezed state in siv centers coupled by diamond waveguide. *Chinese Physics B*, 30(10):100311.

[Maclean et al., 2000] Maclean, N., Pound, P., Wolfe, C., Rudd, A., et al. (2000). A critical review of the concept of patient motivation in the literature on physical rehabilitation. *Soc Sci Med*, 50(4):495–506.

[Malik et al., 2020] Malik, R., Tomer, V. K., Mishra, Y. K., and Lin, L. (2020). Functional gas sensing nanomaterials: A panoramic view. *Applied Physics Reviews*, 7(2).

[Mamin et al., 2013] Mamin, H., Kim, M., Sherwood, M., Rettner, C., Ohno, K., Awschalom, D., and Rugar, D. (2013). Nanoscale nuclear magnetic resonance with a nitrogen-vacancy spin sensor. *Science*, 339(6119):557–560.

[Mandel and Wolf, 1995] Mandel, L. and Wolf, E. (1995). *Optical coherence and quantum optics*. Cambridge university press.

[Manzano, 2020] Manzano, D. (2020). A short introduction to the lindblad master equation. *Aip advances*, 10(2).

[Mariani et al., 2020] Mariani, G., Nomoto, S., Kashiwaya, S., and Nomura, S. (2020). System for the remote control and imaging of mw fields for spin manipulation in nv centers in diamond. *Scientific reports*, 10(1):4813.

[Mauro D. Ariano et al., 2003] Mauro D. Ariano, G., Paris, M. G., and Sacchi, M. F. (2003). Quantum tomography. volume 128 of *Advances in Imaging and Electron Physics*, pages 205–308. Elsevier.

[McEwen, 2007] McEwen, B. S. (2007). Physiology and neurobiology of stress and adaptation: central role of the brain. *Physiological reviews*, 87(3):873–904.

[McFadden, 2002] McFadden, J. (2002). Synchronous firing and its influence on the brain's electromagnetic field. *Journal of Consciousness Studies*, 9(4):23–50.

[McFadden, 2020] McFadden, J. (2020). Integrating information in the brain's em field: the cemi field theory of consciousness. *Neuroscience of consciousness*, 2020(1):niaa016.

[Mekhov and Ritsch, 2012] Mekhov, I. B. and Ritsch, H. (2012). Quantum optics with ultracold quantum gases: towards the full quantum regime of the light–matter interaction. *Journal of Physics B: Atomic, Molecular and Optical Physics*, 45(10):102001.

[Miller et al., 2020] Miller, H. J., Guarnieri, G., Mitchison, M. T., and Goold, J. (2020). Quantum fluctuations hinder finite-time information erasure near the landauer limit. *Physical Review Letters*, 125(16):160602.

[Mohseni et al., 2008] Mohseni, M., Rezakhani, A. T., and Lidar, D. A. (2008). Quantum-process tomography: Resource analysis of different strategies. *Phys. Rev. A*, 77:032322.

[Mortola, 2001] Mortola, J. P. (2001). *Respiratory physiology of newborn mammals: a comparative perspective*. JHU Press.

[Mukhopadhyay et al., 2018] Mukhopadhyay, S. C., Jayasundera, K. P., and Postolache, O. A. (2018). *Modern Sensing Technologies*, volume 29. Springer.

[Munuera-Javaloy et al., 2022] Munuera-Javaloy, C., Puebla, R., D'Anjou, B., Plenio, M. B., and Casanova, J. (2022). Detection of molecular transitions with nitrogen-vacancy centers and electron-spin labels. *npj Quantum Information*, 8(1):140.

[Murube, 2009] Murube, J. (2009). Basal, reflex, and psycho-emotional tears. *The ocular surface*, 7(2):60–66.

[Müstecaplıoğlu et al., 2002] Müstecaplıoğlu, Ö. E., Zhang, M., and You, L. (2002). Spin squeezing and entanglement in spinor condensates. *Physical Review A*, 66(3):033611.

[Newell et al., 1972] Newell, A., Simon, H. A., et al. (1972). *Human problem solving*, volume 104. Prentice-hall Englewood Cliffs, NJ.

[Nezu et al., 2012] Nezu, A. M., Nezu, C. M., and D'Zurilla, T. J. (2012). *Problem-solving therapy: A treatment manual*. springer publishing company.

[Nie et al., 2020] Nie, W., Peng, Z., Nori, F., and Liu, Y.-x. (2020). Topologically protected quantum coherence in a superatom. *Physical Review Letters*, 124(2):023603.

[Nielsen and Chuang, 2010] Nielsen, M. A. and Chuang, I. L. (2010). *Quantum computation and quantum information*. Cambridge university press.

[Nordman et al., 2023] Nordman, J. C., Summers, C., and Ball, K. (2023). The impact of chronic stress on neuroplasticity and abnormal behavior. *Frontiers in Behavioral Neuroscience*, 17:1208351.

[O'brien, 2007] O'brien, J. L. (2007). Optical quantum computing. *Science*, 318(5856):1567–1570.

[Ogunkoya et al., 2024] Ogunkoya, O., Kim, J., Peng, B., Özgüler, A. B., and Alexeev, Y. (2024). Qutrit circuits and algebraic relations: A pathway to efficient spin-1 hamiltonian simulation. *Physical Review A*, 109(1):012426.

[Olatunji et al., 2007] Olatunji, B. O., Cisler, J. M., and Tolin, D. F. (2007). Quality of life in the anxiety disorders: a meta-analytic review. *Clinical psychology review*, 27(5):572–581.

[Ono et al., 2013] Ono, T., Okamoto, R., and Takeuchi, S. (2013). An entanglement-enhanced microscope. *Nature communications*, 4(1):2426.

[Oon et al., 2022] Oon, J. T., Tang, J., Hart, C. A., Olsson, K. S., Turner, M. J., Schloss, J. M., and Walsworth, R. L. (2022). Ramsey envelope modulation in nv diamond magnetometry. *Physical Review B*, 106(5):054110.

[Oshnik et al., 2022] Oshnik, N., Rembold, P., Calarco, T., Montangero, S., Neu, E., and Müller, M. M. (2022). Robust magnetometry with single nitrogen-vacancy centers via two-step optimization. *Physical Review A*, 106(1):013107.

[Palazuelos and De Vicente, 2022] Palazuelos, C. and De Vicente, J. I. (2022). Genuine multipartite entanglement of quantum states in the multiple-copy scenario. *Quantum*, 6:735.

[Paneru et al., 2020] Paneru, D., Cohen, E., Fickler, R., Boyd, R. W., and Karimi, E. (2020). Entanglement: quantum or classical? *Reports on Progress in Physics*, 83(6):064001.

[Panitchayangkoon et al., 2010] Panitchayangkoon, G., Hayes, D., Fransted, K. A., Caram, J. R., Harel, E., Wen, J., Blankenship, R. E., and Engel, G. S. (2010).

Long-lived quantum coherence in photosynthetic complexes at physiological temperature. *Proceedings of the National Academy of Sciences*, 107(29):12766–12770.

[Park, 2012] Park, D. (2012). *Introduction to the quantum theory.* Courier Corporation.

[Parma et al., 2024] Parma, C., Doria, F., Zulueta, A., Lanzone, J., Boscarino, M., Giani, L., Lunetta, C., Vassallo, M., Parati, E. A., Picozzi, M., et al. (2024). An overview of the bodily awareness representation and interoception: Insights and progress in the field of neurorehabilitation research. *Brain Sciences*, 14(4):386.

[Patočka et al., 2004] Patočka, J., Dvořák, A., et al. (2004). Biomedical aspects of chiral molecules. *J. Appl. Biomed*, 2:95–100.

[Paul, 2015] Paul, H. (2015). An introduction to reactive oxygen species. *Journal of cell science and therapy*, 2(2):2–20.

[Pedram et al., 2024a] Pedram, A., Besaga, V. R., Gassab, L., Setzpfandt, F., and Özgür E. Müstecaplıoğlu (2024a). Quantum estimation of the stokes vector rotation for a general polarimetric transformation.

[Pedram et al., 2024b] Pedram, A., Besaga, V. R., Setzpfandt, F., and Özgür E. Müstecaplıoğlu (2024b). Nonlocality enhanced precision in quantum polarimetry via entangled photons.

[Pedram et al., 2024c] Pedram, A., Besaga, V. R., Setzpfandt, F., and Özgür E. Müstecaplıoğlu (2024c). Nonlocality enhanced precision in quantum polarimetry via entangled photons.

[Pedram et al., 2022] Pedram, A., Müstecaplıoğlu, O. E., and Kominis, I. K. (2022). Using quantum states of light to probe the retinal network. *Phys. Rev. Research*, 4:033060.

[Petrini et al., 2020] Petrini, G., Moreva, E., Bernardi, E., Traina, P., Tomagra, G., Carabelli, V., Degiovanni, I. P., and Genovese, M. (2020). Is a quantum biosensing revolution approaching? perspectives in nv-assisted current and thermal biosensing in living cells. *Advanced Quantum Technologies*, 3(12):2000066.

[Peyvasteh et al., 2021] Peyvasteh, M., Popov, A., Bykov, A., Pierangelo, A., Novikova, T., and Meglinski, I. (2021). Evolution of raw meat polarization-based properties by means of mueller matrix imaging. *Journal of Biophotonics*, 14(5):e202000376.

[Pezzè, 2021] Pezzè, L. (2021). Entanglement-enhanced sensor networks. *Nature Photonics*, 15(2):74–76.

[Phan et al., 2014] Phan, N. M., Cheng, M. F., Bessarab, D. A., and Krivitsky, L. A. (2014). Interaction of fixed number of photons with retinal rod cells. *Phys. Rev. Lett.*, 112:213601.

[Piechocinska, 2000] Piechocinska, B. (2000). Information erasure. *Physical Review A*, 61(6):062314.

[Plantzos, 1997] Plantzos, D. (1997). Crystals and lenses in the graeco-roman world. *American Journal of Archaeology*, 101(3):451–464.

[Player and Hore, 2018] Player, T. C. and Hore, P. (2018). Posner qubits: spin dynamics of entangled ca9 (po4) 6 molecules and their role in neural processing. *Journal of the Royal Society Interface*, 15(147):20180494.

[Plenio and Virmani, 2014] Plenio, M. B. and Virmani, S. S. (2014). An introduction to entanglement theory. *Quantum information and coherence*, pages 173–209.

[Plum et al., 2023] Plum, T., Binzberger, R., Thiele, R., Shang, F., Postrach, D., Fung, C., Fortea, M., Stakenborg, N., Wang, Z., Tappe-Theodor, A., et al.

(2023). Mast cells link immune sensing to antigen-avoidance behaviour. *Nature*, 620(7974):634–642.

[Polin and Abman, 2011] Polin, R. A. and Abman, S. H. (2011). *Fetal and neonatal physiology E-book*. Elsevier health sciences.

[Polzik, 2008] Polzik, E. S. (2008). The squeeze goes on. *Nature*, 453(7191):45–46.

[Pradana and Chew, 2021] Pradana, A. and Chew, L. Y. (2021). Entanglement of nitrogen-vacancy-center ensembles with initial squeezing. *Physical Review A*, 104(2):022435.

[Procopio et al., 2024] Procopio, M., Fernández-Cézar, R., Fernandes-Procopio, L., and Yánez-Araque, B. (2024). Neuroscience-based information and communication technologies development in elementary school mathematics through games: A case study evaluation. *Education Sciences*, 14(3):213.

[Propp and van Enk, 2019] Propp, T. B. and van Enk, S. J. (2019). On nonlinear amplification: improved quantum limits for photon counting. *Optics Express*, 27(16):23454–23463.

[Prucnal and Teich, 1982] Prucnal, P. R. and Teich, M. C. (1982). Multiplication noise in the human visual system at threshold: 2. probit estimation of parameters. *Biological Cybernetics*, 43(2):87–96.

[Pugh, 2018] Pugh, Edward N., J. (2018). The discovery of the ability of rod photoreceptors to signal single photons. *Journal of General Physiology*, 150(3):383–388.

[Pulsifer et al., 2004] Pulsifer, M. B., Brandt, J., Salorio, C. F., Vining, E. P., Carson, B. S., and Freeman, J. M. (2004). The cognitive outcome of hemispherectomy in 71 children. *Epilepsia*, 45(3):243–254.

[Pushin et al., 2024] Pushin, D., Kapahi, C., Silva, A., Cory, D., Kulmaganbetov, M., Mungalsingh, M., Singh, T., Thompson, B., and Sarenac, D. (2024). Psychophysical discrimination of radially varying polarization-based entoptic phenomena. *Physical Review Applied*, 21(1):L011002.

[Pushin et al., 2023] Pushin, D. A., Cory, D. G., Kulmaganbetov, M., Silva, A. E., Thompson, B., and Sarenac, D. (2023). Structured light enhanced entoptic stimuli for vision science applications. *Frontiers in Neuroscience*, 17:1232532.

[Pyrkov et al., 2024] Pyrkov, A., Aliper, A., Bezrukov, D., Podolskiy, D., Ren, F., and Zhavoronkov, A. (2024). Complexity of life sciences in quantum and ai era. *Wiley Interdisciplinary Reviews: Computational Molecular Science*, 14(1):e1701.

[Qiu et al., 2021] Qiu, Z., Vool, U., Hamo, A., and Yacoby, A. (2021). Nuclear spin assisted magnetic field angle sensing. *npj Quantum Information*, 7(1):39.

[Quack, 1989] Quack, M. (1989). Structure and dynamics of chiral molecules. *Angewandte Chemie International Edition in English*, 28(5):571–586.

[Radley and Morrison, 2005] Radley, J. J. and Morrison, J. H. (2005). Repeated stress and structural plasticity in the brain. *Ageing research reviews*, 4(2):271–287.

[Rarity et al., 1990] Rarity, J., Tapster, P., Jakeman, E., Larchuk, T., Campos, R., Teich, M., and Saleh, B. (1990). Two-photon interference in a mach-zehnder interferometer. *Physical review letters*, 65(11):1348.

[Ravikumar et al., 2019] Ravikumar, K., Basu, B., and Dubey, A. K. (2019). Analysis of electrical analogue of a biological cell and its response to external electric field. *Regenerative Engineering and Translational Medicine*, 5:10–21.

[Raza et al., 2011] Raza, Z., Alfe, D., Salzmann, C. G., Klimeš, J., Michaelides, A., and Slater, B. (2011). Proton ordering in cubic ice and hexagonal ice; a potential new ice phase. *Physical Chemistry Chemical Physics*, 13(44):19788–19795.

[Reingruber et al., 2013] Reingruber, J., Pahlberg, J., Woodruff, M. L., Sampath, A. P., Fain, G. L., and Holcman, D. (2013). Detection of single photons by toad and mouse rods. *Proceedings of the National Academy of Sciences*, 110(48):19378–19383.

[Riantiningtyas et al., 2024] Riantiningtyas, R. R., Dougkas, A., Bredie, W. L., Kwiecien, C., Bruyas, A., Philouze, P., Giboreau, A., and Carrouel, F. (2024). Investigating oral somatosensory perception and oral symptoms of head and neck cancer patients: insights on eating behaviour. *Supportive Care in Cancer*, 32(5):1–10.

[Riccardi et al., 2020] Riccardi, A., Chruściński, D., and Macchiavello, C. (2020). Optimal entanglement witnesses from limited local measurements. *Phys. Rev. A*, 101:062319.

[Rieke and Baylor, 1998] Rieke, F. and Baylor, D. A. (1998). Single-photon detection by rod cells of the retina. *Rev. Mod. Phys.*, 70:1027–1036.

[Ritz, 2011] Ritz, T. (2011). Quantum effects in biology: Bird navigation. *Procedia Chemistry*, 3(1):262–275.

[Rondin et al., 2014] Rondin, L., Tetienne, J.-P., Hingant, T., Roch, J.-F., Maletinsky, P., and Jacques, V. (2014). Magnetometry with nitrogen-vacancy defects in diamond. *Reports on progress in physics*, 77(5):056503.

[Rosen, 2021] Rosen, S. M. (2021). The strange nature of quantum perception: To see a photon, one must be a photon.

[Rubart, 2004] Rubart, M. (2004). Two-photon microscopy of cells and tissue. *Circulation research*, 95(12):1154–1166.

[Rungta et al., 2001] Rungta, P., Bužek, V., Caves, C. M., Hillery, M., and Milburn, G. J. (2001). Universal state inversion and concurrence in arbitrary dimensions. *Physical Review A*, 64(4):042315.

[Sadato et al., 1996] Sadato, N., Pascual-Leone, A., Grafman, J., Ibañez, V., Deiber, M.-P., Dold, G., and Hallett, M. (1996). Activation of the primary visual cortex by braille reading in blind subjects. *Nature*, 380(6574):526–528.

[Sakakibara et al., 2013] Sakakibara, A., Ando, R., Sapir, T., and Tanaka, T. (2013). Microtubule dynamics in neuronal morphogenesis. *Open biology*, 3(7):130061.

[Sakitt, 1972] Sakitt, B. (1972). Counting every quantum. *The Journal of Physiology*, 223(1):131–150.

[Saleh and Teich, 2019] Saleh, B. E. and Teich, M. C. (2019). *Fundamentals of photonics*. john Wiley & sons.

[Salicari et al., 2023] Salicari, L., Baiesi, M., Orlandini, E., and Trovato, A. (2023). Folding kinetics of an entangled protein. *PLOS Computational Biology*, 19(11):e1011107.

[Sanders, 1992] Sanders, B. C. (1992). Entangled coherent states. *Physical Review A*, 45(9):6811.

[Sapienza et al., 2015] Sapienza, L., Davanço, M., Badolato, A., and Srinivasan, K. (2015). Nanoscale optical positioning of single quantum dots for bright and pure single-photon emission. *Nature communications*, 6(1):7833.

[Sarenac et al., 2020a] Sarenac, D., Kapahi, C., Silva, A. E., Cory, D. G., Taminiau, I., Thompson, B., and Pushin, D. A. (2020a). Direct discrimination of structured light by humans. *Proceedings of the National Academy of Sciences*, 117(26):14682–14687.

[Sarenac et al., 2020b] Sarenac, D., Kapahi, C., Silva, A. E., Cory, D. G., Taminiau, I., Thompson, B., and Pushin, D. A. (2020b). Direct discrimination of structured light by humans. *Proceedings of the National Academy of Sciences*, 117(26):14682–14687.

[Sarenac et al., 2022a] Sarenac, D., Silva, A. E., Kapahi, C., Cory, D., Thompson, B., and Pushin, D. A. (2022a). Human psychophysical discrimination of spatially dependant pancharatnam–berry phases in optical spin-orbit states. *Scientific reports*, 12(1):3245.

[Sarenac et al., 2022b] Sarenac, D., Silva, A. E., Kapahi, C., Cory, D. G., Thompson, B., and Pushin, D. A. (2022b). Human psychophysical discrimination of spatially dependant pancharatnam–berry phases in optical spin-orbit states. *Scientific Reports*, 12(1):3245.

[Scandi et al., 2022] Scandi, M., Barker, D., Lehmann, S., Dick, K. A., Maisi, V. F., and Perarnau-Llobet, M. (2022). Minimally dissipative information erasure in a quantum dot via thermodynamic length. *Physical Review Letters*, 129(27):270601.

[Schimpf et al., 2021] Schimpf, C., Reindl, M., Huber, D., Lehner, B., Covre Da Silva, S. F., Manna, S., Vyvlecka, M., Walther, P., and Rastelli, A. (2021). Quantum cryptography with highly entangled photons from semiconductor quantum dots. *Science advances*, 7(16):eabe8905.

[Schirhagl et al., 2014] Schirhagl, R., Chang, K., Loretz, M., and Degen, C. L. (2014). Nitrogen-vacancy centers in diamond: nanoscale sensors for physics and biology. *Annual review of physical chemistry*, 65:83–105.

[Schlosshauer, 2019] Schlosshauer, M. (2019). Quantum decoherence. *Physics Reports*, 831:1–57.

[Schmidt and Rathjen, 2010] Schmidt, H. and Rathjen, F. G. (2010). Signalling mechanisms regulating axonal branching in vivo. *Bioessays*, 32(11):977–985.

[Schnurr et al., 2007] Schnurr, P. P., Friedman, M. J., Engel, C. C., Foa, E. B., Shea, M. T., Chow, B. K., Resick, P. A., Thurston, V., Orsillo, S. M., Haug, R., et al. (2007). Cognitive behavioral therapy for posttraumatic stress disorder in women: A randomized controlled trial. *Jama*, 297(8):820–830.

[Schreiber, 2023] Schreiber, A. (2023). *General and Comparative Endocrinology: An Integrative Approach*. CRC Press.

[Seeman, 2007] Seeman, N. C. (2007). An overview of structural dna nanotechnology. *Molecular biotechnology*, 37:246–257.

[Sekatski et al., 2009] Sekatski, P., Brunner, N., Branciard, C., Gisin, N., and Simon, C. (2009). Towards quantum experiments with human eyes as detectors based on cloning via stimulated emission. *Phys. Rev. Lett.*, 103:113601.

[Senellart et al., 2017] Senellart, P., Solomon, G., and White, A. (2017). High-performance semiconductor quantum-dot single-photon sources. *Nature nanotechnology*, 12(11):1026–1039.

[Sewani et al., 2020] Sewani, V. K., Vallabhapurapu, H. H., Yang, Y., Firgau, H. R., Adambukulam, C., Johnson, B. C., Pla, J. J., and Laucht, A. (2020). Coherent control of nv- centers in diamond in a quantum teaching lab. *American Journal of Physics*, 88(12):1156–1169.

[Shah et al., 2007] Shah, V., Knappe, S., Schwindt, P. D., and Kitching, J. (2007). Subpicotesla atomic magnetometry with a microfabricated vapour cell. *Nature Photonics*, 1(11):649–652.

[Shannon, 1948] Shannon, C. E. (1948). A mathematical theory of communication. *The Bell system technical journal*, 27(3):379–423.

[Shao et al., 2015] Shao, L.-H., Xi, Z., Fan, H., and Li, Y. (2015). Fidelity and trace-norm distances for quantifying coherence. *Physical Review A*, 91(4):042120.

[Shen et al., 2022] Shen, Y., Xue, X., Jones, A. H., Peng, Y., Gao, J., Tzu, T. C., Konkol, M., and Campbell, J. C. (2022). Near 100% external quantum efficiency 1550-nm broad spectrum photodetector. *Optics Express*, 30(2):3047–3054.

[Shiddiq et al., 2016] Shiddiq, M., Komijani, D., Duan, Y., Gaita-Ariño, A., Coronado, E., and Hill, S. (2016). Enhancing coherence in molecular spin qubits via atomic clock transitions. *Nature*, 531(7594):348–351.

[Shim et al., 2012] Shim, J., Niemeyer, I., Zhang, J., and Suter, D. (2012). Robust dynamical decoupling for arbitrary quantum states of a single nv center in diamond. *Europhysics Letters*, 99(4):40004.

[Shimizu, 2005] Shimizu, H. (2005). Our experience with pediatric epilepsy surgery focusing on corpus callosotomy and hemispherotomy. *Epilepsia*, 46:30–31.

[Shizume, 1995] Shizume, K. (1995). Heat generation required by information erasure. *Physical Review E*, 52(4):3495.

[Shlyakhov et al., 2018a] Shlyakhov, A., Zemlyanov, V., Suslov, M., Lebedev, A. V., Paraoanu, G. S., Lesovik, G. B., and Blatter, G. (2018a). Quantum metrology with a transmon qutrit. *Physical Review A*, 97(2):022115.

[Shlyakhov et al., 2018b] Shlyakhov, A. R., Zemlyanov, V. V., Suslov, M. V., Lebedev, A. V., Paraoanu, G. S., Lesovik, G. B., and Blatter, G. (2018b). Quantum metrology with a transmon qutrit. *Physical Review A*, 97:022115.

[Silverstein et al., 2002] Silverstein, A., Silverstein, V. B., and Nunn, L. S. (2002). *Touching and Feeling*. Lerner Publications.

[Sim et al., 2012] Sim, N., Cheng, M. F., Bessarab, D., Jones, C. M., and Krivitsky, L. A. (2012). Measurement of photon statistics with live photoreceptor cells. *Phys. Rev. Lett.*, 109:113601.

[Singh et al., 2024] Singh, P., Dosovitskiy, G., and Bekenstein, Y. (2024). Bright innovations: Review of next-generation advances in scintillator engineering. *ACS nano*.

[Sirsi, 2004] Sirsi, S. (2004). Spin squeezing, entanglement and correlations. *Journal of Optics B: Quantum and Semiclassical Optics*, 6(11):437.

[Sivak et al., 2023] Sivak, V., Eickbusch, A., Royer, B., Singh, S., Tsioutsios, I., Ganjam, S., Miano, A., Brock, B., Ding, A., Frunzio, L., et al. (2023). Real-time quantum error correction beyond break-even. *Nature*, 616(7955):50–55.

[Sk and Panigrahi, 2022] Sk, R. and Panigrahi, P. K. (2022). Protecting quantum coherence and entanglement in a correlated environment. *Physica A: Statistical Mechanics and its Applications*, 596:127129.

[Song et al., 2017] Song, W., Yang, W., An, J., and Feng, M. (2017). Dissipation-assisted spin squeezing of nitrogen-vacancy centers coupled to a rectangular hollow metallic waveguide. *Optics Express*, 25(16):19226–19235.

[Spagnolo et al., 2011] Spagnolo, N., Vitelli, C., Paternostro, M., De Martini, F., and Sciarrino, F. (2011). Hybrid methods for witnessing entanglement in a microscopic-macroscopic system. *Physical Review A*, 84(3):032102.

[Sporns et al., 2005] Sporns, O., Tononi, G., and Kötter, R. (2005). The human connectome: a structural description of the human brain. *PLoS computational biology*, 1(4):e42.

[Stratonovich, 1966] Stratonovich, R. L. (1966). The transmission rate for certain quantum communications channels. *Probl. Peredachi Inf.*, 2:45–57.

[Streltsov et al., 2017] Streltsov, A., Adesso, G., and Plenio, M. B. (2017). Colloquium: Quantum coherence as a resource. *Reviews of Modern Physics*, 89(4):041003.

[Sundar, 1996] Sundar, K. (1996). Amplitude-squeezed quantum states produced by the evolution of a quadrature-squeezed coherent state in a kerr medium. *Phys. Rev. A*, 53:1096–1111.

[Suter and Jelezko, 2017] Suter, D. and Jelezko, F. (2017). Single-spin magnetic resonance in the nitrogen-vacancy center of diamond. *Progress in nuclear magnetic resonance spectroscopy*, 98:50–62.

[Svoboda and Yasuda, 2006] Svoboda, K. and Yasuda, R. (2006). Principles of two-photon excitation microscopy and its applications to neuroscience. *Neuron*, 50(6):823–839.

[Szigeti et al., 2021] Szigeti, S. S., Hosten, O., and Haine, S. A. (2021). Improving cold-atom sensors with quantum entanglement: Prospects and challenges. *Applied Physics Letters*, 118(14).

[Szwed et al., 2017] Szwed, M., Bola, Ł., and Zimmermann, M. (2017). Whether the hearing brain hears it or the deaf brain sees it, it's just the same. *Proceedings of the National Academy of Sciences*, 114(31):8135–8137.

[Taniguchi, 2010] Taniguchi, A. (2010). Live cell-based sensor cells. *Biomaterials*, 31(23):5911–5915.

[Taylor and Bowen, 2016] Taylor, M. A. and Bowen, W. P. (2016). Quantum metrology and its application in biology. *Physics Reports*, 615:1–59.

[Tedeschi and Calhoun, 1996] Tedeschi, R. G. and Calhoun, L. G. (1996). The posttraumatic growth inventory: Measuring the positive legacy of trauma. *Journal of traumatic stress*, 9:455–471.

[Teich et al., 1982a] Teich, M. C., Prucnal, P. R., Vannucci, G., Breton, M. E., and McGill, W. J. (1982a). Multiplication noise in the human visual system at threshold: 1. quantum fluctuations and minimum detectable energy. *J. Opt. Soc. Am.*, 72(4):419–431.

[Teich et al., 1982b] Teich, M. C., Prucnal, P. R., Vannucci, G., Breton, M. E., and McGill, W. J. (1982b). Multiplication noise in the human visual system at threshold: 3. the role of non-poisson quantum fluctuations. *Biological Cybernetics*, 44(3):157–165.

[Teich and Saleh, 1989] Teich, M. C. and Saleh, B. E. (1989). Squeezed state of light. *Quantum Optics: Journal of the European Optical Society Part B*, 1(2):153.

[Testa, 1982] Testa, B. (1982). The geometry of molecules: Basic principles and nomenclatures. In *New Comprehensive Biochemistry*, volume 3, pages 1–47. Elsevier.

[Thatcher and Campbell, 1993] Thatcher, G. R. and Campbell, A. S. (1993). Phosphonates as mimics of phosphate biomolecules: ab initio calculations on tetrahedral ground states and pentacoordinate intermediates for phosphoryl transfer. *The Journal of Organic Chemistry*, 58(8):2272–2281.

[Tinsley et al., 2016a] Tinsley, J. N., Molodtsov, M. I., Prevedel, R., Wartmann, D., Espigulé-Pons, J., Lauwers, M., and Vaziri, A. (2016a). Direct detection of a single photon by humans. *Nature communications*, 7(1):12172.

[Tinsley et al., 2016b] Tinsley, J. N., Molodtsov, M. I., Prevedel, R., Wartmann, D., Espigulé-Pons, J., Lauwers, M., and Vaziri, A. (2016b). Direct detection of a single photon by humans. *Nature Communications*, 7(1):12172.

[Tirandaz et al., 2017] Tirandaz, A., Taher Ghahramani, F., and Salari, V. (2017). Validity examination of the dissipative quantum model of olfaction. *Scientific Reports*, 7(1):4432.

[Togawa et al., 2011] Togawa, T., Tamura, T., and Öberg, P. Å. (2011). Biomedical sensors and instruments.

[Tononi, 2008] Tononi, G. (2008). Consciousness as integrated information: a provisional manifesto. *The Biological Bulletin*, 215(3):216–242.

[Tóth and Apellaniz, 2014] Tóth, G. and Apellaniz, I. (2014). Quantum metrology from a quantum information science perspective. *Journal of Physics A: Mathematical and Theoretical*, 47(42):424006.

[Tóth and Gühne, 2005] Tóth, G. and Gühne, O. (2005). Entanglement detection in the stabilizer formalism. *Physical Review A—Atomic, Molecular, and Optical Physics*, 72(2):022340.

[Tóth et al., 2009] Tóth, G., Knapp, C., Gühne, O., and Briegel, H. J. (2009). Spin squeezing and entanglement. *Physical Review A*, 79(4):042334.

[Truhlar, 2010] Truhlar, D. G. (2010). Tunneling in enzymatic and nonenzymatic hydrogen transfer reactions. *Journal of Physical Organic Chemistry*, 23(7):660–676.

[Tuniyazi et al., 2021] Tuniyazi, A., Mu, T., Jiang, X., Han, F., Li, H., Li, Q., Gong, H., Wang, W., and Qin, B. (2021). Snapshot polarized light scattering spectroscopy using spectrally-modulated polarimetry for early gastric cancer detection. *Journal of Biophotonics*, 14(9):e202100140.

[Turner et al., 2007] Turner, J. A., Holtzman, S., and Mancl, L. (2007). Mediators, moderators, and predictors of therapeutic change in cognitive–behavioral therapy for chronic pain. *Pain*, 127(3):276–286.

[Ullah et al., 2022] Ullah, K., Köse, E., Yagan, R., Onbaşlı, M. C., and Müstecaplıoğlu, Ö. E. (2022). Steady state entanglement of distant nitrogen-vacancy centers in a coherent thermal magnon bath. *Physical Review Research*, 4(2):023221.

[Unruh, 1995] Unruh, W. G. (1995). Maintaining coherence in quantum computers. *Physical Review A*, 51(2):992.

[Vahlbruch et al., 2007] Vahlbruch, H., Chelkowski, S., Danzmann, K., and Schnabel, R. (2007). Quantum engineering of squeezed states for quantum communication and metrology. *New Journal of Physics*, 9(10):371.

[van der Reep et al., 2023] van der Reep, T. H. A., Molenaar, D., Löffler, W., and Pinto, Y. (2023). Quantum detector tomography applied to the human visual system: a feasibility study. *J. Opt. Soc. Am. A*, 40(2):285–293.

[van der Velden, 1946] van der Velden, H. A. (1946). The number of quanta necessary for the perception of light of the human eye. *Ophthalmologica*, 111(6):321–331.

[Vandersypen and Chuang, 2005] Vandersypen, L. M. and Chuang, I. L. (2005). Nmr techniques for quantum control and computation. *Reviews of modern physics*, 76(4):1037.

[Vandersypen et al., 2001] Vandersypen, L. M., Steffen, M., Breyta, G., Yannoni, C. S., Sherwood, M. H., and Chuang, I. L. (2001). Experimental realization of shor's quantum factoring algorithm using nuclear magnetic resonance. *Nature*, 414(6866):883–887.

[Vanier, 2005] Vanier, J. (2005). Atomic clocks based on coherent population trapping: a review. *Applied Physics B*, 81:421–442.

[Vaseashta and Dimova-Malinovska, 2005] Vaseashta, A. and Dimova-Malinovska, D. (2005). Nanostructured and nanoscale devices, sensors and detectors. *Science and Technology of Advanced Materials*, 6(3-4):312–318.

[Viola et al., 1999] Viola, L., Knill, E., and Lloyd, S. (1999). Dynamical decoupling of open quantum systems. *Physical Review Letters*, 82(12):2417.

[Vitagliano et al., 2014] Vitagliano, G., Apellaniz, I., Egusquiza, I. L., and Tóth, G. (2014). Spin squeezing and entanglement for an arbitrary spin. *Physical Review A*, 89(3):032307.

[Vivoli et al., 2016] Vivoli, V. C., Sekatski, P., and Sangouard, N. (2016). What does it take to detect entanglement with the human eye? *Optica*, 3(5):473–476.

[Voss, 2013] Voss, P. (2013). Sensitive and critical periods in visual sensory deprivation. *Frontiers in psychology*, 4:664.

[Walls and Zoller, 1981] Walls, D. and Zoller, P. (1981). Enhanced sensitivity of a gravitational wave detector. *Physics Letters A*, 85(2):118–120.

[Walls, 1983] Walls, D. F. (1983). Squeezed states of light. *nature*, 306(5939):141–146.

[Wang et al., 2006] Wang, C., Adeyeye, A., and Singh, N. (2006). Magnetic antidot nanostructures: effect of lattice geometry. *Nanotechnology*, 17(6):1629.

[Wang and Sanders, 2003] Wang, X. and Sanders, B. C. (2003). Spin squeezing and pairwise entanglement for symmetric multiqubit states. *Physical Review A*, 68(1):012101.

[Wang et al., 2023] Wang, Y., Xia, S., Lv, M., Chen, J., Chen, J., and Su, S. (2023). A fundamental lower bound of the cost for bit reset. *Physics Letters A*, 481:129009.

[Wang et al., 2012] Wang, Z.-H., De Lange, G., Ristè, D., Hanson, R., and Dobrovitski, V. (2012). Comparison of dynamical decoupling protocols for a nitrogen-vacancy center in diamond. *Physical Review B*, 85(15):155204.

[Watts et al., 2021] Watts, D., Bordes, J., Brown, J., Cherlin, A., Newton, R., Allison, J., Bashkanov, M., Efthimiou, N., and Zachariou, N. (2021). Photon quantum entanglement in the mev regime and its application in pet imaging. *Nature communications*, 12(1):2646.

[Webb, 1996] Webb, R. H. (1996). Confocal optical microscopy. *Reports on progress in physics*, 59(3):427.

[Weber et al., 2010] Weber, J., Koehl, W., Varley, J., Janotti, A., Buckley, B., Van de Walle, C., and Awschalom, D. D. (2010). Quantum computing with defects. *Proceedings of the National Academy of Sciences*, 107(19):8513–8518.

[Weingarten et al., 2016] Weingarten, C. P., Doraiswamy, P. M., and Fisher, M. (2016). A new spin on neural processing: quantum cognition. *Frontiers in human neuroscience*, 10:218250.

[Wiles et al., 2002] Wiles, R., Ashburn, A., Payne, S., and Murphy, C. (2002). Patients' expectations of recovery following stroke: a qualitative study. *Disability and rehabilitation*, 24(16):841–850.

[Wineland et al., 1994] Wineland, D. J., Bollinger, J. J., Itano, W. M., and Heinzen, D. (1994). Squeezed atomic states and projection noise in spectroscopy. *Physical Review A*, 50(1):67.

[Wineland et al., 1992] Wineland, D. J., Bollinger, J. J., Itano, W. M., Moore, F., and Heinzen, D. J. (1992). Spin squeezing and reduced quantum noise in spectroscopy. *Physical Review A*, 46(11):R6797.

[Wood et al., 2010] Wood, A. M., Froh, J. J., and Geraghty, A. W. (2010). Gratitude and well-being: A review and theoretical integration. *Clinical psychology review*, 30(7):890–905.

[Wootters, 2001] Wootters, W. K. (2001). Entanglement of formation and concurrence. *Quantum Inf. Comput.*, 1(1):27–44.

[Wu et al., 2022] Wu, D., Li, Z., Shi, Z., Guo, H., Tang, J., and Liu, J. (2022). High-sensitivity temperature sensing on an ensemble of nitrogen-vacancy centers in diamond. *Japanese Journal of Applied Physics*, 61(8):086502.

[Wu et al., 2024] Wu, W., Zhu, J., Yao, Y., and Lan, Y. (2024). Can molecular quantum computing bridge quantum biology and cognitive science? *Intelligent Computing*.

[Wu et al., 2016] Wu, Y., Jelezko, F., Plenio, M. B., and Weil, T. (2016). Diamond quantum devices in biology. *Angewandte Chemie International Edition*, 55(23):6586–6598.

[Xie et al., 2021] Xie, T., Zhao, Z., Kong, X., Ma, W., Wang, M., Ye, X., Yu, P., Yang, Z., Xu, S., Wang, P., et al. (2021). Beating the standard quantum limit under ambient conditions with solid-state spins. *Science Advances*, 7(32):eabg9204.

[Xin et al., 2022] Xin, L., Chapman, M., and Kennedy, T. (2022). Fast generation of time-stationary spin-1 squeezed states by nonadiabatic control. *PRX Quantum*, 3(1):010328.

[Xu et al., 2019a] Xu, C., Wu, X., Huang, G., and Mei, Y. (2019a). Rolled-up nanotechnology: materials issue and geometry capability. *Advanced materials technologies*, 4(1):1800486.

[Xu et al., 2019b] Xu, C., Zhang, L., Huang, S., Ma, T., Liu, F., Yonezawa, H., Zhang, Y., and Xiao, M. (2019b). Sensing and tracking enhanced by quantum squeezing. *Photonics Research*, 7(6):A14–A26.

[Xu et al., 2024] Xu, Q., Zhou, L.-X., Feng, T.-F., Qiu, S.-F., Li, S.-W., Zhang, W.-J., Luo, H., and Zhou, X.-Q. (2024). Experimental quantum state compression from two identical qubits to a qutrit. *Science China Physics, Mechanics & Astronomy*, 67(7):270311.

[Yan et al., 2010] Yan, F., Yang, M., and Cao, Z.-L. (2010). Optimal reconstruction of the states in qutrit systems. *Physical Review A*, 82(4):044102.

[Yang et al., 2022] Yang, X., Yin, H., Zhang, F., and Nie, J. (2022). Quantum coherence protection by noise. *Laser Physics Letters*, 19(7):075202.

[Yao et al., 2024] Yao, F., Dong, K., Ke, W., and Fang, G. (2024). Micro/nano perovskite materials for advanced x-ray detection and imaging. *ACS nano*.

[Yao et al., 2021] Yao, Y., Schlömer, H., Ma, Z., Venuti, L. C., and Haas, S. (2021). Topological protection of coherence in disordered open quantum systems. *Physical Review A*, 104(1):012216.

[Yau et al., 1977] Yau, K., Lamb, T. D., and Baylor, D. A. (1977). Light-induced fluctuations in membrane current of single toad rod outer segments. *Nature*, 269(5623):78–80.

[Ye and Zoller, 2024] Ye, J. and Zoller, P. (2024). Essay: Quantum sensing with atomic, molecular, and optical platforms for fundamental physics. *Physical Review Letters*, 132(19):190001.

[Yuste, 2005] Yuste, R. (2005). Fluorescence microscopy today. *Nature methods*, 2(12):902–904.

[Zeh, 1973] Zeh, H. D. (1973). Toward a quantum theory of observation. *Foundations of Physics*, 3(1):109–116.

[Zeilinger, 2007] Zeilinger, A. (2007). Long-distance quantum cryptography with entangled photons. In *Quantum Communications Realized*, volume 6780, pages 44–51. SPIE.

[Zhang et al., 2024a] Zhang, L., Besaga, V. R., Rühl, P., Zou, C., Heinemann, S. H., Wang, Y., and Setzpfandt, F. (2024a). Probing polarization response of monolayer cell cultures with photon entanglement. (arXiv:2401.10789). arXiv:2401.10789 [physics, physics:quant-ph].

[Zhang et al., 2022] Zhang, M., Yu, H.-M., Yuan, H., Wang, X., Demkowicz-Dobrzański, R., and Liu, J. (2022). Quanestimation: An open-source toolkit for quantum parameter estimation. *Physical Review Research*, 4(4):043057.

[Zhang et al., 2018] Zhang, T., Liu, G.-Q., Leong, W.-H., Liu, C.-F., Kwok, M.-H., Ngai, T., Liu, R.-B., and Li, Q. (2018). Hybrid nanodiamond quantum sensors enabled by volume phase transitions of hydrogels. *Nature communications*, 9(1):3188.

[Zhang et al., 1990] Zhang, W.-M., Gilmore, R., et al. (1990). Coherent states: theory and some applications. *Reviews of Modern Physics*, 62(4):867.

[Zhang et al., 2024b] Zhang, Y., He, Z., Tong, X., Garrett, D. C., Cao, R., and Wang, L. V. (2024b). Quantum imaging of biological organisms through spatial and polarization entanglement. *Science Advances*, 10(10):eadk1495.

[Zhu et al., 2024] Zhu, R., Li, W., Zhen, Z., Zou, J., Liao, G., Wang, J., Wang, Z., Chen, H., Qin, S., and Weng, Y. (2024). Quantum phase synchronization via exciton-vibrational energy dissipation sustains long-lived coherence in photosynthetic antennas. *Nature Communications*, 15(1):3171.